Transilvania University of Brașov

HABILITATION THESIS

LASER WELDING AND SURFACE ENGINEERING OF ADVANCED MATERIALS

Domain: Industrial engineering

Author: Assoc. Prof. Dr. Elena Manuela STANCIU

University: Transilvania University of Brașov

BRAŞOV, 2023

CONTENT

ACKNOWLEDGEMENT

The Transilvania University of Brasov is gratefully acknowledged for providing technical resources and academic support, facilitating the successful conduction of research activities.

This Habilitation thesis incorporates research that has received partial support from various grants:

7th Framework Programme of the EU (SFERA 2 Grant Agreement n. 312643) is gratefully acknowledged for the access to solar reactors.

Sectoral Operational Programme Human Resources Development (SOP HRD), financed from the European Social Fund and by the Romanian Government under the project number POSDRU/159/1.5/S/134378 is gratefully acknowledged.

Romanian National Program for Research in the framework of the Project No." PCCA 243/2014 Advanced Metallic Materials used for the New Generation of Nuclear Power Plant 4R – NUCLEARMAT is acknowledged.

PRO-DD (POS-CCE, O.2.2.1., ID 123, SMIS 2637, ctr. No 11/2009) is gratefully acknowledged for providing the infrastructure used in this habilitation thesis.

This Habilitation thesis is the result of the collective efforts and support of many, and I extend my Acknowledgement to all members of the Materials Engineering and Welding department from the Transilvania University of Brasov. I extend my sincere gratitude to all my collaborators from Politehnica University of Bucharest, Politehnica University of Timișoara, and University las Palmas de Gran Canaria. A special acknowledgment goes to the laboratories LAMET and ERAMET at Politehnica University of Bucharest for their invaluable contributions.

The habilitation thesis, titled "Laser Welding and Surface Engineering of Advanced Materials," is founded on the research activities undertaken by the author in collaboration with:

Balteș Liana	Moldovan Edit
Croitoru Cătălin	Pascu Alexandru
Geantă Victor	Roată Ionuț Claudiu
Hulka Iosif	Țierean Mircea Horia
Uțu Dragoș	Voiculescu Ionelia

REZUMAT

Teza de abilitare intitulată **Sudarea și prelucrarea cu laser a materialelor avansate** prezintă o sinteză a rezultatelor științifice în domeniul tehnologiei laser ale autoarei, pornind de la obținerea titlului de doctor inginer în domeniul inginerie industrială.

Teza este redactată în limba engleză, are 124 de pagini și este structurată în 4 secțiuni distincte, respectiv: **B1 Realizări profesionale, B2 Realizări științifice , B3 Evoluția carierei și B4 Bibliografia.**

Lucrarea debutează cu prezentarea succintă a realizărilor profesionale ale autoarei în domeniul ingineriei industriale după obținerea titlului de doctor inginer în anul 2011. Tehnologia de prelucrare cu laser este domeniul principal al cercetărilor științifice prezentate în această teză de abilitare, domeniu care a permis o continuare fireasca a tezei de doctorat intitulată Research on Nd:YAG Laser Welding of Stainless Steel Thin-Walled Components, susținută în 2011 la Universitatea Politehnică din București, și a disertației intitulate Laser Welding of Austenitic Stainless Steel Thin Components, susținută în 2011 la Universitatea Politehnică din Madrid. Profesional, autoarea își începe activitatea în anul 2011 ca cercetător științific la SC Optoelectronica-2001 SA, Măgurele, unde a profesat până în 2016, când s-a angajat la Universitatea Transilvania din Brașov, având gradual didactic de șef de lucrări. Prima parte a tezei, intitulată **Realizări profesionale**, prezintă succint evoluția în cariera didactică și activitatea de cercetare a autoarei. Aceasta a făcut parte din 16 proiecte de cercetare științifică și a publicat numeroase articole științifice dintre care 41 sunt indexate în baza de date Web of science core colection.

Cea de-a doua secțiune a tezei, **B2 Realizări științifice**, este structurată în 5 capitole și abordează comprehensiv domeniul tehnologiei de prelucrare cu laser, fiind prezentate în detaliu cercetări fundamentale privind sudarea, depunerea cu pulberi, texturarea și procesarea superficială cu fascicul laser a diferitelor materiale convenționale sau materiale avansate de tipul FeCrAl.

Capitolul 1 al tezei, intitulat *Baze teoretice și motivare*, debutează prin expunerea motivației care a stat la baza realizării prezentei teze de abilitare. Proprietățile extraordinare ale radiației electromagnetice provenită din surse naturale sau artificiale, sunt exponentul care face posibilă utilizarea radiației laser pentru o gamă largă de cercetări fundamentale în domeniul

industrial. Pe parcursul capitolului este dezvoltat treptat conceptul tehnologiei laser și sunt prezentate principalele caracteristici ale radiației electromagnetice.

În continuare**, Capitolul 2**, intitulat *Procese care utilizează fasciculul LASER*, descrie cele mai importante metode de procesare cu laser, procese care sunt utilizate de care autoare în cadrul activităților de cercetare științifică. Printre acestea, sudarea cu laser este una dintre principalele aplicații ale laserului în industrie și este abordată detaliat în cadrul acestui capitol. Principiul sudării prin conducție, sudarea cu laser în modul key-hole sunt concepte fundamentale care stau la baza studiilor de caz prezentate pe parcursul lucrării. De asemenea, depunerea cu fascicul laser și texturarea cu laser sunt prezentate atât conceptual cât și din punct de vedere experimental, fiind prezentate rezultate proprii despre depunerile cu pulberi înalt aliate și armate cu particule de carbură de wolfram. La finalul acestui capitol este introdus conceptul de tratament termic cu laser în conjuncție cu topirea superficială cu laser și sunt detaliate aplicațiile acestei tehnici în industrie. Este evidențiată aplicativitatea tehnicilor de procesare superficială, topire / retopire cu laser, la materialele avansate de tipul FeCrAl destinate utilizării în centralele nucleare de generație a 4-a. Acest capitol oferă o perspectivă comprehensivă asupra modului în care autoarea a integrat diferitele procese bazate pe tehnologia laser în raport cu literatura de specialitate.

Capitolul 3, *Cercetări experimentale privind sudarea cu laser a oțelurilor inoxidabile*, este dedicat descrierii a trei studii experimentale privind sudarea cu laser a oțelurilor inoxidabile. Optimizarea parametrilor la sudarea cu laser a oțelurilor AISI 321 este realizată prin determinarea influenței puterii laserului, a duratei pulsului și a frecvenței, asupra geometriei cordonului sudat. Rezultatele studiului prezentat au permis obținerea unor valori clare privind parametrii optimi de proces pentru sudarea cu pulsuri laser în domeniul milisecundelor. Contribuțiile originale ale autoarei în acest domeniu sunt evidențiate și prin realizarea unor îmbinări eterogene sudate între oțel carbon și oțel inoxidabil (AISI 1010 – AISI 321). Rezultatele studiului au arătat că puterea laserului, respectiv densitatea de putere este parametrul principal care influențează distribuția elementelor chimice în cordonul sudat. Conform celui de-al treilea studiu prezentat în acest capitol, sudabilitatea oțelurilor inoxidabile poate fi îmbunătățită și prin utilizarea unui flux activ, de tipul SiO_2, care să îmbunătățească gradul de absorbție a fasciculul laser. Rezultatele cercetărilor din acest capitol, diseminate in trei publicații științifice, permit o evaluare obiectivă a capabilității tehnologiei laser în realizarea de îmbinări sudate între materiale de același fel sau diferite, utilizând sisteme laser care funcționează in regim continuu sau pulsat.

Capitolul 4 prezintă cercetările științifice din domeniul procesării superficiale cu laser a materialelor avansate de tipul FeCrAl. Topirea și retopirea superficială cu laser reprezintă soluția propusă de autoare pentru creșterea rezistentei la coroziune, dar și a durității aliajelor FeCrAl, aliaje destinate în special utilizării în centralele nucleare de generație a 4-a. Rezultatele din acest capitol sunt obținute în urma colaborării directe cu laboratoarele LAMET și ERAMET din cadrul Universității Politehnice din București și a derulării proiectului Materiale metalice avansate pentru noile generații de centrale nuclear, 4R, NUCLEARMAT (Contract PCCA 243/2014) la care autoarea a fost responsabil.

Topirea superficială cu laser este o tehnică modernă de prelucrare a suprafețelor care implică modificări microstructurile și morfologice datorate topirii / retopirii materialului și datorită ciclului rapid de încălzire-răcire a zonei prelucrate. Această tehnică de procesare este fundamentul studiului prezentat în capitolul 5, intitulat *Metodă avansată de procesare cu laser în lichid*.

Capitolul 5 descrie o tehnologie originală de procesare superficială cu laser folosind un lichid, astfel încât să se poată realiza un tratament termo-mecanic, coroborat cu microalierea suprafeței prelucrate. Conceptul original prezentat în acest capitol se bazează pe fenomenul de cavitație în lichid, acetat de nichel, iar rezultatele obținute au validat eficacitatea tehnologiei propuse. Cavitația în lichid, în acest context, se dovedește a fi o metodă inovatoare de a realiza procesarea termo-mecanică, dar și microalierea cu nichel a suprafeței prelucrate.

A treia secțiune a tezei, **B3 Evoluția carierei,** prezintă succint planurile de dezvoltare a carierei didactice și de cercetare. Dezvoltarea continuă a aptitudinilor profesionale, utilizarea tehnicilor moderne de predare-învățare precum și actualizarea permanentă a cursurilor sunt obiective principale ale autoarei în evoluția carierei academice.

Activitatea de cercetare a autoarei va continua în domeniul tehnologiei laser și sunt descrise succint trei direcții viitoare de cercetare:

1. Determinarea unei metode pentru monitorizarea în timp real a procesării cu laser
2. Sudarea eterogenă a titanului cu oțel inoxidabil
3. Proiectarea de noi materiale de tipul HEA și prelucrarea superficială cu laser

Ultima parte a tezei, **B4 Bibliografia**, prezintă referințele bibliografice asociate acestei lucrări.

B Scientific and professional achievements and the evolution and development plans for career development

B1. Professional achievements

The Habilitation thesis entitled **Laser welding and surface engineering of advanced materials** reflects the continued development and growth of my research activities, originating from the defending of my doctoral thesis in September 2011. My academic career and professional trajectory can be outlined as follows:

Emerging into the domain of welding engineering in 2008, I graduated from the Faculty of Engineering and Management of Technological Systems at the University Politehnica of Bucharest. My specialty is on Welding Equipment and Technology. Subsequently, in 2010, I continued my academic path by completing the master's program in Welding Engineering at the same institution.

In 2008, my activity into the Industrial Engineering field starts with enrollment in the doctoral program at the Faculty of Engineering and Management of Technological Systems at the University Politehnica of Bucharest. In 2011, I successfully defended my doctoral thesis entitled "Research on Nd:YAG Laser Welding of Stainless Steel Thin-Walled Components." This experimental research-based thesis in the field of laser welding technology was undertaken in collaboration with the Centro Laser department at the Universidad Politécnica de Madrid. This collaborative with Centro Laser, enhanced my technical skills and expertise in laser technology. Simultaneously, from 2009 to 2011, I pursued a Master of Laser Technology from the Applied Physics Department ETS Ingenieros Industriales at Universidad Politécnica de Madrid, resulting in a master's thesis on "Laser Welding of Austenitic Stainless Steel Thin Components."

After finished the master and doctoral studies, my professional activity in research continued as CSIII researcher from 2011 to 2016 at the R&D company Optoelectronica 2001 SA, Magurele, Bucharest.

In this interval spanning, I have been principal researcher, being involved in research activities based on exploration of diverse applications of laser technology, contributing to various experimental studies under both national and international research grants. My main research activities include laser processing, particularly welding and heat treatment, alongside the

development of innovative materials for solar cell applications and also an emphasis on advanced alloys such us FeCrAl.

Since 2016 I start my affiliation with Transilvania University of Brasov as lecturer, being involved into two main trajectories: teaching and research. These dual directions have numerous interdisciplinary pursuits that synergistically complement my academic activity. Pedagogical responsibilities, research leadership, knowledge propagation, conference participation, projects proposals, and beyond are examples of main activities. In the same time, my proactive involvement in the Advanced Welding Eco-Technologies research center within the R&D Infrastructure of Transilvania University of Brasov continuously improve my skills and knowledge in the laser welding technology.

The teaching is the most important activity in my career, encompassing the delivery of courses, seminars, and hands-on laboratories in the field of materials science, materials technology, non-destructive testing, and mechanical processing at bachelor's and master's degree levels. Concurrently, my dedication to mentoring and guiding undergraduate and master's students in their final projects has enriched my pedagogical experience. A totally of 14 undergraduate students and 5 master's students have been under my tutelage for their final projects.

My pedagogical strategies have been meticulously enhanced by constant refinement based on students feedback. The enrichment of the courses content is made by using real-world engineering case studies and by integration of contemporary technological developments into the curriculum.

My expertise in industrial engineering is based on fundamental and applied research, sustained by investigations into diverse topics such as laser welding across various alloys, laser process optimization, laser-based surface treatments, and advanced material development within the sphere of industrial engineering. These research activities were the foundation of numerous projects undertaken over the past 12 years.

As **project director and principal investigator**, I have managed one national PCCA grant and two international research grants SFERA II (Solar Facilities for the European Research Area), projects that attest to my research leadership:

1. Advanced Metallic Materials for New Generation Nuclear Power Plants, 4R, NUCLEARMAT (PCCA 243/2014, as **principal investigator / project responsable**).
2. Solar Synthesis of Functional Carbonaceous under Constant Electric Charge - SFERA III" (2019, France).

3. Corrosion and Wear Behavior of NiCrBSi Coatings Fabricated by Laser Cladding, European Solar Research Infrastructure for Concentrated Solar Power - SFERA II" (2016, Italy).

At the same time, my role as a **project team member** has been pronounced across various national and international research grants, such us:

1. "Studies Concerning the Real-Time Monitoring of the Laser Welding/Cutting Process" and "New Methods for Cutting Metallic Waste". Third party project with EU private sector (2015-2018, Netherlands). Project coordinated by Prof. Mircea Horia Țierean from Transilvania University of Brasov.

2. **Key person** of "Reclamation of Gallium, Indium and Rare-Earth Elements from Photovoltaics, Solid-State Lighting and Electronics Waste"- RECLAIM, FP7 grant type, grant agreement no: 309620 https://cordis.europa.eu/project/id/309620/reporting, Project coordinated by Brânduș Comănescu from Optoelectronica – 2001 SA, Măgurele.

3. "Perovskites for Photovoltaic Efficient Conversion Technology", 8 SEE grant type, EEA-JRP-RO-NO-2013-1, Project coordinated by Prof. Mihaiela Iliescu from Optoelectronica – 2001 SA, Măgurele.

4. "Compact biophotonic platform for drug allergy diagnosis" – COBIOPHAD, H2020 grant type, Grant agreement no: 688448, Project coordinated by Dr. Necșoiu Teodor from Optoelectronica – 2001 SA, Măgurele.

5. "Improvement of Electric Contact Corrosion Resistance", SFERA II type project (2014, Italy). Project coordinated by Dr. Ionut Roată from Transilvania University of Brasov

6. "Mechanical proprieties improvement of Cu10Al laser cladded on aluminium", SFERA II type project (2014, Spain). Project coordinated by Dr. Ionut Roată from Transilvania University of Brasov.

7. "Residual stress relieve of Ni based coatings fabricated by laser cladding", SFERA II type project (2015, France). Project coordinated by Prof. Pascu Alexandru from Transilvania University of Brasov.

8. "Synthesis of carbon nanotubes using solar radiation and Al_2O_3-Mn/Cu_2O catalyst", SFERA II type project (2016, France). Project coordinated by Prof. Pascu Alexandru from Transilvania University of Brasov

9. "Al_2O_3/TiO_2 cladding in pre-placed powder geometry using concentrated solar radiation", SFERA II type project (2017, France). Project coordinated by Prof. Pascu Alexandru from Transilvania University of Brasov.
10. "Corrosion improvement of FeCrAl alloys designed for Molten Salt Reactors", SFERA II type project (2017, Italy). Project coordinated by Prof. Pascu Alexandru from Transilvania University of Brasov.
11. "Research on the Development of Diode-Pumped Laser Equipment Family for Medical Applications, Especially Urology" - ELASMEDURO, POS-CCE type project, No.159/2011. Project coordinated by Brânduș Comănescu from Optoelectronica – 2001 SA, Magurele.
12. "Advanced and Extended Functionality Complex System for Document Examination and Scientific Research in the Field of Forensic", grant type PN-II-IN-DPST-2012-1-0026. Project coordinated by Dr. Necșoiu Teodor from Optoelectronica – 2001 SA, Măgurele.
13. "Application of Laser Techniques for Manufacturing Real-Time Microfluidic-Based Biosensors SOLE", grant type PN-II-PT-PCCA-2013-4-1992, grant number 34/01.07.2014. Project coordinated by Dr. Necșoiu Teodor from Optoelectronica – 2001 SA, Măgurele.

The dissemination of my scientific activity has been made through publications in journals indexed within the Web of Science Core Collection and other international databases (BDI). Besides participation at international conferences, workshops and seminaries, my dissemination activity, on 25.11.2023, can be summarised as following:

1. **Web of Science Core Collection:**
   - 41 articles indexed, accumulating a total of 216 citations (excluding self-citations).
   - H-index of 9.
2. **Scopus Database:**
   - 59 articles indexed, with a combined total of 321 citations.
   - H-index of 10.
3. **Google Scholar Database:**
   - 78 articles listed, gathering a total of 423 citations.
   - H-index of 12 and an i10-index of 13.

The dissemination activity is also augmented by realising of two patents:

- Patent of Invention, No. 133180/30.08.2022, for FeCrAl(Y) alloy types and a method for obtaining a product from this alloy, by V. Geantă, I. Voiculescu, R. Ștefănoiu, V. Fugaru, E.M. Stanciu, A. Pascu, C. Postolache, M.R. Ioan.
- Patent of Invention, No. 132082/28.06.2019, for a Printer for Depositing Ultra-Thin Layers with Different Physico-Chemical Properties, by I. Mihaiela, M. Lazar, I. Pintilie, L. Vladareanu, T. Necsoiu, V. Stancu, A.G. Tomulescu, C. Besleaga Stan, M. Sima, L.N. Leonat, E. M. Stanciu, B. Comansescu, A.V. Enuica.

Furthermore, my commitment to advancing scientific activity is completed with my key role in the organizing committees of international events like the International Conference on Materials Science and Engineering – BraMat 2019 and Bramat 2022. Additionally, I have the role of reviewer for ISI journals, including Optics and laser engineering and Materials Today Proceedings.

The scientific results presented in this Habilitation thesis are rooted within the following research grants, scientific papers, presentations in international conferences and peer-reviewed journals subsequent to the research and defence of my PhD thesis in 2011.

Research grants

1. Advanced Metallic Materials for New Generation Nuclear Power Plants, 4R, NUCLEARMAT (PCCA 243/2014, as **Principal investigator / Project responsable**

Scientific papers

1. Stanciu E.M., Pascu A., Tierean M.H., Roata I.C., Voiculescu I., Hulka I., Croitoru C., Dissimilar Laser Welding of AISI 321 and AISI 1010, Technical Gazette, ISSN 1330-3651, Vol. 25/No. 2, 2018, I.F. 0.72.
2. Stanciu E.M., Pascu A., Roata I.C., Croitoru C., Tierean M.H., Laser welding of dissimilar materials, Materials Today-Proceedings, 19, pp 1066-1072, ISSN 2214-7853, 2019.
3. Stanciu E.M., Pascu A., Gheorghiu I., CMT Welding of Low Carbon Steel Thin Sheets, IOP Conference Series: Materials Science and Engineering, 209, 2017, 012051
4. Stanciu E.M., Pascu A., Roată I.C., Croitoru C., Tierean M., Mirza Rosca J., Hulka I., Solar radiation synthesis of functional carbonaceous materials using Al_2O_3/TiO_2-Cu-HA doped catalyst, Applied Surface Science 438, pp 33–40, 2018, ISSN 0169-4332, I.F. 5.15, **Q1**.
5. Stanciu E.M., Pascu A., Roată I.C., Iatan C., Moldovan E.R. and Tierean M.H., Millisecond pulsed laser welding of AISI 316 stainless steel, IOP Conf. Series: Materials Science and Engineering, IOP Publishing, 1251, 2022, 012012

6. Stanciu E.M., Pascu A., Croitoru C., Roata I. C., Cristea D., Tierean M.H., Hulka I., Petre I.M., Mirza Rosca J. C., Functional Surfaces via Laser Processing in Nickel Acetate Solution, Materials, 2023, 16, 3087, I.F. 3.4, **Q2**.
7. Voiculescu, V. Geanta, E.M. Stanciu, D.A. Jianu, C. Postolache, V. Fugaru, Effect of Irradiation and Temperature on Microstructural Characteristic of FeCrAl Alloys, Acta Physica Polonica A, 134(1), pp 116-118, 2018, I.F. 0.725
8. Hulka, I.; Utu, I.D.; Avram, D.; Dan, M.L.; Pascu, A.; Stanciu, E.M.; Roata, I.C. Influence of the Laser Cladding Parameters on the Morphology, Wear and Corrosion Resistance of WC-Co/NiCrBSi Composite Coatings. Materials 2021, 14, 5583, **Q1**.
9. Moldovan E.R., Doria C.C., Ocana J.L., Baltes L.S., Stanciu E.M., Croitoru C., Pascu A., Roata I.C., Tiereanu M.H., Wettability and Surface Roughness Analysis of Laser Surface Texturing of AISI 430 Stainless Steel, Materials, 2022, 15(8), 2955, I.F. 3.4, **Q2**.
10. Geanta V., Voiculescu I., Tenciu D., Baschir L., Stanciu E.M., Pascu A., Effect of laser processing on the microstructure of the FeCrAl alloys, Journal of Optoelectronics and Advanced Materials, 2020, 22(7-8), pp 411-418, I.F. 0.63

Presentations in international conferences

1. Pascu A., Stanciu E. M., Cuculea D., Ardelean G., Iatan C., Moldovan E. R., Machedon T., Influences of the Nozzle Shape on Bead Appearance and Morphology in Coaxial Laser Cladding, International Conference on Innovative Research, May 26th to 27th, 2022, Iasi – Romania, ISSN Print 2601-4580.

Moreover, unpublished results have been adjoined for a better presentation of the scientific contents of the thesis.

The present habitation thesis satisfies and surpasses the indicated minimum criteria set by the Romanian National Council for Titles, Diplomas, and Certificates (Industrial Engineering and Management domain), as outlined in OMENCS Nr. 6129/20.12.2016 [MO, I, 123/15.02.2017). The criteria are presented and summarised as following:

<table>
<tr><td colspan="3">MINIMUM CRITERIA</td><td>Minimum requested</td><td>Accomplished</td></tr>
<tr><td colspan="3">A1. Teaching & training</td><td>130</td><td>139.8</td></tr>
<tr><td colspan="3">A2. Research</td><td>300</td><td>640.34</td></tr>
<tr><td colspan="3">A3. Recognition & impact of research activity</td><td>100</td><td>174.50</td></tr>
<tr><td colspan="3">MANDATORY MINIMUM TERMS SUBCATEGORIES</td><td>Minimum requested</td><td>Accomplished</td></tr>
<tr><td colspan="3">A.1.1.1. Books / chapters in engineering as author (first author)</td><td>2</td><td>3</td></tr>
<tr><td colspan="3">A.1.1.2. Didactic textbook, laboratory guidance / applications (first author)</td><td>4 (2)</td><td>4 (2)</td></tr>
<tr><td colspan="5">A.2.1. Articles in ISI Thomson Reuters journals & proceedings</td></tr>
<tr><td rowspan="4">of which</td><td colspan="2">Minimum 8 articles in ISI Thomson Reuters journals and proceedings – <u>from the last promotion (2018)</u></td><td>8</td><td>15</td></tr>
<tr><td rowspan="3">of which</td><td>in ISI Thomson Reuters journals</td><td>3</td><td>15</td></tr>
<tr><td>as first author in ISI Thomson Reuters journals</td><td>3</td><td>4</td></tr>
<tr><td>in a Q1 or Q2 rated journal</td><td>1</td><td>12</td></tr>
<tr><td colspan="3">A.2.2. Articles in journals and volumes of scientific events indexed in international databases - <u>from the last promotion</u></td><td>8</td><td>10</td></tr>
<tr><td colspan="5">A.2.5 Research grants (obtained by competition)</td></tr>
<tr><td rowspan="2">A.2.5.1 As director/responsible</td><td>International grant</td><td rowspan="2">2</td><td>2 director</td></tr>
<tr><td>National grant</td><td>1 responsible</td></tr>
<tr><td rowspan="2">A.2.5.2 As member/participant</td><td>International grant</td><td>-</td><td>9</td></tr>
<tr><td>National grant</td><td>-</td><td>15</td></tr>
</table>

B2. Scientific achievements

LASER WELDING AND SURFACE ENGINEERING OF ADVANCED MATERIALS

Chapter 1. BACKGROUND AND MOTIVATION

Since completing my Ph.D. thesis in 2011, I have been attracted by the field of industrial engineering, particularly by the application of various light sources in materials processing. Light, is a fundamental form of electromagnetic radiation and has proven to be a versatile tool in engineering processes, being used in a wide range of applications such as welding, cladding, surface melting, cutting, and the synthesis of micro and nano-carbonaceous materials. One of the most interesting facts of light-based materials engineering is its ability to utilise the properties of electromagnetic radiation for diverse applications. Light, originating from both artificial sources like lasers and specialised lamps, as well as natural sources such as sunlight, can have a broad spectrum of wavelengths. Each wavelength can alter the material in a different way and special designed artificial light sources have been developed to produce intense and focused beams, allowing for precise modifications at micro and nanoscales. Simultaneously, sunlight, Earth's primary natural light source, start to be used through concentrated solar power (CSP) systems for experimental or large-scale industrial applications. As researcher, I have been involved in various projects that employed natural (sunlight) or artificial light (lasers) to synthesis or to process materials. Below is depicted the "power" and capabilities of the sunlight to produce carbon nanotubes, in controlled conditions, as resulted from the project Synthesis of carbon nanotubes using solar radiation and Al_2O_3-Mn/Cu_2O catalyst.

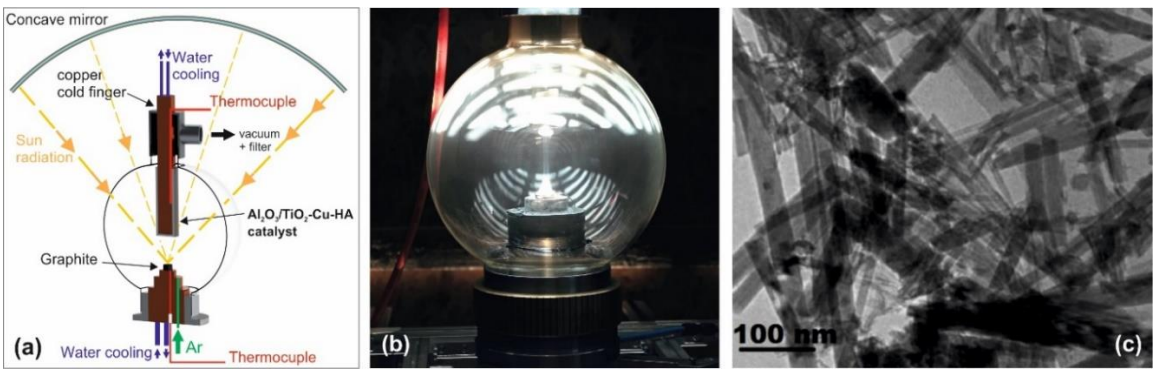

Figure 1.1 Solar synthesis of the carbon nanotubes using a pure graphite target; a) schematic representation of the set-up, b) solar reactor, c) obtained CNT's [STE18].

This is only one example of how the natural light can be used for synthesis of advanced materials where precise control over size and composition is achieved through carefully designed processing conditions. The sun light, even if is the greener source of energy, has considerable limitation for engineering applications and to overcame these down backs have been created state of the art laser generators with high quality and power light beams. Nowadays, the entire industrial engineering field benefits on the laser technology. In the field of welding, lasers have revolutionized the process by enabling high-precision fusion of metals, ensuring superior weld quality and minimizing thermal distortion. Cladding, a technique used for surface modification, utilizes focused light beams to deposit protective layers onto substrates, enhancing their mechanical and corrosion-resistant properties. Surface melting, another cutting-edge application, involves the controlled melting of a material's surface using laser, resulting in improved surface characteristics and performance.

As an engineer, professor, and researcher, I am deeply involved in the field of laser technology used to various engineering applications. The relevance of the laser technology into the nowadays research activity is proved by the 27000+ article published and indexed by Clarivate Analytics in the last five years.

Figure 1.2 Articles related with laser technology for industrial applications. On 05.11.2023.

The focus of this Habilitation thesis is to address existing gaps in the field of laser processing, specifically concerning the welding of materials with similar or dissimilar compositions, surface engineering techniques involving the addition of a new layer through cladding, and surface treatments such as heat treatment, surface remelting, and in-liquid processing of materials.

1.1 Fundamentals of laser technology

The field of LASER technology involves the utilization of advanced devices that are specifically engineered for the emission and amplification of radiation at the quantum level. The success of their functioning is based on the complex interaction between two separate physical components: a gain medium, commonly known as an active or laser medium, and an optical resonator. The gain medium contains a variety of materials, including high-purity rare-earth-doped crystals, glasses, gaseous molecules, semiconductors, and dyes. These materials undergo the process known as energy pumping. The optical resonator, which includes an optical cavity or resonating cavity, encloses the gain medium and is composed of several mirrors. These mirrors give feedback to the system, resulting in the generation of resonant stationary waves, namely longitudinal modes or transverse modes. The synchronization of these waves is done with great precision to match the frequency at which electrons move from a state of high energy (excited state) to a state of reduced energy, which is a characteristic feature of the particular gain medium being used. There are several energy pumping techniques that can be employed, such as resonant energy transfer, chemical reactions, and the utilization of electrical and magnetic fields. These methods are of high significance in facilitating the gathering of energy within the active medium. This previously mentioned energy can be successfully gathered and later released by the process of stimulated emissions, which occurs under the influence of laser radiation.

The acronym LASER is derived from the phrase "**Light Amplification by Stimulated Emission of Radiation**," which simply describes the fundamental quantum phenomenon that facilitates the functioning of LASER systems. A LASER system is a device that has been designed to produce and enhance electromagnetic radiation in several domains, including X-ray, UV, visible, infrared, or microwave. This capability is based on the principle of stimulated emission, as previously addressed. The resulting radiation shows properties of great coherence, monochromaticity, and a substantially higher power density.

The laser functions as a quantum radiation amplifier when it is stimulated by external radiation in certain specified cases. On the other hand, in cases when the photons initially created within the device cavity spontaneously induce stimulated emission, the laser functions as a quantum radiation generator.

Basically, the laser is a complex device that employs a solid, liquid, or gaseous active medium coupled to a resonant optical cavity. This active medium has a particular chemical composition

and well-defined properties, and it obtains external energy through a process known as pumping [URS86].

Pumping can be accomplished through either electrical or optical means. Optical pumping involves the use of a luminous source (flash) that induces excitation in the atomic or molecular species residing in the active medium. This excitation involves the transition of electrons from the ground energy level to a higher energy state, resulting in the absorption of energy. In accordance with the dual corpuscle-wave principle, subsequent transitions between higher and lower energy levels result in the emission of energy quanta or photons. A photon, a particle associated with light, is capable of transferring kinetic energy to a single electron, thereby altering the electron's energy level. According to the Planck relation, the quantum of energy supplied by a photon, denoted E, is inversely proportional to the wavelength of light radiation, denoted and measured in meters [AND08, ION05]:

$$\Delta E = h \cdot c / \lambda \quad (1.1)$$

where $c = 3 * 10^8$ m/s represents the speed of light in a vacuum and $h = 6.626 * 10^{-34}$ J·s is the Planck constant.

Characteristics of the laser beam

Based on the phenomenon of stimulated emission, the laser emits electromagnetic radiation that differs from those emitted by conventional sources due to its unique characteristics. Important laser beam parameters include beam intensity, focalization, and radiation wavelength. Coherence, monochromaticity, intensity, and temporal beam distribution distinguish laser radiation.

Table 1.1 explains the primary characteristics of laser radiation and emphasizes its most important industrial applications. In addition, the table specifies the appropriate laser generator variety for each application.

The main properties of laser radiation and its applications. Table 1.1.

Laser beam proprieties	Heat treatments	Welding	Hole processing	Cutting	Holography	Measure-ments	Alloying	Electronics
Coherence	X	X	X	X	X			X

Directionality	X	X	X	X		X		X
High intensity	X	X	X	X	X			X
Monochromaticity						X	X	X
Small divergence	X	X	X	X	X	X	X	X
Efficiency	X	X	X	X				
Active medium	Ruby, Glass Nd, YAG-Nd, CO_2-N_2-He				He-Ne-Argon Ruby YAG-Nd	He-Ne	He-Ne	Argon Krypton

Laser systems operate within the domain of the electromagnetic spectrum, emitting radiations that span the visible spectrum and extend into the infrared and ultraviolet wavelength regions (Fig. 1.3).

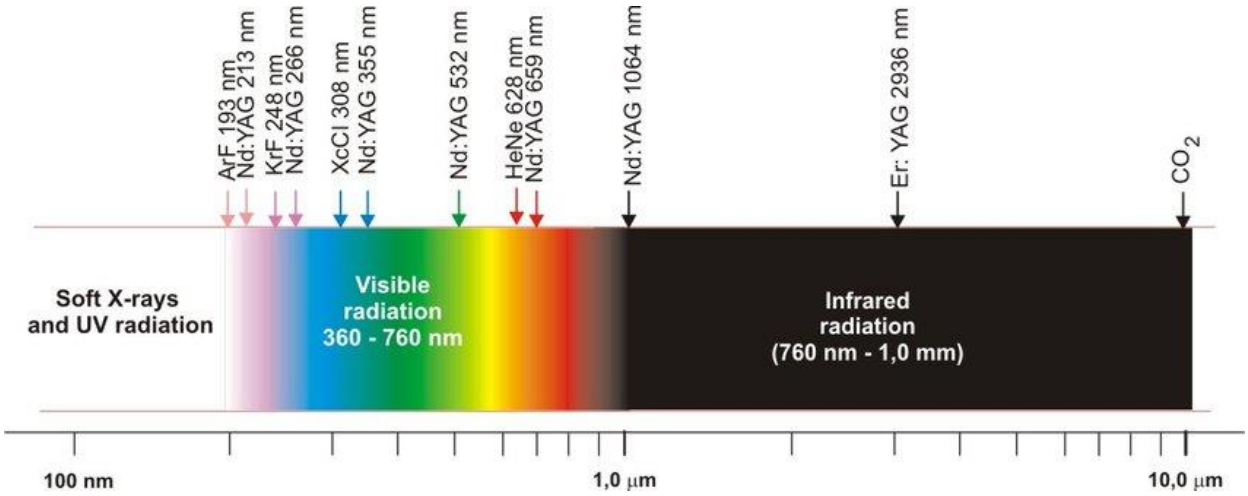

Figure 1.3. Electromagnetic spectrum [MAR08].

The main proprieties of the laser beam are coherency, collimation and monochromatic properties.

Coherency

Coherence of a laser beam is the property of its constituent light waves to maintain a constant and fixed phase relationship over time and space. The coherence arises from the underlying physics of stimulated emission and the coherent amplification process within the laser cavity.

In stimulated emission, when an incoming photon interacts with an excited atom, it triggers the emission of an identical photon. This process results in the creation of light waves that possess the same frequency and phase. As these waves propagate, they maintain their phase alignment, exhibiting a high degree of temporal and spatial correlation.

A source emits a series of light particles, known as quanta, with a specific coherence length. The coherence length refers to the distance traveled by a light source before experiencing changes in coherence. The coherence length, denoted as l_{coh} , is contingent upon both the wavelength, represented by λ, and the bandwidth, indicated as Δλ [ION05]:

$$l_{coh} = \frac{\lambda^2}{\Delta\lambda} \tag{1.2}$$

When the radiation source possesses a significantly broad bandwidth, it leads to a diminished coherence length, hence resulting in the absence of interference events. The coherence time can be defined as [AAF08]:

$$t_{coh} = \frac{l_{coh}}{c} \tag{1.3}$$

where is the speed of light.

The laser's ability to maintain coherence is very important in obtaining highly focused and narrow beams of light that allows processing of various materials.

Collimation

The collimation or directionality property of a laser beam is its ability to preserve an almost parallel and uniform distribution of light waves as it travels through space. In other words, a collimated laser beam does not disperse or diverge excessively as it travels, remaining focused across great distances.

This unique property is a consequence of the laser's design and the physics determining how laser light is generated. Using mirrors and the laser's active medium, light waves are tightly confined and aligned within a laser. This alignment ensures that the light waves exiting the laser stay arranged and coherent, resulting in minimal dispersion.

Due to the diffraction phenomenon, the laser beam must have a certain divergence, which, for most lasers, is extremely reduced (fig. 1.4.). Laser emission directionality depends on the way of achieving the stimulated light emission, on the wavelength λ and on the beam diameter d_f . The minimum divergence of the laser beam may be assessed with relation 1.4 [AAF08]:

$$\theta_{min} = \frac{1.22\lambda}{d_f} \tag{1.4}$$

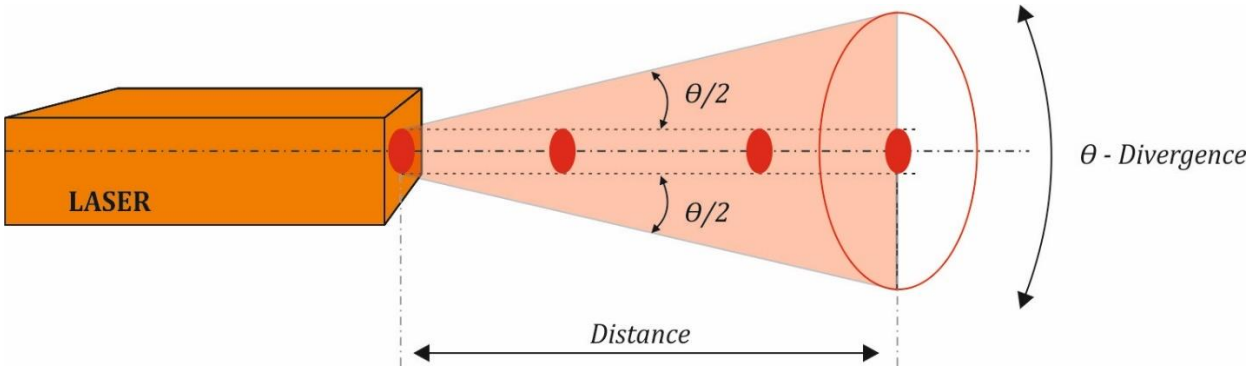

Figure 1.4. Divergence of a laser beam [AAF08].

Monochromaticity

Monochromaticity of a laser beam is the essential property of a laser to emit light at a single, precise wavelength or color. This characteristic is a direct result of the basic physics of stimulated emission in a laser system. The main phenomenon in laser generation, stimulated emission, assures that photons produced by stimulated emission have the same energy and, therefore, wavelength. This consistency is a result of the requirement that the photon emitted must have the same energy as the photon that initiated the emission. Therefore, the active medium of a laser, whether it is a solid, liquid, or gas, generates photons with a highly specific energy level, which corresponds directly to a specific wavelength.

Monochromaticity is given by Planck's [HEC17, HAN98]:

$$\nu_0 = \frac{E_2 - E_1}{h} \tag{1.5}$$

Monochromaticity depends on the characteristics of the resonant cavity and is connected to the fact that the stimulated emission takes place. The bandwidth $\Delta\nu_c$ of a resonant cavity is given by the relation:

$$\Delta\nu_c = \frac{c-(1-R)}{L} \tag{1.6}$$

while the bandwidth of the laser radiation $\Delta\nu_{osc}$ is much less:

$$\frac{\Delta\nu_{osc}}{\nu} = \frac{4h\cdot(\Delta\nu_c)^2}{P} \tag{1.7}$$

where P is the laser power, and h is the Planck's constant.

The spectral purity of laser radiation represents the ratio between radiation bandwidth and its frequency, according to relation:

$$s = \frac{\Delta\nu}{\nu} \tag{1.8}$$

Spectral purity is determined by the stimulated emission phenomenon, which requires induced photons to possess the same properties as inductive photons. The photons emitted are initially spontaneous photons that occupy the entire range of energy levels. The essential function is played by the resonant cavity, which, based on the natural transition width, selects and amplifies certain characteristic frequencies.

The distance between two such cavity resonant frequencies or modes can be expressed as follows:

$$\Delta\nu_i = \nu_{i+1} - \nu_i = \frac{c}{2L} \tag{1.9}$$

where c is the speed of light and L is the distance between the resonant cavity mirrors.

This emission of photons at a single wavelength contrast with traditional light sources, such as incandescent bulbs and fluorescent lights, in which photons are emitted across a diverse spectrum of wavelengths. The monochromatic nature of laser light is a fundamental property that allows for its wide range of industrial applications.

1.2 LASER beam parameters

1.2.1 Laser wavelength

The wavelength of a laser is the length of a single cycle of the electromagnetic wave and is measured in units of nanometers (nm). Depending of the laser type the emitted light is at different wavelengths and have a high influence on the material that is being processed.

The interaction between the laser beam and the material is influenced by the material's optical properties and the laser's wavelength. When incident laser radiation is directed onto a metallic material, three phenomena occur: some of the radiation is reflected from the material's surface (ρ), some is absorbed by the material (α), and some passes through the material (τ) [WIE08]. Equations 1.10 – 1.11 establish the ratio of how the values of the laser radiation flux parameters change.

$$(\rho) = \frac{Reflected\ radiation}{Incident\ radiation}\ (0 \leq \rho \geq 1) \tag{1.10}$$

$$(\beta) = \frac{Absorbed\ radiation}{Incident\ radiation}\ (0 \leq \beta \geq 1) \tag{1.11}$$

$$(\tau) = \frac{Transmited\ radiation}{Incident\ radiation}\ (0 \leq \tau \geq 1) \tag{1.12}$$

Absorption is a key factor in laser welding, as it determines how much of the laser energy is absorbed by the material. This absorbed energy is then converted into heat, which melts and fuses the material. The absorption of the electromagnetic radiation in a material follows the Beer-Lambert law, given by

$$I(z) = I_0 \cdot e^{-\beta z} \tag{1.13}$$

where I(z) is the intensity at z depth, Io is the incident radiation, β is the absorption coefficient influenced by the medium, radiation wavelength, and intensity. Laser radiation consists of electric (E) and magnetic fields (H). When it meets charged particles, like electrons of the material, it induces them a motion through the electric force from the electric field, E. If the laser radiation's frequency doesn't match the particle's natural vibration, no light is emitted or absorbed. Instead, a forced movement and vibration of particle occurs. This interaction, namely "inverse bremsstrahlung," involves photons being absorbed in by free or bound electrons. These vibrating electrons can either radiate again (reflected and transmitted light) or their motion can be restricted by the material's structure, turning the energy into heat. Phonons make the structure vibrate, and this heat transfer is governed by Fourier's laws of heat conduction. With enough absorbed energy, molecular bonding stretches, causing melting. Further heating leads to molecular vibrations that weaken bonding, resulting in evaporation. The vapor can still absorb radiation but not very effectively, as it only has bound electrons. If the absorption is strong enough, the electrons break free, and the vapor turns into a plasma.

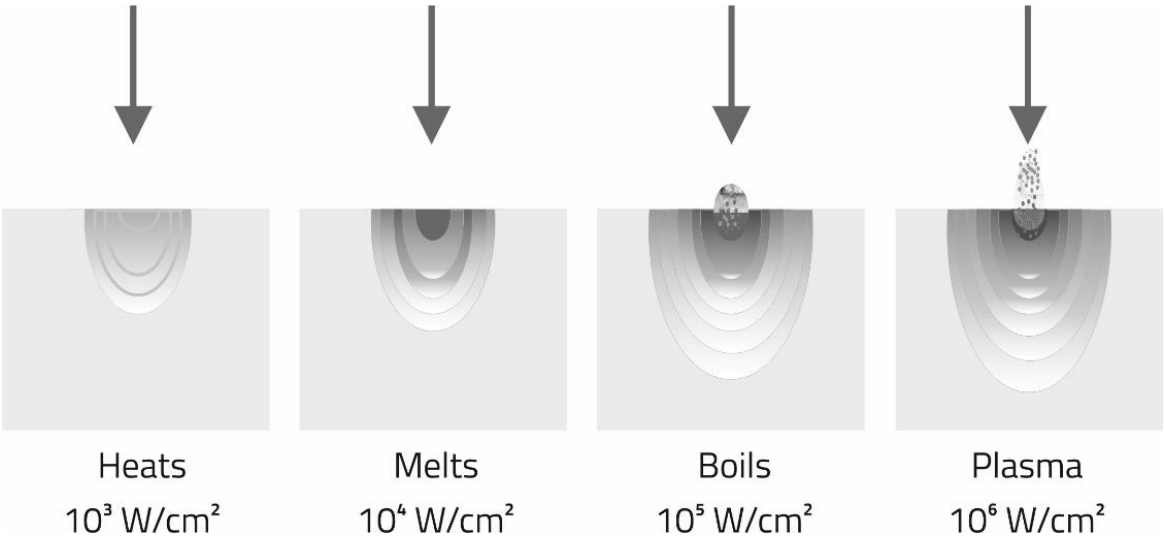

Figure 1.5 Phenomena during absorption

Besides absorption, reflectivity of materials plays a crucial role in laser processing. A wide range of materials exhibit a high coefficient of reflection when exposed to longer wavelengths.

The optical characteristics of metals at a wavelength of 1060 nm are shown in Table 1.2 [TOY05]. It should be noted that optical properties are temperature-dependent. The smaller the wavelength of photons, the easier they are absorbed into the surface of metallic materials. The photon population density increases with temperature, so at higher temperatures increase the possibility of interaction between electrons and the material.

Optical proprieties of materials Table 1.2

Material	k	n
Al	8.50	1.75
Cu	6.93	0.15
Fe	4.44	3.81
Ni	5.26	2.62
Pb	5.40	1.41
Ti	4.00	3.80
Zn	3.48	2.88
Glass	0.10	0.50

1.2.2 Laser power density

The laser power density, or irradiance, is the most important parameter in laser processing because it is a measure of the amount of laser power (energy per unit time) delivered per unit area of the laser spot diameter. Analytically, the laser power density (P) can be expressed as:

$$Pd = \frac{P}{A}[W/m^2] \quad (1.14)$$

Where:

- Pd is the laser power density.
- P is the total optical power of the laser beam (W).
- A is the area of laser spot cross-section (m^2).

Consequently, the laser power density is dependent on the diameter of the laser beam. A small laser spot will increase the power density delivered to the surface of the material, which will influence the laser-material interaction phenomena. The power density is crucial in processes such as laser heat treatment, cladding, and welding because it determines the material melting rate, heat affected zone, and overall process quality.

The laser spot diameters often employed for welding typically range from 0.3mm to 1mm, whereas for laser cladding, the range is typically 1mm to 3mm, depending on the specific

method utilized. Heat treatments can be conducted utilizing spot sizes ranging from 1 to 5 mm.

Considering a laser beam with a flat top shape, table 1.3 shows the laser power density of a 1kW continuous laser with a laser spot diameter of 0.4mm vs. a 0.8 mm.

Laser power density of a 1kW CW laser with 0.8 and 0.4 laser spot diameter. Table 1.3

0.8 mm laser spot	0.4 mm laser spot
Laser cross section area = $\pi * (R)^2$	Laser cross section area = $\pi * (R)^2$
Radius = Diameter / 2 = 0.8 mm / 2 = 0.4 mm = 0.0004 meters	Radius = Diameter / 2 = 0.4 mm / 2 = 0.2 mm = 0.0002 meters
Area = $\pi * (0.0004\ m)^2 = 5.026 \times 10^{-7}$ meters^2	Area = $\pi * (0.0002\ m)^2 = 1.256 \times 10^{-7}$ meters^2
Power density = Laser power / Laser area	Power density = Laser power / Laser area
Pd = 1000 W / 5.026×10^{-7} m² = 1.98×10^6 W/m²	Pd = 1000 W / 1.256×10^{-7} m² = 7.95×10^6 W/m²
Pd = 1.98×10^6 W/m² * 0.0001 = 0.198 kW/cm²	Pd = 7.95×10^6 W/m² * 0.0001 = 0.795 kW/cm²

In addition to laser power density, the duration of laser-material interaction has major significance. The interaction time in case of a continuous wave (CW) laser is directly correlated with the speed at which laser processing is made.

The interaction time when using pulsed lasers is determined by the duration of the individual laser pulses. Each pulse is characterized by its pulse width or pulse duration, and the overall process is influenced by the laser power density of each pulse, the pulse repetition rate, and, of course, the processing speed.

In this case, the laser power density of a 1kW pulsed laser with a laser spot diameter of 0.8mm and a pulse duration of 0.5 ms will be:

Laser power density of a 1kW pulsed laser with pulse duration of 0.5 ms. Table 1.4

0.8 mm laser spot	0.4 mm laser spot
Laser cross section area = $\pi * (R)^2$	Laser cross section area = $\pi * (R)^2$
Radius = Diameter / 2 = 0.8 mm / 2 = 0.4 mm = 0.0004 meters	Radius = Diameter / 2 = 0.4 mm / 2 = 0.2 mm = 0.0002 meters
Area = $\pi * (0.0004\ m)^2 = 5.0265 \times 10^{-7}$ meters^2	Area = $\pi * (0.0002\ m)^2 = 1.256 \times 10^{-7}$ meters^2
Pulse energy = Average Power [W] * Pulse Width [s]	Pulse energy = Average Power [W] * Pulse Width [s]
Energy per Pulse = 1000 W * 0.005 s = 5 Joules	Energy per Pulse = 1000 W * 0.005 s = 5 Joules
Pulse power density = Pulse laser power / Laser area	Pulse power density = Pulse laser power / Laser area
Pd = 5 J / 5.026×10^{-7} m² = 9.94×10^6 W/m²	Pd = 5 J / 1.256×10^{-7} m² = 3.98×10^7 W/m²
Pd = 9.94×10^6 W/m² * 0.0001 = 0.99 kW/cm²	Pd = 3.98×10^7 * 0.0001 = 3.98 kW/cm²

The table shows the power density of each pulse without considering the repetition rate. If we add the repetition rate, the results will be:

Laser power density of a 1kW pulsed laser with pulse duration of 0.5 ms and 10Hz. Table 1.5

0.8 mm laser spot	**0.4 mm laser spot**
Laser cross section area = $\pi * (R)^2$	Laser cross section area = $\pi * (R)^2$
Radius = Diameter / 2 = 0.8 mm / 2 = 0.4 mm = 0.0004 meters	Radius = Diameter / 2 = 0.4 mm / 2 = 0.2 mm = 0.0002 meters
Area = $\pi * (0.0004\ m)^2 \approx 5.0265 \times 10^{-7}$ meters^2	Area = $\pi * (0.0002\ m)^2 \approx 1.256 \times 10^{-7}$ meters^2
Pulse energy = Average Power [W] * Pulse Width [s]	Pulse energy = Average Power [W] * Pulse Width [s]
Energy per Pulse = 1000 W * 0.005 s = 5 Joules	Energy per Pulse = 1000 W * 0.005 s = 5 Joules
Laser power [W] = Energy per Pulse [J] * Repetition Rate [Hz] = 5 J * 10 Hz = 50 W	Laser power [W] = Energy per Pulse [J] * Repetition Rate [Hz] = 5 J * 10 Hz = 50 W
Power density = Laser power / Laser area	Power density = Laser power / Laser area
Pd = 50 W / 5.026×10^{-7} m² = 9.94×10^7 W/m²	Pd = 50 W / 1.256×10^{-7} m² = 3.98×10^8 W/m²
Pd = 9.94×10^6 W/m² * 0.0001 = 9.94 kW/cm²	Pd = 3.98×10^8 W/m² * 0.0001 = 39.8 kW/cm²

1.2.3 Laser pulse shape

Pulsed lasers release light in short optical pulses, compared with continuous lasers that emit an uninterrupted beam of light. Therefore, in case of the pulsed lasers, the light is emitted as a pulse with a precise pulse duration or pulse width. Each pulse is formed by a certain number of photons and, depending of the laser type, the number of photons can be realised as pulses in the range of milliseconds up to pulses in the range of femtoseconds (10^{-15} second or 1/1000 picosecond). This characteristic of the pulsed lasers is very important being the key factor that influence the interaction between the laser and material.

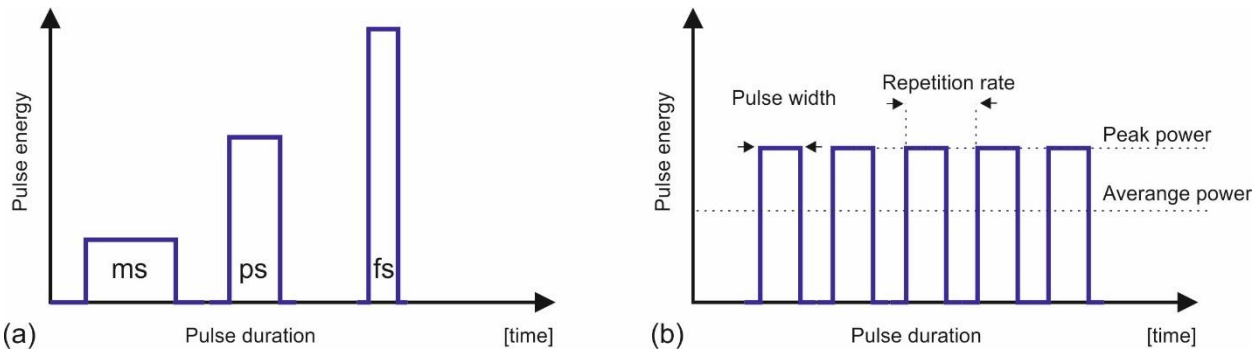

Figure1.6 a) Non scale representation of laser pulses, b) ideal rectangular pulse train.

The average power of the pulsed lasers is calculated by multiplying the number of pulses (Pn) with the pulse's energy (Pe) divided on the time of pulses (t).

$$P_{averange} = \frac{Pn \cdot Pe}{t} \tag{1.15}$$

$$R = \frac{Pn}{t} \tag{1.16}$$

and therefore

$$P_{averange} = R \cdot Pe \tag{1.17}$$

where R is the repetition rate.

At a constant pulse energy, the average power will increase proportionally with the repetition rate.

Processing with pulsed lasers involve more parameters that needs to be set up but also increased control over the laser-material interaction. Laser average power, pulse width and repetition rate determine the amount of energy that is absorbed into the material. Another important key factor of pulsed laser beam is that the pulse duration can be modulated in order to fine tune the distribution of power over the pulse duration. This modulation can be also a decisive factor that influence the material heating, melting or ablation during the laser processing. Figure 1.7 shows the most common type of *pulse geometry*:

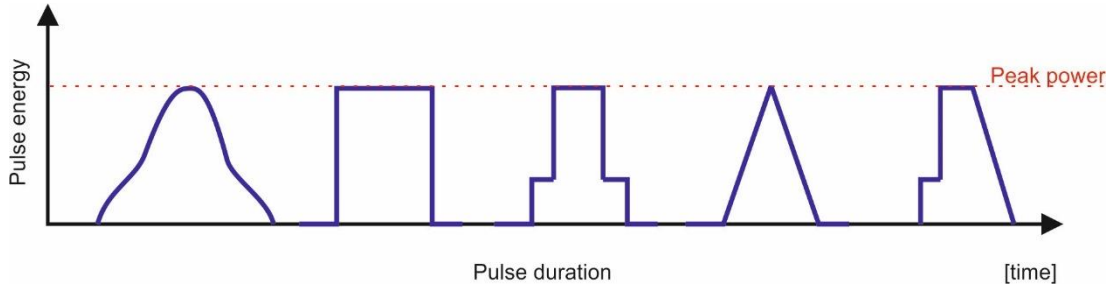

Figure 1.7 Various *pulse geometry* used for materials processing

1.2.4 Laser focal distance and deep of focus

The laser focal distance and depth of field/focus are interdependent parameters, and very important in laser processing by determining the energy density on the material surface and the positioning of the laser focus related to the material. Both parameters are key factors when utilizing low-power lasers, where maximizing the utilization of available power for material processing is mandatory and obtaining the smallest laser spot diameter is desirable. The spot diameter is influenced by various factors, such us the type of laser, the quality of the laser beam, and the focusing optics. As illustrated in Figure 1.8, a short focal length results in

a smaller laser spot diameter. If a larger focal length is used than a proportional increasing of the laser spot diameter will occur. It is a basic physics principle but is very important for laser welding of materials. A larger depth of field allows for higher tolerance in the distance between the focusing optics and the material. This is advantageous in welding application when a high distance between (500 – 1500 mm) the welding head and material are desired due to positioning / access limitations. Also, a higher focusing distance and a high depth of field can be advantageous in situations where there are variations in the material surface or when working with irregular shapes.

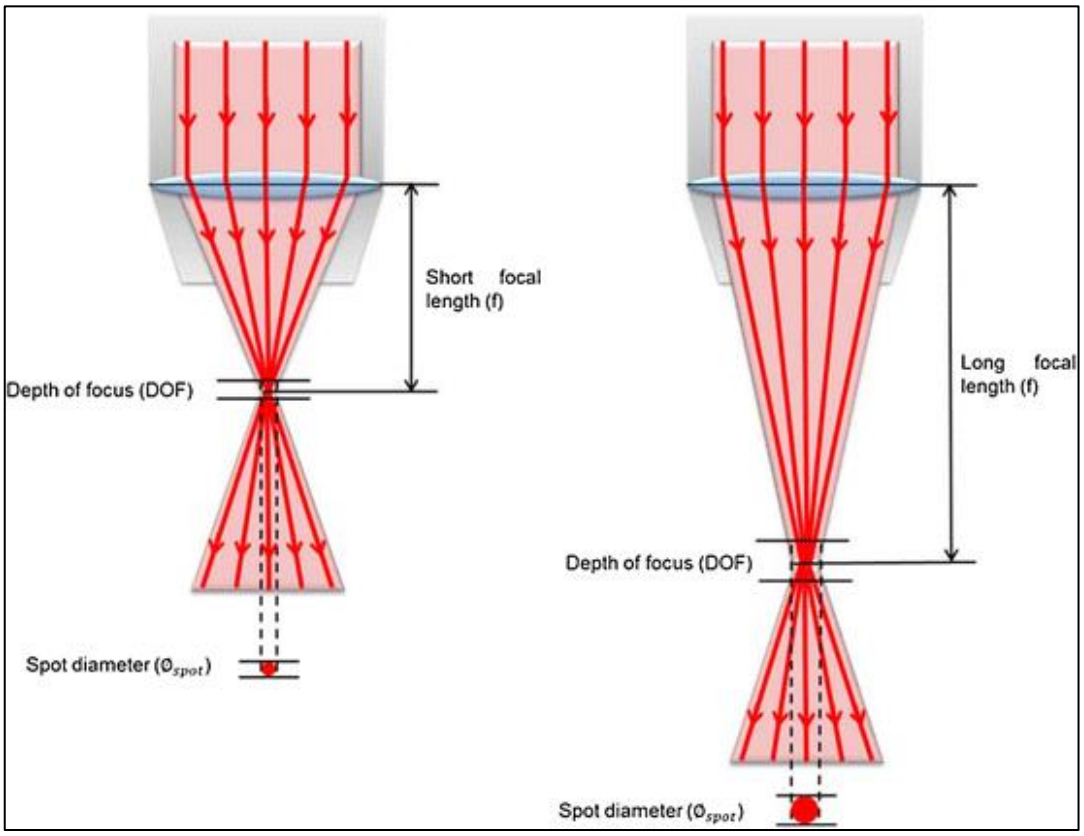

Figure 1.8 Laser spot diameter and deep of focus as different focal length [MAR17].

Attention should be paid to focal length because a very large depth of field can diminish the energy density, affecting the efficiency of material processing. In applications where precision is important, a smaller depth of field and a small laser spot is used to maintain a concentrated and well-defined interaction zone, but it is a solution only for thin materials. In case of thicker material, a higher focal distance and focal depth is required to welding or cutting the material.

CHAPTER 2. DIFFERENT PROCESSES, SAME THERMAL SOURCE: LASER BEAM

Lasers have emerged as cutting-edge tools in materials processing and are now in direct competition with conventional methods for operations such as cutting, welding, heat treatment, and surface alloying. The unique characteristics of laser beams have introduced a higher degree of precision and repeatability into material processing applications when compared to traditional techniques. In industrial engineering, lasers find their primary application in laser cutting, closely followed by laser marking. These applications have evolved and are well-established technologies within the field of materials processing. As presented in figure 2.2, laser cutting stands out as the most widely utilized laser application in the industry.

On the other hand, laser welding, additive manufacturing, heat treatment, and surface processing represent more intricate operations that continue to be subjects of active research. Researchers are dedicated to defining the optimal techniques and parameters for these processes.

The primary objective of this Habilitation thesis is to address certain knowledge gaps within the domain of laser welding and surface processing and to expand the current understanding of laser welding techniques and surface processing methodologies.

To achieve this objective, the thesis presents various research studies in the field of laser processing for industrial applications, conducted primarily at the Advanced Welding Eco-Technologies Research Center, situated at the research facilities of Transilvania University of Brasov.

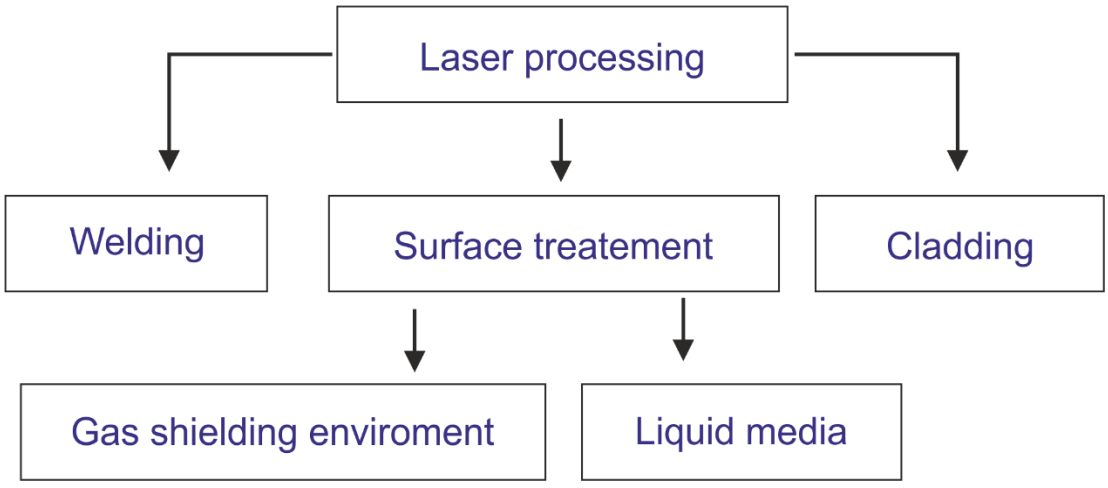

Figure 2.1. Laser processes that are addressed in this Habilitation thesis.

2.1. Laser welding

2.1.1 Techniques and principles

Laser welding of metallic materials represents a special category within the broader spectrum of fusion welding techniques. In contrast to conventional joining methods, which often exhibit inherent drawbacks such as heightened stress and strain resulting from continuous heat input, variability in welding quality depending on the operator's skill, reduced overall efficiency, and limited applicability to thin plates, laser welding has emerged as a compelling solution poised to address the challenges of the 21st century in the field of joining processes.

Among the various laser processing techniques, in 2020 welding ranks fourth in terms of its prevalence in the industrial laser beam applications, as depicted in Figure 2.2. The thermal energy delivered by the laser beam offers the capacity to concentrate significant energy onto small surfaces, facilitating the creation of narrow and deep welds. Furthermore, this method delivers high productivity and process repeatability, all while eliminating the need for physical contact between the workpiece and the welding head.

To obtains a quality welded joint, two distinct challenges arise:

1. Ensuring the precise alignment between the pieces to be welded.
2. Ensuring the precise alignment between the pieces and the laser head or, more specifically, the laser beam itself.

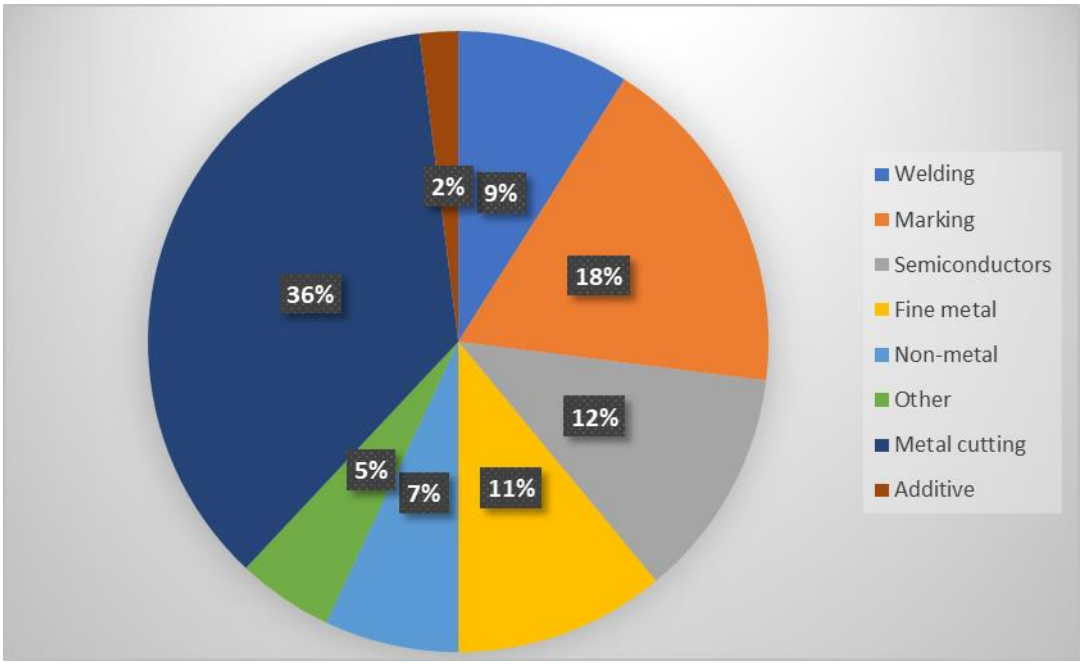

Figure 2.2 Utilisation of laser for industrial application [***LAS].

Laser beam welding can be done in two main ways: continuously or in a pulsed manner. In this process, the laser beam is directed at the material's interface, where it is absorbed, but not totally. Phenomena of reflection and diffraction plays an important role in the process.
Commonly, protection of the melted metal pool is made using an inert gas introduced through the laser welding head. A diagram illustrating the laser welding process is shown in Figure 2.3.

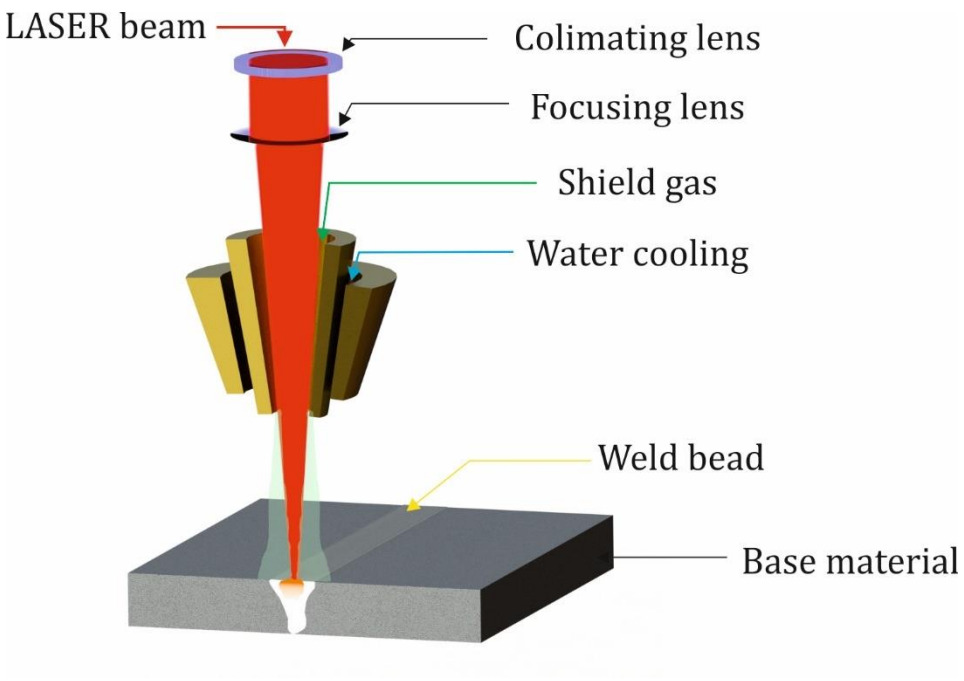

Figure 2.3 3D schematic representation of the laser welding principle.

The choice between welding with or without filler material depends on the type of material and its thickness. For materials with high thickness or grooved sides, or in cases of dissimilar joints that present metallurgical compatibility challenges, filler material in the form of wire or powder may be used to fill gaps. Using filler material provides more flexibility in positioning the base materials and closing gaps between components.
Regarding the positioning of the laser beam relative to the workpieces, several notable orientations exist: horizontal plane welding, vertical plane welding with lateral movement (left-right), movement from top to bottom, from bottom to top, and overhead welding. These orientations result in different characteristics in the flow of the weld pool. When welding workpieces with complex shapes that are in motion, these basic welding positions can be combined.
The laser welding process can be carried out either continuously or in pulses. Laser radiation is absorbed at the material interface, and protecting the molten metal pool involves introducing an inert gas through the laser welding head. Depending on the specific application

and the thickness of the components, protection of the molten pool can also be achieved by directing the flow of gas laterally. The root of the seam can be shielded by manipulating the gas flow within the component-holding device.

Optimizing welding parameters depends on the irradiation mode in relation to the nature and thickness of the workpiece material. Irradiation can occur either continuously or in pulses. Typically, the welding speed and the distance between the laser welding head and the workpiece remain constant throughout the process. Focusing can be directed towards the surface of the workpieces or within the material itself. In addition to ensuring sufficient penetration, it is crucial to prevent workpiece deformation during welding. Workpiece deformation could lead to significant fluctuations in thermal flux density at the workpiece surface, potentially compromising the welding process.

2.1.2 Conduction welding

Laser conduction welding can be achieved in two ways: direct heating and energy transfer. In direct heating, the materials surface absorbs the laser energy, and then the energy conducts inside the material, as the name "conduction mode welding." This type of welding can be realised using relatively low laser beam intensity. During the conduction welding process, semi-spherical welding bead and a nearby heat-affected zone are formed similarly to conventional processes like electrical arc welding. This method is particularly useful for thinner materials or when full penetration is not needed. The welding process occurs quickly, influencing the joint geometry and resulting in fine granulation with improved mechanical properties. Continuous welding, can be achieved by overlapping welding spots or by using a continuous wave beam and it is suitable for materials that absorb infrared radiation, where the laser energy creates a melted layer, leading to the formation of a welded joint upon solidification.

One of the advantages of laser welding is the ability to change the welding types, such as from conduction to keyhole welding, depending on the laser beam power density and duration respectively, the laser welding speed. Both welding types, conduction and keyhole welding can be achieved by using continuous wave lasers or pulsed ones. Continuous welding offers high productivity and faster welding speed compared to pulse welding.

In conduction welding mode, there is one condition; it is required that the material surface temperature to exceed the melting temperature but not reach the vaporization temperature.

The optimal parameters for conduction welding vary for different materials and trials must be done in order to determine when conduction welding changes into keyhole welding.
Despite some initial limitations, the conduction welding process has some advantages. It has better stability and heat control, and it can be used instead of keyhole and conventional welding. Large spot diameters laser beam in this mode reduces the problems created by components misalignments, and the laser system doesn't demand high beam quality. Weld without pores and splashes can be obtained in conduction welding mode.

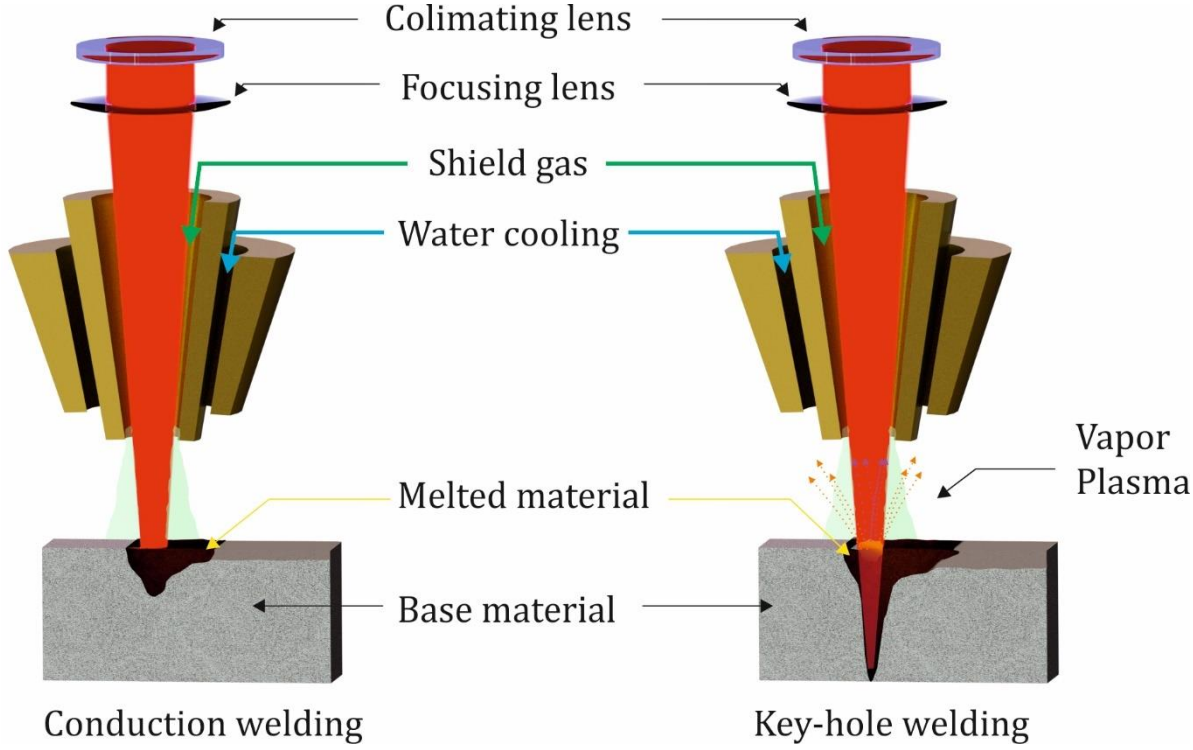

Figure 2.4 3D representation of the laser welding process in a) conduction mode and b) key-hole mode.

The main disadvantage of the conduction welding process is the limited penetration depth, especially in case of processing reflective materials. The process efficiency, which measures how much laser energy is absorbed by the material, is lower in conduction mode compared to keyhole mode. The laser materials interaction phenomena depend on multiple conditions and therefore the point when conduction mode ends and keyhole welding starts is not precisely defined, but it generally occurs when the laser power is not sufficient to cause boiling or when vaporization is insignificant. Figure 2.4 shows the schematic of conduction and the keyhole mode.

2.1.3 Keyhole laser welding

The keyhole laser welding it differs significantly from conduction welding. The keyhole mode welding relies on achieving a high-power density, causing the formation of a void / hole similar in appearance with a 'keyhole' in the material. In this mode, the laser beam penetrates the material with such intensity that it creates a localized cavity, or keyhole, within the molten pool. This keyhole is mainly a vapor-filled void surrounded by molten material. The high power density causes rapid evaporation of the material, and the resulting pressure creates the keyhole. One important factor in the keyhole welding process is achieving a power density sufficient to cause boiling in the molten pool. This leads to the creation of the keyhole and enables the laser beam to penetrate deeply into the material. The power density required for keyhole welding is typically higher than that used in conduction welding.

The boundary between conduction and keyhole it generally occurs when the power density surpasses a certain threshold, often considered to be around 10^6 W/cm^2. This value is heavily used in literature as the minimum power density at which the laser welding can be done. It is not always correct because this value is independent of welding speed or beam diameter. Moreover, in case of laser processing / welding besides laser power is very important the material absorption / reflection factor which influence the occurrence of boiling or vaporization of the material.

Keyhole laser welding has several advantages, such as deeper penetration compared to conduction welding. The high-power density allows for the creation of a well-defined keyhole, resulting in a more profound weld. This mode is particularly useful for thicker materials or when strong weld penetration is required.

In keyhole welding mode, attention should be paid to process parameters as excessive power density can lead to instability and ununiform keyhole formation. In the same time, the process is more sensitive to the reflective properties of the material, as higher reflectivity can reduce the absorption of laser energy and make keyhole formation more difficult.

2.2 Laser welding in scientific research

Nowadays, the laser welding offers a versatile and precise method for joining materials, particularly in applications requiring high precision, such as microelectronics, medicine, and aerospace. It provides advantages in terms of weld quality and the ability to create welds

unattainable through conventional welding methods. However, successful laser welding requires careful consideration of factors like material characteristics, temperature control, and process parameters to maintain the optimal balance of energy input and output. Researchers continue to explore and optimize laser welding processes to unlock its full potential in various industrial applications. Laser welding is suitable for welding various iron-based steels, stainless steels, and nonferrous alloys.

One of the topics addressed by this habitation thesis is laser welding in similar and dissimilar configuration. My experience in this topic starts in 2010 and continue to be a key focus area in my current research this subchapter been a lead-in into the topic of stainless-steel welding in similar and dissimilar joint configuration.

Laser welding of stainless steel

In the latest years, stainless steel has become one of the most used alloys in areas where corrosion resistance is a vital material performance. Laser welding is commonly used in the automotive industry to join stainless steel components, offering high precision and speed, making it suitable for producing various structural components as well as in aircraft and aerospace applications due to its corrosion resistance and strength. In the medical field, stainless steel is a preferred material because of its biocompatibility and resistance to corrosion. Laser welding is a precise technique for assembling surgical instruments, implantable devices, and medical equipment. It ensures the highest quality and reliability standards are met.

The family of stainless-steel grades is large including austenitic, ferritic, martensitic and duplex steels and among them, several grades are preferred for utilization in industry and a special attention is paid for weldability of this steels. Thus, austenitic steels have the best impact resistance qualities at low temperatures and the maximum resistance at high temperatures, whereas martensitic steels are the hardest at room temperature. Stainless steels have a variety of mechanical qualities that, together with their high corrosion resistance, make them design-universal for engineering [FOL88]. Austenitic grades like AISI 304, 308, 316, and 321 are preferred for various applications requiring welded joints.

These grades are versatile and widely used for creating durable welded joints in medicine or in industries such as chemical, food, and construction. The choice of stainless-steel grades,

especially austenitic ones, plays a vital role in ensuring the reliability of welded structures across diverse sectors.

As a consequence, austenitic stainless steels such as AISI 316 and AISI 321 have become the subject of numerous studies exploring material behaviour during laser welding in order to identify the optimal parameters and welding set-ups.

It is important to note that the laser joining method for stainless steel can be done in two different wave modes: continuous mode for welding joints with a high thickness and pulsed mode for thinner parts where precise control of the energy is very important.

Continuous laser welding of AISI 317, a preferred choice owing to its superior corrosion resistance compared to AISI 316 and AISI 321, was made in a recent study by Ceyhun Kose [CEY22]. He obtained good welded joints using AISI 317 of 3mm sheets on which applied a PWHT that increased the ductility and impact toughness.

For thicker materials, such as AISI 316 LN with a thickness of 11mm, alternative techniques can be used. Pavan et al. [PAV23] successfully employed a hybrid process involving laser beam and MIG welding to achieve optimal results. In this context, precise alignment between the laser beam and the MIG torch was determined as been a critical factor. Through the utilization of Hybrid Laser Welding (HLW), a high joint efficiency of 101% was attained for AISI 316 LN, as reported by Pavan.

When dealing with thicker materials, various welding techniques can be used, including hybrid welding, preheating, post-heating treatments, and welding assisted by vibration, among others. Conversely, the welding of thin sheets using lasers presents a more intricate challenge. One of the primary concerns is the rapid cooling of the welded bead and the potential for root burnout. These issues have been addressed through optimization of process parameters and the utilization of pulsed lasers.

The mechanism underlying pulsed welding seams, characterized by low residual stress, robust mechanical properties, and an aesthetically pleasing appearance, relies on a well-balanced sequence of high-energy pulses. These pulses are precisely defined by their pulse energy and density, as highlighted in the literature [PEI21, CHL21, KUM17].

Nevertheless, pulsed welding is susceptible to thermal cracking due to rapid cooling. In response to this issue, Zhang et al. [PEI21] use a novel approach involving the modelling of pulse shapes to control over the crystallization process during the cooling phase. Laser-welded structures are prone to residual stress and strain due to the thermal expansion coefficient and relatively low heat conductivity of stainless steel in the 300 series. Shenghong

et al. [SHE22] investigated the effects of oscillating laser beam characteristics, such as amplitude and frequency, on residual stress in 316 stainless steel using Goldak's double-ellipsoidal finite element technique.

While stainless steel is primarily selected for its exceptional corrosion resistance properties, the research on austenitic stainless steels have revealed that the corrosion resistance performance in the heat-affected zone (HAZ) is affected by laser heat input [JIA22]. It is noteworthy that the choice of shielding gas can also have a high influence on the hardness of laser beam-welded (LBW) specimens. Suman et al. [SUM19] have reported lower hardness values when using argon as a shielding gas. Furthermore, for LBW seams, the width of the joint is mainly influenced by laser power, while the pulse width assumes a main role in determining the ultimate strength of 316 stainless steel [KUM17].

To date, there has been a many reports and studies on stainless steel welding; however, the comprehensive exploration of process parameters for pulsed beams remains a relatively understudied domain. The overall quality of welding outcomes is dependent upon a of various factors, including the fine variations in process parameters.

Laser welding of heterogenous materials

It is known that the most processable and less time-consuming process to assembly two components is by welding but challenges arise if the materials are not similar. In recent years, there has been an increase of investigations conducted in the field of heterogeneous welding, with a specific focus on its utilization within industrial applications. The laser technology has allowed the emergence of heterogeneous weldings between materials that have matching melting and vaporization temperatures. Heterogeneous joints, characterized by a combination of various materials, are widely used in various applications to avoid the use of costly materials such as stainless steel. The development of various material combinations for welded structures has been motivated by economic and environmental factors. In order to attain optimal performance of these welded joints, it is imperative to use appropriate welding techniques that effectively mitigate potential challenges, including the formation of nonhomogeneous regions within the fusion zone, the development of brittle layers accompanied with increased internal stresses, and the presence of secondary phases, among various other factors.

Nowadays, laser welding is the best technology to be used for dissimilar welding due to high concentration of energy and the high welding speed. With those two characteristics the high-quality welding joints of stainless steel, titanium, copper, aluminium in various combination has become possible. From economic reasons a high interest is addressed in welding of stainless steel with carbon steel, usually known as black and white joints [IOD11, IOR10] being commonly used in the fabrication of chemical installations, power generating installations, and are also prevalent in the petrochemical, nuclear, and automotive sectors [MIS14, LIP05, KLI07]. Depending on the chemical composition of the steel and stainless-steel type at the in case of heterogenous joints a diffusion area with a distinct chemical composition from both the base materials and the weld can be formed in the fusion zone [IIS10] [STA14]. In case of welding dissimilar materials that include two different steels, there is a carbon diffusion phenomenon to the material with a higher content of alloying elements, where carbon exhibits a strong affinity. Consequently, at the interface with the alloyed steel, carbon increases, leading to the formation of carbides at the grain boundaries. This weakens the cohesion of the metallic matrix and promotes inter-crystalline corrosion. Therefore, it is essential to control carbon diffusion and limit the dilution effect. Laser welding proves advantageous in this regard as it reduces the size of diffusion areas due to the high concentration of linear energy.

Furthermore, in the case of stainless steel, chromium precipitation on the grain boundaries can be mitigated by utilizing a high laser welding speed, which decrease the weld bead exposure to high temperatures [LOK09, LIM05, YAN10].

In my experience, structural and operational key factors in heterogenous joints, are variation in alloying elements, surface reflectivity, heat conductivity rate, and thermal expansion coefficients of the base materials. Of course, in conjunction with the process parameters, which have the main influence on the welding process. All these factors have been investigated and reported in the literature. According to Khan et al. [KRK12], the factors that influence the weld bead geometry in dissimilar laser welding of AISI 304 and AISI 340 stainless steel include laser power and incident beam angle. A welding in black and white configuration (laser spot welds between low carbon and austenitic stainless steels) was successfully conducted by Torkamany, obtaining positive results in terms of tensile-shear monotonic loading [TOR12]. Baghjari et al. [BAG14] reports on a more difficult research, defect free welding of AISI 420 stainless steel to kovar alloy while reducing hot crack development in the weld zone.

Mousavi achieved favourable outcomes in the laser welding of AISI 321 and AISI 630 stainless steels, employing a circular butt weld configuration [AKB09]. Anawa revealed improvements in the mechanical properties of ferritic/austenitic (F/A) joints by employing monitored experimental settings regarding laser power [ANA08]. In term of dissimilar laser welding of stainless steel, valuable research was present by Kose C. [KOS22] showing that AISI 904L super austenitic stainless steel can be successfully weld with AISI 317L. In depth characterisation using EBSD electron microscopy analyses revealed that content of γ grains increased after a post weld heat treatment was applied and their direction chanced in the [101] and [001] direction after compared with [111] and [101] in as welded condition. As effect was determined an increasing of toughness while the tensile strength and resistance to bending decrease. As indicated in the literature an additional factor that should be considered for the stainless steel-carbon steel welded joints, respectively the fast cooling. Due to the fast cooling of the metal bath, which can cause an incomplete δ-γ transformation [JOH05, YGZ10, ARI11, KHA12], delta ferrite phase is possible to be formed with a negative impact on the corrosion resistance of the weld bead. Moreover, delta ferrite phase is more susceptible to grain boundary corrosion as the material thickness decreases.

2.3 Laser surface engineering: Methods and applications

As previously stated, laser surface treatment, in addition to laser welding and cutting, is a new technology of surface engineering used to improve material properties such as corrosion resistance, hardness, wear and friction behavior, heat resistance, surface strength, and so on. There are several techniques in surface engineering that involve laser beams, all of which been used to increase the component lifespan, to recondition or to improve overall surface tribological features can be used with a continuous or pulsed laser beam, but all are based on one of the following 3 principle:

I. Laser surface engineering by adding a material.

II. Laser surface engineering by removal the base material.

III. Laser surface engineering without changing the surface topography.

All three processes offer versatile solutions for surface engineering and can comply with specific application requirements across various industries. The choice of technique depends on the desired surface properties and the proprieties of the material being processed.

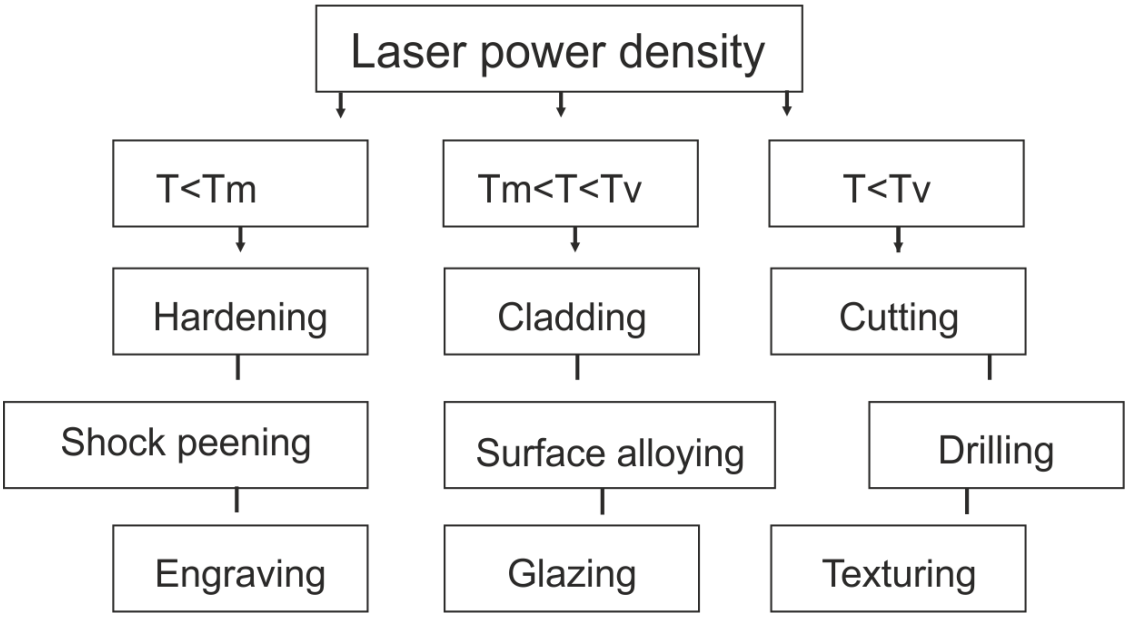

Figure 2.5 Laser surface processing depending on the surface temperature [ANA20]

The main important factors that influence all the laser processing methods are the laser power density and the laser-surface interaction time. Depending on that, surface melting or vaporisation will emerge or not. If the temperature at the surface (T) is lower than the materials melting temperature (Tm) then surface topology will not be changed and only subsurface solid-state transformation will appear as for the heat treatment processing, hardening or engraving. If the temperature is higher enough then melting or vaporisation (Tv) of the surface will occur. Laser cladding, glazing or surface alloying need a superficial melting of the surface and cutting, drilling or surface texturing need the material vaporisation. A special case is represented by the laser shock processing where surface topography is changed due to mechanical action of the laser pulse but without melting.

2.3.1 Laser caldding

Laser cladding is a modern technique of deposition in which the laser beam is used as thermal source and a cladding material in form of powder is melted on the surface of the base material. Metallurgical bonding is obtained by superficially melting and mixing with the substrate [PAS16]. The filler material can be in the form of powder and feeded coaxially or of-axis with the laser beam, or the powder can be preplaced on the material surface in the form of a paste. Also, prior the laser melting, the powder cand be preplaced by using another spraying process like thermal spraying.

Nowadays, the laser cladding with coaxial powder injection is the best technology available for reconditioning or to enhancing of new surfaces. Even if the laser cladding is the best techniques to apply a coating with superior tribological characteristic, the process is dependent on the numerous process and set-up parameters.

As presented in the figure 2.6, the overall quality of the cladded layer is a result of the matching of various parameters that are the subject of ongoing research in the community of coatings researchers. Parameters like laser power [YON23, YAX23], pulse duration [ZHE21], repetition rate [WEI23], powder feed rate [LON23], cladding speed [HUL21], beam profile [XIN24] are investigated and optimised in scientific studies.

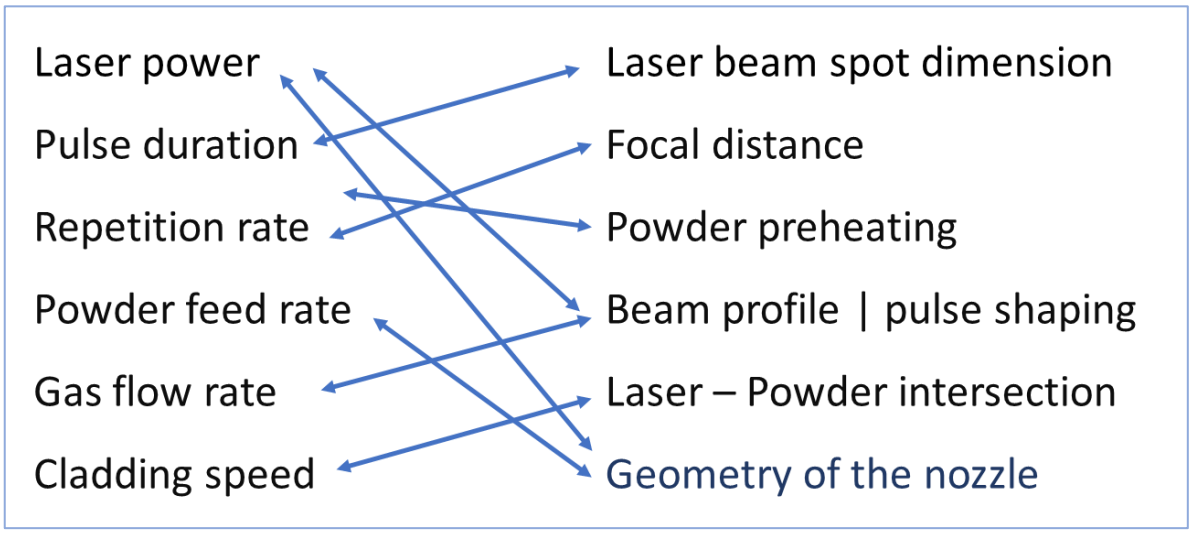

Figure 2.6 Interdependence of laser cladding process parameters [PAS22].

Not on the last, the cladding nozzle, respectively the angle of the feeding powder has a major influence in the case of coaxial laser cladding. Usually, the coaxial powder injection can be realised at angles between 15 and 40 degrees. As I and my colleagues presented at the ICIR International Conference [PAS22] in 2022, the laser cladding head can completely change the shape of the cladded layer. Figure 2.7 presents a case study realised using 20-, 25- and 32-degree cladding nozzles. Each cladding has a different geometry of the sprayed powder which will interact differently with the laser beam.

Depending on the nozzle angle a different interaction between the powder and the laser beam will be employed. In each case, the focal point of the laser can be positioned in the same spot with the power, above the intersection tip of the powder steam of below the intersection point of the injected powder. Moreover, besides the point of intersection between the powder and the laser beam, an important parameter is the relative position of that point related with base material surface.

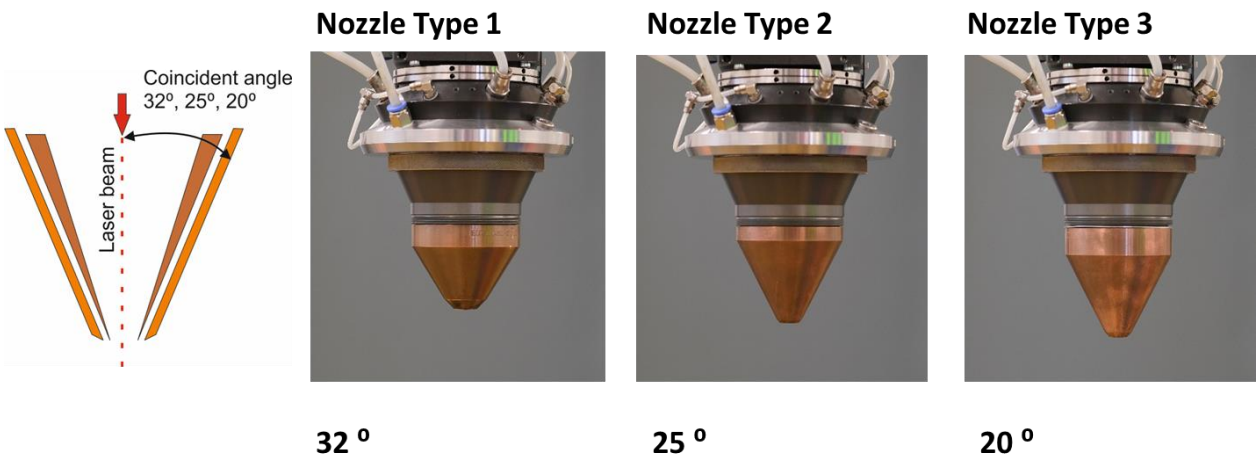

Figure 2.7 Examples of different cladding heads. Precitec WC 50, focal lens 200 mm [Center for Advanced Eco-Technologies at UNITBV Research Facilities] [PAS22].

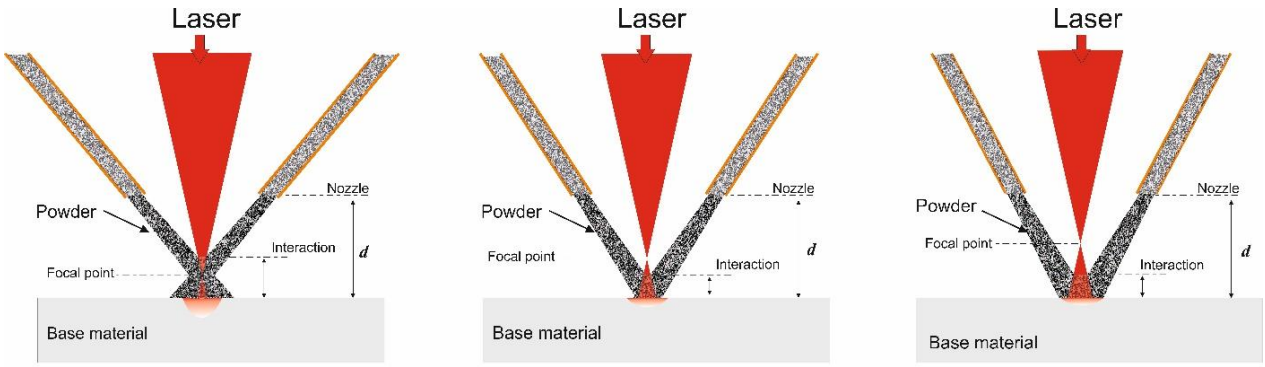

Figure 2.8 Schematic representation of laser beam – powder steam intersection area at 32-, 25- and 20-degree [PAS22].

The angle of the cladding unit influences the shape of the powder steam and also the area and location of the intersection point between the laser beam and the powder. It is an important parameter because this will further influence the quantity of the melted powder, the quantity of the absorbed and reflected of the laser beam. Depending on the intersection point the laser beam will have a different power density because of the variable radius of the beam as illustrated in figure 2.8.

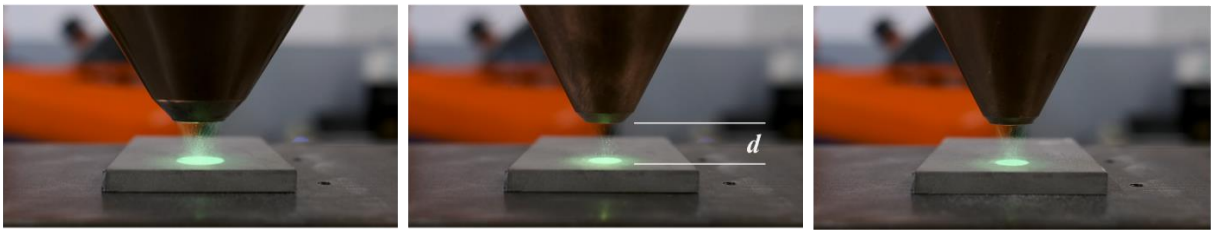

Figure 2.9 Powder spraying geometry at 32-, 25- and 20-degree. Stand-of distance, d=11mm; [Center for Advanced Welding Eco-Technologies at UNITBV Research Facilities].

This is important in controlling the geometry of the cladded laser and also the dilution of the cladding with the base material. This variable of the technological set-up was investigated using a Ni-based powder and three co-axial cladding units with 20-, 25- and 32-degree angle of powder injection. The set-up was completed using a 1kW continuous laser and a robotic arm, the powder being feed et by a designed powder feeder (Therematec). Nichel based powder with chemical composition of Ni17Cr2.5B4Fe4Si0.5C and S235 low carbon steel of 8 mm have been used for the experiments.

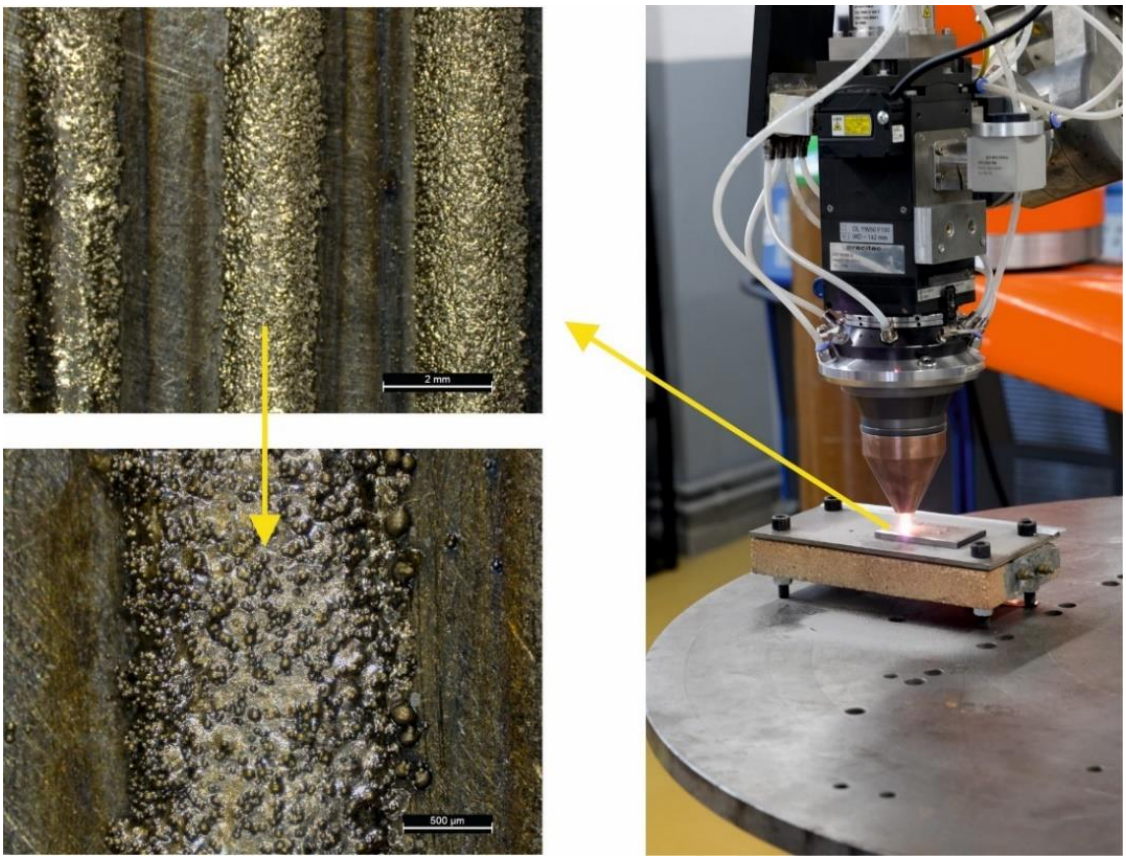

Figure 2.10 Experimental frame used for testing various cladding units and the general appearance of the cladded track. Stand-of distance, d=11mm. [Center for Advanced Welding Eco-Technologies at UNITBV Research Facilities] [PAS22].

Figure 2.10 presents the experimental set-up and the macro appearance of the cladded tracks which have been fabricated using different cladding units.

By the carrying out of multiple tests with different parameters, it was determined that the control of the powder injection angle has the potential to influence the rate of dilution. The cross-section of two cladded track obtained with similar parameters reveal that dilution is mainly affected by the cladding unit, respectively 32-degree vs 20–degree the angle.

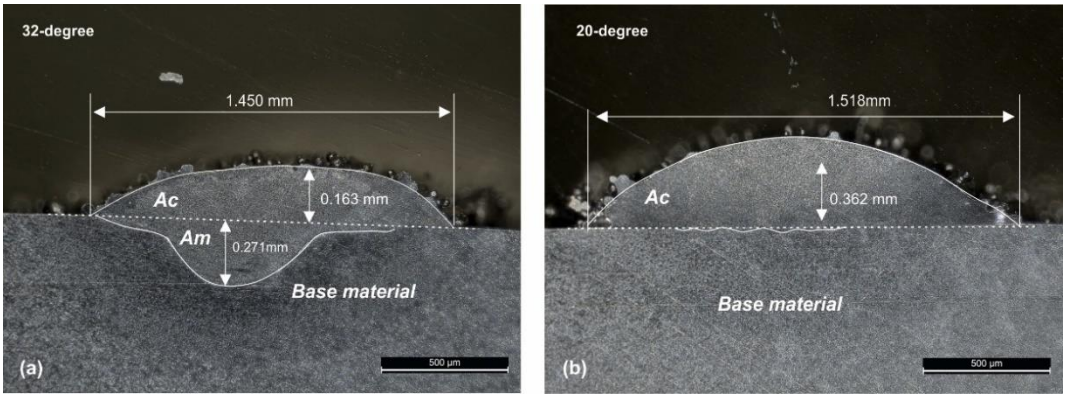

Figure 2.11 Examples of how the cladding head angle can influence the dilution. Laser power 800W, cladding speed 25 cm/min, (a) 32°-degree angle of powder injection and (b) 20°-degree angle of powder injection [PAS22].

Dilution in case of coatings is defined as:

$$Dilution(areas\ ratio) = \frac{A_m}{A_m + A_c} \tag{2.1}$$

Where Am is the melted area and the Ac is the cladded area as depicted in figure 2.11. The main difference between the two tracks is the melted area of the base material that indicate a high dilution with the cladded material. This is not desired in the laser cladding processes because a high degree of dilution between materials means that diffusion phenomena of chemical elements of the substrate into the cladded layer will occur.

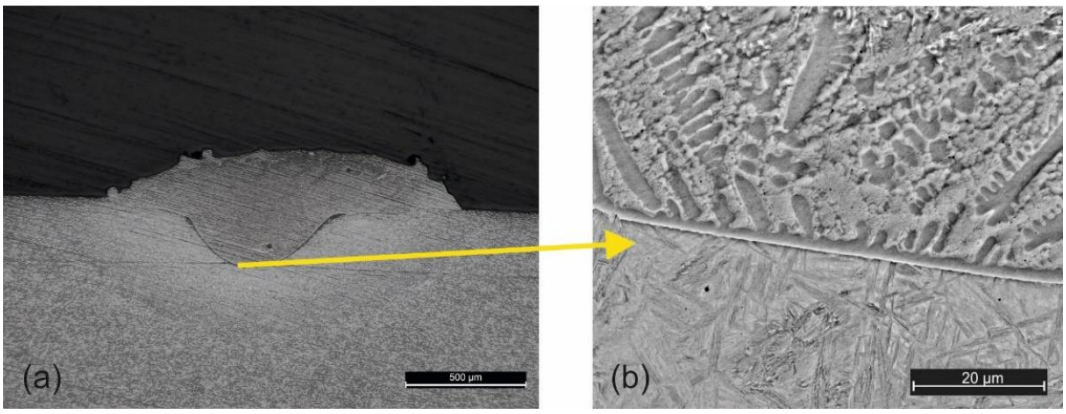

Figure 2.12 Detail view of the diffusion line [PAS22].

A high degree of diffusion will negatively impact the mechanical proprieties of the cladded material, eg. low hardness, chemical resistance of wear resistance of the coating.

The negative effects resulting from a significant dilution encountered as a result of increased power density are illustrated in figure 2.12, which indicates the presence of a diffusion boundary between materials. The observed separation line is a distinct dendritic structure that serves as a boundary between the substrate and the cladded layer. This separation line is most

evident in the case of the sample which was produced using cladding head no. 1 (fig. 2.7 and 2.8).

This highlights that the laser cladding process is significantly influenced by the process parameters and the configuration of the laser cladding set-up, since the cladding head /nozzle can impact both the geometry of the cladding layer and mechanical proprieties.

According to my observations, the utilization of a nozzle with a low incidence angle, specifically categorized 15 - 20 degrees, has the potential to produce coatings of superior quality.

Powders

In addition to process parameters, the selection of materials significantly impacts the quality of the cladded layer, therefore playing a critical role in achieving a superior result. One major advantage of the laser cladding process is its capability to utilize a wide range of alloyed powders, including those with commercially available compositions or specifically designed recipes.

Typically, powders ranging from 10 to 100 μm in size, based primarily on iron, nickel, or cobalt, are commonly utilized for cladding processes in order to enhance corrosion resistance, wear resistance, or achieve high levels of hardness. Powders consisting of pure compositions of nickel (Ni), aluminum (Al), titanium (Ti), and cobalt (Co) are often used as matrices for hard phases, such as zirconia or tungsten carbide (WC).

Due to its versatility, the cladding process with powders is used in various applications that request special materials with good proprieties in term of erosion, cavitation, abrasion, corrosion, heat resistance etc [PAS17]. Finding new alloys and adapting the process parameters to various conditions imposed by the advanced materials is a continuous quest in the scientific research. In a detailed study Zhang et al. [ZHA23] optimise the process parameters to control the dilution of 15-5PH alloy on U75V pearlitic steel during the laser cladding. In this particular case the increased dilution was beneficial due to the strengthening effect of diffused carbon into the cladding. Increased hardness and wear resistance was declared. Downside of higher dilution is the increased cracking susceptibility. Wei at al. [WEI23] limit the dilution percent for Co-based and Ni-based alloys on 1Cr12 substrate and obtain 5.4 % and 3.1 % dilution rate for NiCrMoNb+WC and Stellite 6 respectively. Good corrosion resistance and tribological results were obtained. The general opinion among numerous studies is that achieving a high-quality coating requires a precise alignment of materials, process parameters, and set-up.

An effective approach presented in several study papers is to use a ductile matrix and a hard phase in order to increase the wear resistance. The disadvantage of this combination is that the soft material and the carbides have different thermal expansion rates, which increases the cracking susceptibility of the deposited layer. Farahmand and al. [PAR14] have use an inductive heating for laser cladding of Ni-60%WC onto carbon steel as a solution for the reducing of cracks. In the same study was revelated that addition of nano-WC particles and La_2O_3 can increase the homogeneity and refine the microstructure of the coating. Laser cladding assisted by inductive heating is an option to reduce the cracking but increased heating can damage the WC. In order to mitigate the dissolution of WC particles in the melted bath, Wang et al. [WAN17] conducted a study on the effect of process parameters on the integrity of WC particles. They identified three mechanisms of dissolution-diffusion-precipitation of WC particles during laser irradiation and concluded that a higher cladding speed is advantageous in reducing the negative impacts on WC particles. Another way for reducing cracking susceptibility and preserving the WC particle integrity is to precisely tune the soft matrix in order to promote the encapsulation of the hard phases. In a recent study Guo et al [GUO23] design a new class of cladding alloy based on a soft Co matrix and a hard Co one reinforced with WC particles. For cladding of Co-5wt%WC alloy on Inconel 718 base material was added 5, 10, and 15 wt% Cu as supplementary soft matrix. The results highlights that a certain amount of Cu acts like a solid lubrifiant increasing the wear behaviour room temperature and CuO reduce the friction at high temperatures, 600°C.

A particular method studied at Center for Advanced Eco-Technologies at UNITBV Research Facilities [HUL21] is to use a distinctive blend of WC-Co with NiCrBSi and NiAl compositions. The addition of NiAl into the blend is expected to enhance the bonding capacity between the material and the substrate. Consequently, this original adaptation allows the use of a lower laser density, which prevent the damaging of WC particle.

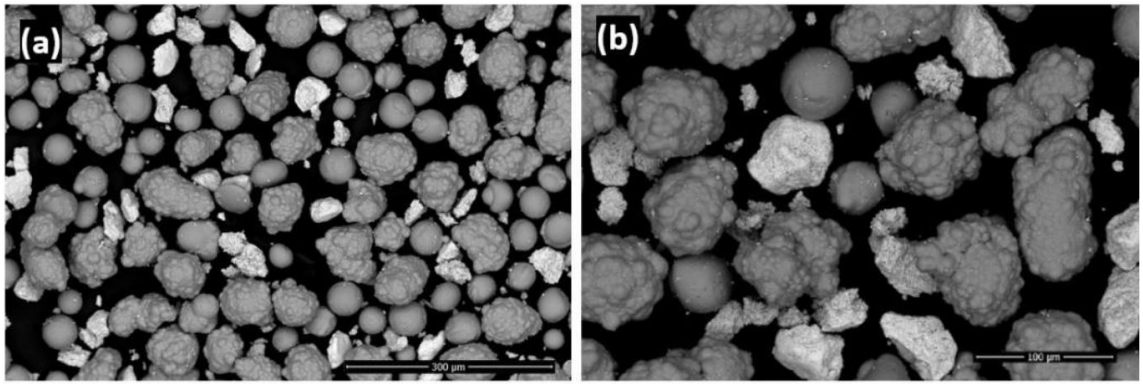

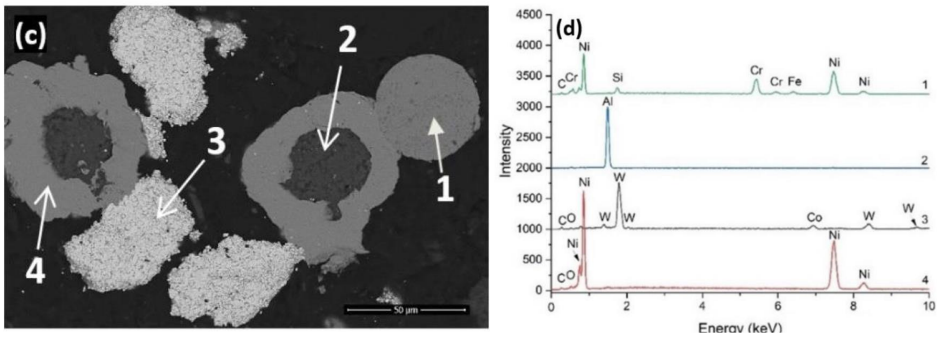

Figure 2.13 Detailed analysis of METCO 439 NS powder, a and b general appearance, c) cross-section of the particle, d) EDS microanalysis of each particle [HUL21].

Commercial powder Metco 439 NS (table 2.1) alloyed with NiAl was used as coating material on AISI 5140 steel substrate for determination of optimal preheating temperature and cladding speed. Figure 2.13 shows the electron microscopy of the mixed powder composed form of WC-Co/NiCrBSi/NiAl and the EDS microanalyses of each particle cross-section sowing uniform geometry and distribution of the WC-Co within the powder.

Chemical composition of the powder Table 2.1

Chemical compozition	WC-12Co	Ni	Al	Cr	B	Fe	Si	C
Element [%]	50	balance	2.8	5.8	1.3	1.4	1.4	0.3

Continuous diode laser coupled with a PRECITEC YC50 were employed for fabricating single cladded tracks and overlapped ones using variable cladding speeds. Substrate preheating at 320 °C was considered for a uniform thermal gradient during the cladding process.

As preliminary tests, 10 individual cladded tracks were made using laser power of 720 W, powder feed rate of 4g/min and linear increasing of cladding speed from 15 to 105 cm / min.

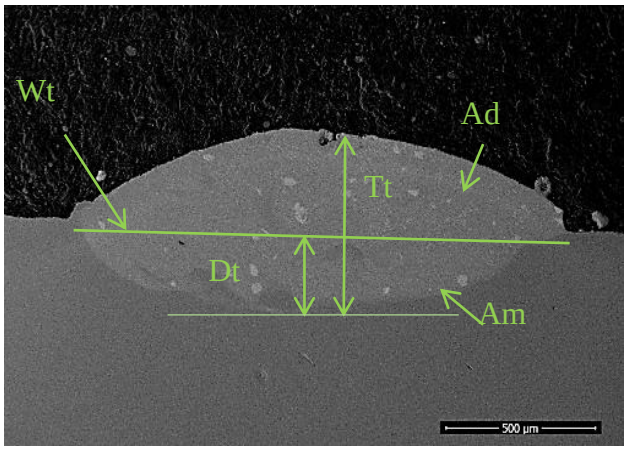

Figure 2.14 Back scattered electron micrograph of a laser cladded single track indicating the main geometrical dimensions [HUL21].

Figure 2.14 show the backscattered analyse of the sample no. 4 revealing a dense, defect-free coating with relatively uniform distribution of the hard phases. It can be observed that dilution is high being a direct consequence of the substrate preheating. Dilution rates between 38 and 56 % were obtained showing that cladding speed has a major impact on the melted area and on dilution phenomena. Although the high dilution rates, in the present case, it is advantageous in reducing the cracking susceptibility of the coating.

The second part of the study was conducted on partially overlapped tracks using the optimal process parameters window as determined for the single tracks. Table 2.2 summarise the parameters used for cladded tracks maintain the same experimental strategy, linear variation of the processing speed.

Laser cladding parameters Table 2.2

Parameter Coating	Power [W]	Cladding Speed [cm/min]	Energy Density [J/mm^2]	Powder Feeding [g/min]	T Preheat [°C]	Ar [L/min]
Coating 1	720	45	80	4	320	14
Coating 2		55	65.4			
Coating 3		65	55.3			
Coating 4		75	48			
Coating 5		85	42.3			

Five samples were fabricated using the same experimental frame. Dense, uniform cladded layers with reduced cracking susceptibility have been obtained using a 320 °C substrate preheating.

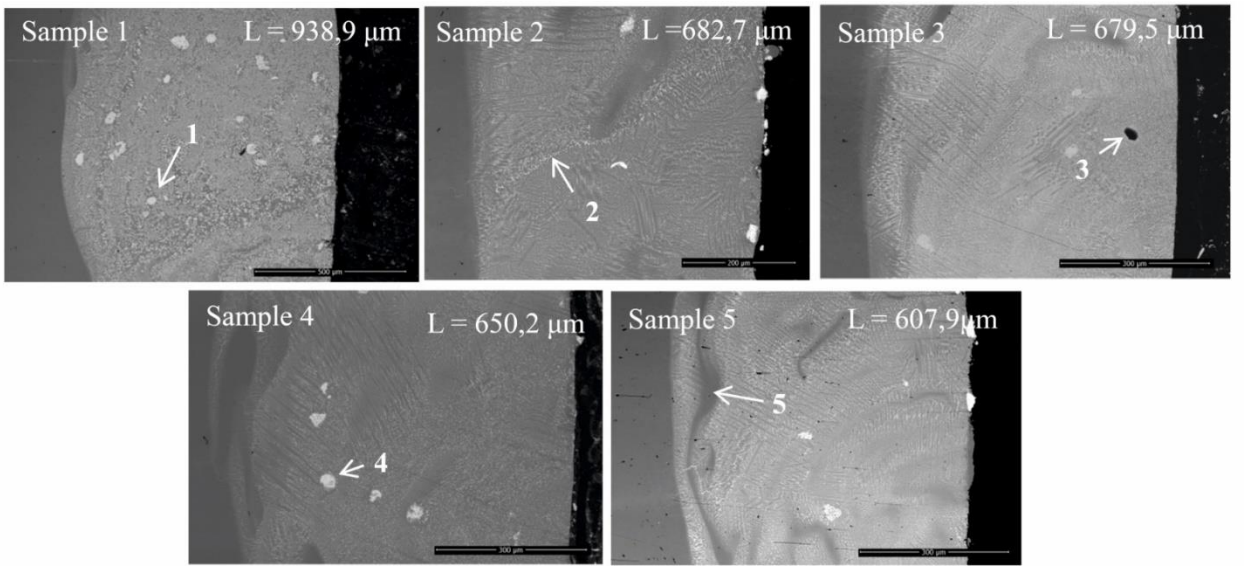

Figure 2.15 SEM micrographs of samples 1 to 5 [HUL21].

Figure 2.15 presents the cross section of samples 1 to 5 at various magnification highlighting dense coatings with good adherence to the substrate and without any visible cracks. Thickness between 607.9 μm and 938.9 μm were obtained and as expected, decreasing of the thickness occurred at higher speeds [HUL21].

The laser cladding process features high speed, fast melting and solidifying of materials, whereby the particles, when reaching the molten substrate, may undergo complete melting, partial melting, or remain in an unmelted state. In the cladded area (fig. 2.15), it can be observed WC phases that don't have complete melting or have only partially melted. The particles are dispersed in the entire cladded area. However, in the bottom region of the cladding, the agglomeration of WC phases is evident due to a higher density of these particles. The optimal laser cladding speeds are between 55 and 65 cm/min, which can give good melting of WC-Co particles as seen in the micrographs of Samples 2 and 3. Higher speeds above 65 cm/min will reduce the laser energy and will result in thinner cladded layer. As a result, the carbide-based particles do not have enough energy to melt, as seen in Figure 2.15, Sample 4.

The interface between overlapped cladding tracks (Sample 2) and certain pores (Sample 3) may be visible in several areas of the cladding layer. Darker regions as presented in the micrographs of Samples 4 and 5, are rich iron patches intermingled with the coating as a result of the vortex created by the laser beam during cladding.

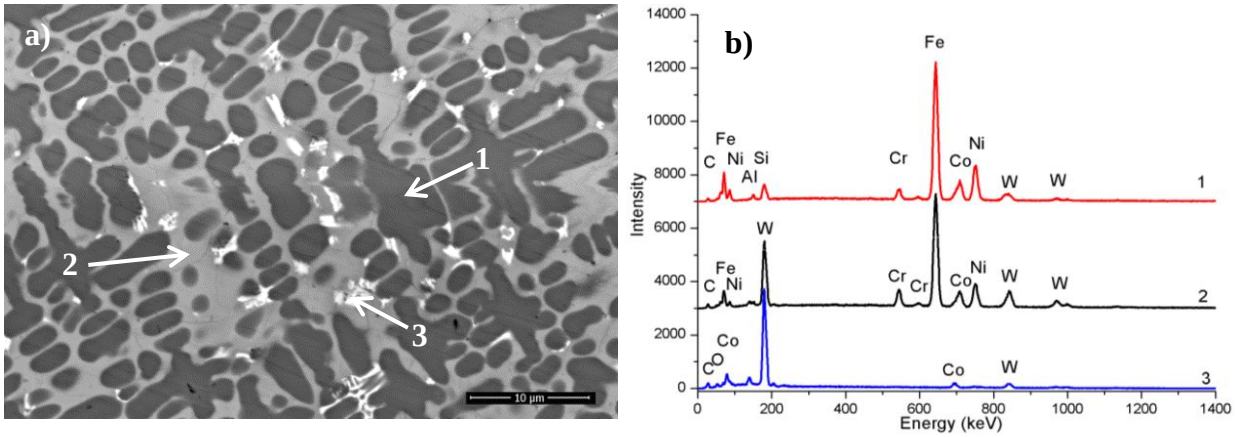

Figure 2.16 Microstructure of the sample 4 and the EDS analysis in the 1, 2 and 3 micro spots [HUL21].

The microstructure of the cladded layer is formed of dendrites with branch tree growth and an Ni rich eutectic matrix. Dendrites with a high concentration of Ni solid solution containing Cr, Fe, Co, and Si are surrounded by interdendritic zones with a high carbide content and Fe. The

diffusion of iron in the cladded coatings is expected to enhance the creation of coarse dendritic formations and impact their size and shape. The bright phases in the micrograph are mostly composed of tungsten carbide-rich areas, as corroborated by the EDS spectra shown in Figure 2.16.

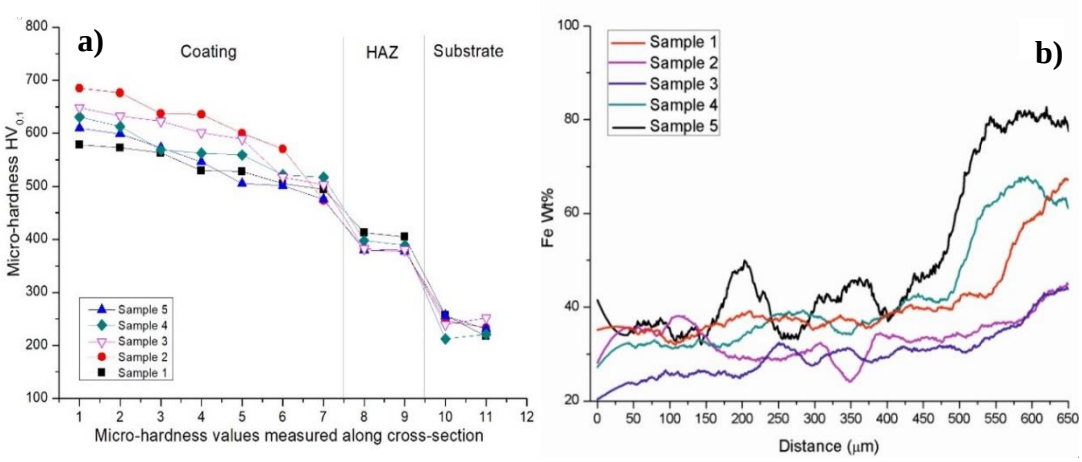

Figure 2.17. Microhardness measurements from top of the coating to the substrate (a) and Fe wt% content from top of the coatings to the substrate (b) [HUL21].

The cladded layers are characterised by a high hardness compared with the base material. Figure 2.17 shows the evolution of hardness depending on the process parameters, mainly the cladding speed for the partially overlapped tracks. It can be observed that for all samples the microhardess is decreasing closer to the interface with the base material and that sample 2 exhibits the higher microhardness. The result is in accordance with the EDS analyses of iron as depicted in the graph b from fig. 2.16 that shows a low amount of iron diffused for this sample [HUL21].

The study shows that cladding speed is an important element that influence the mechanical properties of the cladded material. At the same time, material has an important role in reducing the cracking susceptibility of alloys that include hard phases such as WC. Alloying with NiAl and applying a preheating temperature have been proved as good methods to further reduce the cracking susceptibility and to preserve the integrity of hard particles.

2.3.2 Laser texturing

In laser texturing the laser beam is used to induce ablation, melting or vaporization of a material from a solid surface, resulting in the modification of its topography through the formation of small holes, grooves, or irregular shapes. Laser surface texturing (LST) is a

technique used to enhance the adhesion, friction behaviour, and hydrophilic / hydrophobic properties of different surfaces, as well as to increase their compatibility for coating, claddings or painting applications. The process is highly dependent on various parameters but, among them, the

- Laser power,
- Pattern distribution / overlapping
- Geometry of each texture

are currently used to fine tuning the surface proprieties.

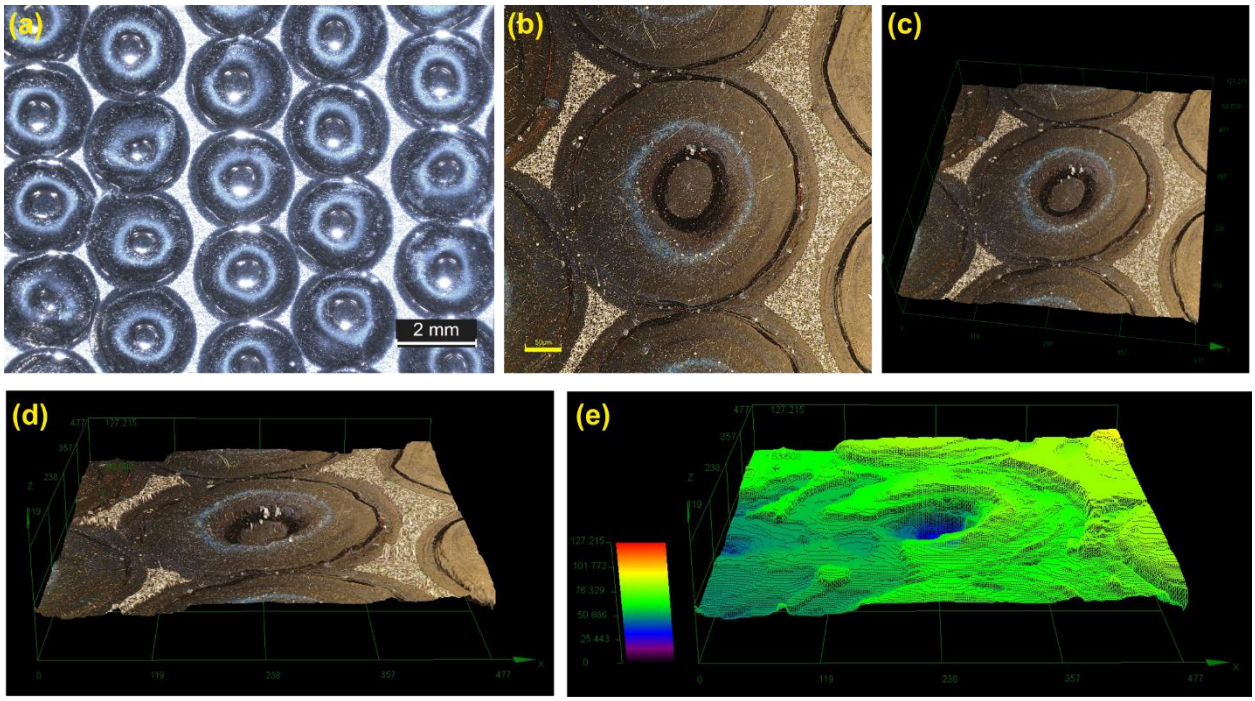

Figure 2.18 Macro texturing on stainless steel surface, a) top view of the textured surface, b), c), d) and e) 3D profile of the textured pattern.

Figure 2.18 presents an example of macro texturing realised at the Center for Advanced Welding Eco-Technologies within UNITBV Research Facilities with a pulsed laser at 10 kW peak power / pulse. This macro texturing, visible on the stainless-steel surface, exemplifies the capabilities of laser technology in creating distinct patterns and textures. Figure 2.18 shows how each laser pulse creates the specific round, *gaussian*, pattern on the material surface. These modifications are particularly relevant in industries where surface properties significantly impact performance. The texturing of materials surface can enhance adhesive bonding between various polymers and is the best solution to create weldings between metal and plastics. Nowadays the joining of metal with plastics is a must in order to produce

lightweight structures. Currently, metals can be successfully laser welded with plastics (PET) and texturing of the metal part is mandatory for increasing the adhesion strength by mechanical lock of the plastic into the texture of the metal part [MOL17]. Good results have been reported by Yanlong Luan [YAN23] for joining of AISI 304 with polyethylene terephthalate by using laser transmission welding and an overlapped geometry. He obtained good mechanical anchoring (35.26 MPa tensile strenght) of the PET in the stainless-steel plate by texturing grooves of 69µm depth and 21µm width.

Complementary, the laser micro texturing can be used for fine tuning the stainless-steel surfaces to obtain new proprieties such us hydrophobic or non-wetting surfaces [MOL22]. Figures 2.19 show an example of micro texturing of AISI 430 using an Nd: Fiber laser in the nanosecond range capable of repetition rate up to 1000 kHz. In this case an octagonal pattern was used for increasing of the surface area with various tribological application. The pattern was obtained by 40% overlapping each pulse to create a continuous ablation of the material in the desired geometry.

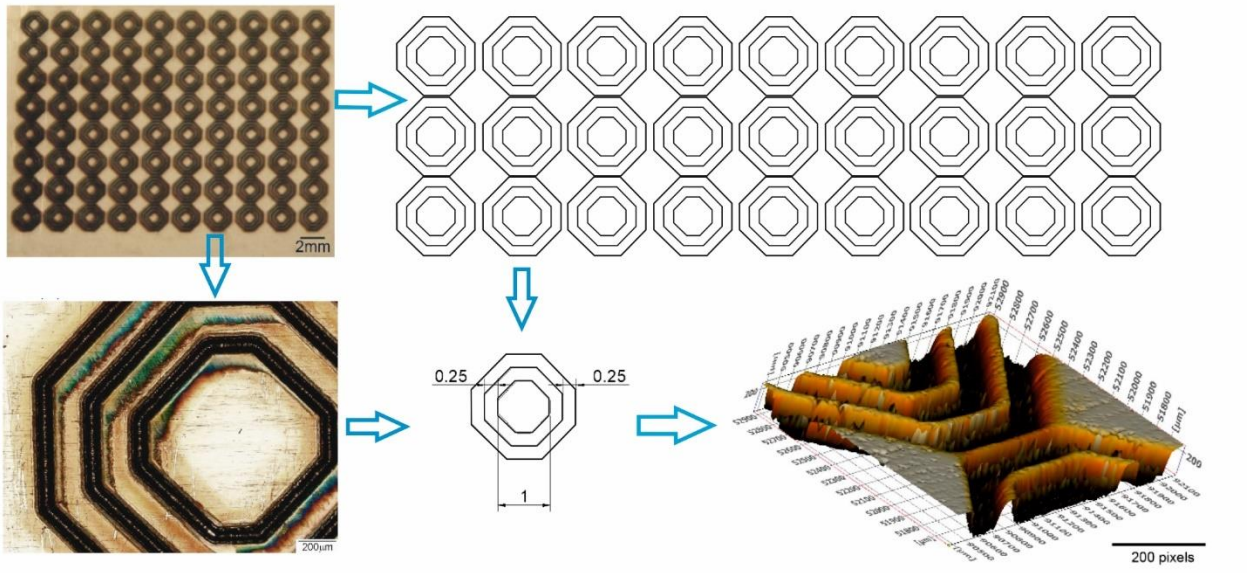

Figure 2.19 Micro texturing of AISI 430 using an octagonal pattern [MOL22].

It should be mentioned that for macro texturing are usually used pulsed lasers in the range of millisecond (fig. 2.18) with diameters of 500 to 1500 µm which can produce large texture on the material but also a heat affected area surrounding the processed surface, compared with the micro texturing that is realised with lasers within short pulse range of picoseconds or nanoseconds (fig.2.19) without thermal damaging of the surface.

2.3.3 Laser surface heat treatment

The heat treatment process, similar to other laser processes, has significantly altered the field of precision surface engineering by providing enhanced control onto the material properties and microstructural development.

Basically, the heat treatment is the simplest laser processing technique as the laser beam is focused on the material surface, leading to rapid localised and controlled heating, followed by controlled cooling. The heat transfer is governed by the inverse Bremsstrahlung effect. Precise temperature modulation may be achieved by changing the laser power and focus, allowing the modification of the material surface properties through grain refinement and phase transformations.

Nowadays the laser heat treatment is a wide term. The laser can be used for a variety of heating processes that allows engineers to obtain specific proprieties of metallic surfaces. Commonly, there are three main processes that use the laser as heating source: laser transformation hardening, annealing, and laser surface melting. The laser transformation hardening is the most used process and besides laser annealing do not involve changing of the material topography but only heating and cooling as depicted in fig. 2.20.

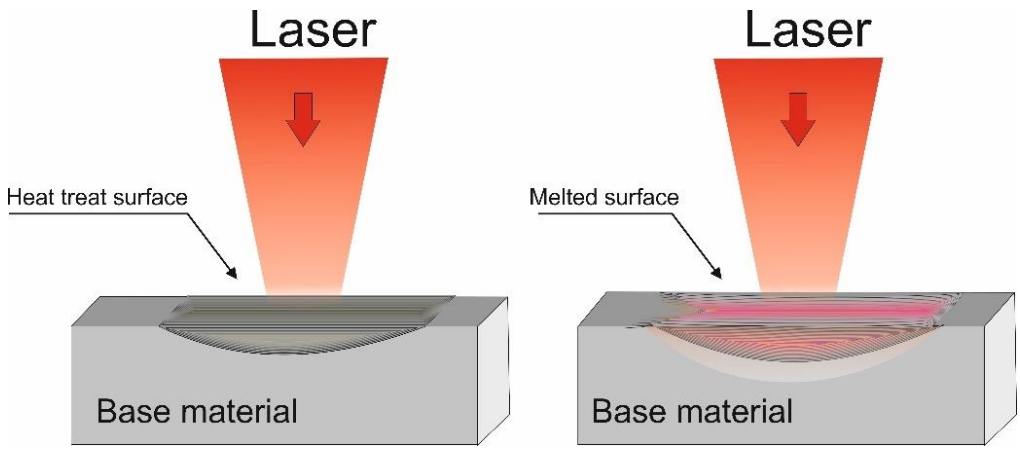

Figure 2.20 Principle of the laser heat treatment.

In case of laser transformation hardening, there are three main factors that determine the efficacy of the process.

1. Temperature must be above the austenitizing zone.
2. During the transition between heating and cooling phases, the substrate must be maintained at the austenitizing temperature for a duration sufficient to facilitate carbon diffusion.

3. The component/material to have enough mass for self-quenching to happen, ensuring that the cooling rate meets the critical quenching rate requirement.

The wavelength of the laser, the focal distance and the spot geometry, the pulse length and repetition rate in case of pulsed lasers are only several additional parameters that must be considered for a successful heat treatment. Attention should be paid to the surface finish, as it has the potential to impact the rate of laser radiation absorption.

The advantages of the laser heat treatment extend far beyond traditional heat treatment methods. Its non-contact and precise localisation of the treated area obviate the risks of contamination and material distortion. The main characteristic, to induce rapid heating and cooling rates ensures the formation of unique microstructures with specific properties, including exceptional hardness, enhanced wear resistance, and high-temperature stability. Additionally, the non-uniform heating gradient allows for fine tuning of local property.

New developments if the laser technology and automation with robotic systems further increase precision and efficiency of the process for surface engineering applications.

The main advantage of the laser technology rise from the possibility to control the energy and thus to obtain the controlled melting of the surface. By doing that, the topography of the surface can be altered and depending on the final application the surface, can be subjected to other manufacturing operation to smooth the surface. Compared with laser heat treatment, in case of surface melting, a thin layer of the substrate is melted and quickly solidified. By doing so, all the constituents are dissolved, uniformly distributed in the melt, and immediately solidified giving the possibility to refine the microstructure and to control the distribution of the carbon or other elements in the subsurface layer of the material.

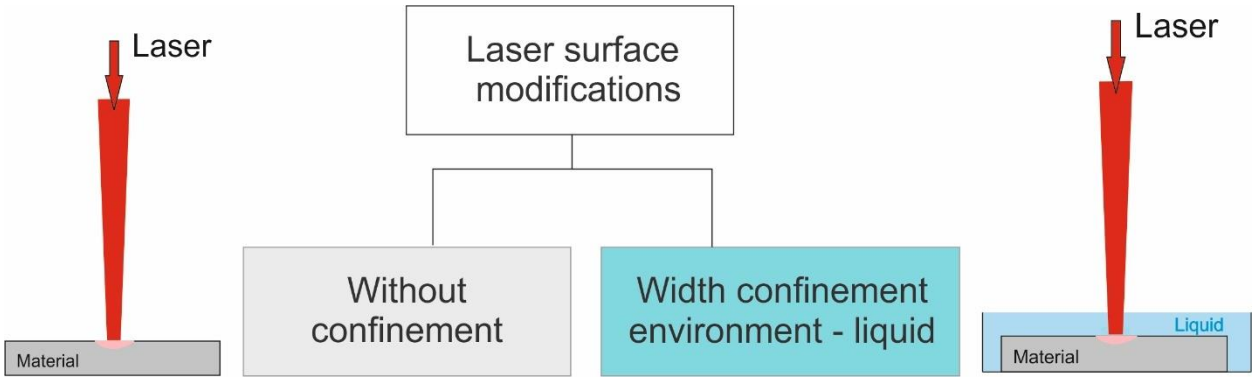

Figure 2.21 Laser surface processing.

Cast irons, nickel aluminium bronze, iron chromium aluminium and HEA alloys are few examples of materials that are currently subjected to laser surface melting. As presented in

figure 2.21, the process of laser surface modification / melting can be realised in two ways. The surface melting can be realised in air / controlled atmosphere usually an inert gas like argon/helium or it can be realised using a confined environment, e.g. water or other liquid. If confined media is used, besides surface melting, other phenomena will be involved (cavitation, shock waves). Both techniques are further discussed on this Habilitation thesis.

2.4 Laser surface engineering in scientific research

In recent years, there has been considerable focus on the exploration of effective methods for enhancing the performance of metallic components. This involves the use of surface modification techniques that are both energy-efficient and cost-effective. In order to enhance the mechanical properties and resistance to wear and corrosion of metallic materials, a range of techniques can be utilized, including bulk or surface treatments using heat or thermochemical processes, as well as the deposition of protective coatings. Laser processing has been widely utilized as an effective technique for micro-processing and/or microalloying of metallic surfaces within the field of standard processes. The latest advance of laser technology has enabled the processing of materials through a multitude of distinctive methods, marking a significant advancement in the field of surface engineering.

Basically, for the surface modification can be used two principles, i) melting of the surface or ii) altering the surface by shock processing. In the second case the surface modification can be with or without the surface melting.

Laser surface melting shielded by argon gas is a common technique to improve the hardness, wear and corrosion resistance. In 2023, Lidong et al. [LID23] use the laser melting process to enhance the corrosion resistance of the C45E steel by using a pulsed laser and optimised parameters in term of spot overlap rate. The corrosion resistance of the remelted surface increased 3 times. Improving the corrosion resistance and resistance to cavitation erosion of AISI 304 by laser surface melting was attended by Cao et al. [CAO23]. He obtained good results in term of corrosion resistance by fine tuning the process parameters to obtain a remelted surface with better self-repairing and re-passivation ability. Corrosion resistance is the key features in many industrial applications. Laser surface melting of Al-Co-Ce-La alloy was investigated by Sayed et al. Corrosion resistance was improved compared with the as cast material by refining the microstructure and reducing the $Al/Al_{11}Ce_3$ eutectic composition.

The laser surface melting can be realised using continuous or pulsed laser. Both types have advantages and disadvantages mostly due to the laser-material interaction. Pulsed lasers,

especially the ones with short pulse duration, will produce a shock wave at the interaction with the material. If the intention is to heat treat, melt and ad a shock wave then a confining media can be used to amplify the shock wave produced by the plasma formation.

The use of laser technology for material processing in liquid environments have great potential as a method to enhance the surface characteristics of metallic materials. This technique offers several advantages, including enhanced absorption, confinement, wave transmission, vaporization, and liquid convection effects [HOF17]. Currently, there is an increasing amount of research focused on using underwater laser processing techniques to mitigate the undesirable thermal effects associated with laser processing, such as minimizing the heat-affected zones. These techniques include underwater laser welding [WAN18, GUO17, ZHA06], cutting [SHI18, SHI17], cladding [FEN18, WEN19], and peening in liquid medium [ZHU12]. The utilization of lasers in an aqueous environment presents significant challenges due to the multitude of characteristics and variables that could affect an already intricate technology.

The formation of a plasma plume inside a liquid environment happens when the laser irradiation is above a certain threshold within a concentrated area. Upon reaching the threshold, there is a fast increase in temperature of the liquid in close proximity, subsequently leading to its forceful expansion and the release of a shock wave. The enlargement of the heated volume also leads to the creation of a cavitation bubble, with a maximum threshold radius ranging from 1 to 3 mm [PHU20]. The continued increasing of the cavitation bubbles will result in their subsequent collapse, so creating a shock wave. According to the research conducted by Zhong [ZHO20, LEE11], it has been shown that during the collapse of a bubble, a narrow zone of intense heat is generated around the surface of the bubble, with temperatures reaching as high as 9700 °C [LEE11]. The thermal and chemical impacts in materials processing are attributed to the superheated area, whereas the mechanical processing is mostly attributed to the shock wave.

The laser processing in liquid media may be classified into two primary groups based on the physical processes involved: continuous wave (CW) and long pulse laser processing (milliseconds, microseconds), and ultrashort laser processing in nanoseconds, picoseconds, and femtoseconds. The primary distinctions are in the manner in which the pulse interacts with the material, specifically including heat conduction inside the material, the process of melting, vaporization, and the production of plasma during extended laser pulses.

The interaction between ultrashort laser pulses, namely those with picosecond (ps) and femtosecond (fs) durations, and the material may be described as having a negligible thermal

effect. Instead, the interaction is primarily characterized by a straightforward transition from solid to vapor due to the short timescale and high intensity of the laser pulse. This is followed by the formation of a plasma with high intensity [HAM16, LEI11]. In liquid media, these processes generate kinetic energy in the form of shock waves and additional pressure known as plasma-induced pressure. Additionally, they result in the development of cavitation bubbles, which have the advantageous ability to mechanically affect the material being irradiated [XIA17, KAN19]. Additionally, the generation of plasma inside a liquid medium might induce thermochemical reactions that are advantageous for the formation of nanoparticles, thus offering a possible alternative to traditional chemical approaches.

Plasma or low intensity plasma is not expected to be created at power densities lower than 10^6–10^7 W/cm^2. Instead, the primary effect observed is an explosive boiling phenomenon that leads to the generation of vapor pressure.

The occurrence of thermocavitation phenomena may be achieved when the liquid exhibits a significant absorption of the laser wavelength, as evidenced by the research conducted by J. P. Padilla-Martinez et al. [PAD14, PAD11, KOR11].

As observed in the literature, the utilization of low power continuous or long pulsed lasers for laser processing in liquid has become prevalent in many applications such as welding, heat treatment, and cutting. This technique relies on constant delivery of heat to the material surface. In a study form 2016, Nikolic et al. [NIK16] utilized an adaptive neural fuzzy inference system to enhance the prediction accuracy of water-jet aided underwater laser cutting parameters. According to Shin et al. [SHI19], laser cutting was employed to cut stainless steel with a maximum thickness of 60 mm. The cutting process was conducted in a water environment utilizing a continuous ytterbium fibre laser. Significant advancements have been achieved in terms of efficiency and the mitigation of secondary waste, rendering them applicable for the dismantling of nuclear reactors. In a recent scientific study, Xiangru Feng [FCZ19] revealed the use of titanium and the application of a zinc-based coating onto a substrate composed of nickel aluminium bronze, utilizing an underwater laser cladding configuration. The analysis of the samples indicated an enhancement in the resistance to corrosion and a refinement in the microstructure of the coating at the grain boundaries. In an additional study, the research group mentioned in reference [FEN19] examines the interactions of laser, water, and the substrate, emphasizing the advantages of utilizing underwater laser cladding with titanium rods. As previously mentioned, the utilization of ultra-short laser pulses has the capability to generate a shock wave inside a liquid medium, hence

enhancing the fatigue strength and resistance of a given material. This technique is commonly referred to as Laser Ablation in Liquid (LAL) or Laser Peening in Liquid (LPL). In contrast to other laser processing techniques, laser peening is described as a cold process. The hardness of AISI 316 stainless steel was enhanced using the process of femtosecond laser ablation in water, as demonstrated by Hoppious et al. [HOP18].

In their study, Wang et al. [WAN18] employed water and aluminium foil as the confinement layer in the laser peening process of 5083 Al alloy. This approach resulted in an enhanced hardness of the material surface, achieved by the formation of a precisely regulated micro-dimple array on the treated surface. In addition, Wang et al. [WAN19] effectively enhanced the microhardness and wear resistance of NiTi shape memory alloy with the application of high-pressure shock waves using laser shock peening carried out in distilled water.

In contrast to laser shock peening, laser heat treatment (hardening) is a processing method that enables the attainment of higher levels of heating and cooling for the materials being treated. The standard laser heat treatment (LHT) typically employs air or argon quenching as a cooling method for the treated region. The heating process can be performed using either continuous or pulsed laser systems. Lapounge and colleagues [LAP19] conducted a comprehensive investigation on the behavior of martensitic and dual-phase steel under various temperature conditions during the laser heat treatment process. The authors state that the relationship between the spot size of the laser and the thickness of the material has considerable significance, as it exhibits a direct correlation with the surface properties.

The intricate nature of the phenomena associated with liquid media laser processing was observed in the results detailed in several scientific articles. Telrandhe [TEL18] employed finite element analysis to estimate the area of the heat-affected zone resulting from the motion of a laser heat source. In their study, Sehyeok and Hyungson [OHS19] employed a three-dimensional thermal simulation technique to predict the distribution of hardness in H13 high-speed steel tools subjected to laser heat treatment. The results demonstrated a remarkable accuracy of 94.4% in predicting the hardness distribution based on the temperature gradient. In addition, Hyungson Ki [KIH12] presents a process map that correlates mathematical models with actual data for the laser heat treatment of AISI 1035 and 1020. Additionally, previous studies have shown the optimization of laser processing settings in order to achieve a consistent surface hardness [KEN04, MAH19, MAH10]. Nevertheless, the entire potential of laser heat treatment/alloying in a liquid medium remains incompletely known.

CHAPTER 3. EXPERIMENTAL INVESTIGATIONS INTO LASER WELDING OF STAINLESS STEEL

3.1. Laser welding of stainless steel

As presented in chapter 2, stainless steel is one of the most used materials for engineering applications where high corrosion resistance is necessary. Among the numerous grades of stainless steel, the AISI 316L is well-known not just for its resistance to corrosive environments but also for its exceptional weldability. In this chapter, I am presenting the results of the extensive experimental research about laser welding of austenitic stainless steel.

3.1.1 Concept Overview

Stainless steel and especially AISI 316L, a widely used material in various industries, demands precise welding techniques to maintain the high corrosion resistance.
The presented study, address to systematically optimise and fine-tuning the key welding process parameters to achieve high quality weld. When using pulsed laser is mandatory to determine the intricate relationship between laser parameters (such as laser power, pulsed duration, pulse repetition and focal length), shielding gases, and material properties, in order to ensures a good geometrical appearance, low distortion, and maximum mechanical behaviour. To do that, I have conducted numerous studies [STA22] regarding the optimisation of parameters for the laser welding process of stainless steels.
The optimal laser power, pulse duration and repetition rate were determined by employing the method of varying only one parameter at a time within a series of experimental tests.

3.1.2 Methodology, Resources, and Outcomes

Stainless steel AISI 316L was used as base material for achieving experimental fusion lines and butt welding. This austenitic stainless steel, enriched with molybdenum, exhibits a high resistance to a wide range of corrosive media, including acidic, alkaline, and chloride environments. Its low carbon content enhances corrosion resistance and also mitigates the detrimental effects of carbide precipitation during welding. Plain sheets of 100x100x1 mm having the chemical composition as presented in Table 3.1 were used as coupon for the laser processing.

Chemical composition of the base material Table 3.1.

Material	Element wt. (%)								
	C %	Si %	Mn %	P %	S %	Cr %	Ni %	Mo %	N %
AISI 316L	0.03	0.75	2	0.004	0.003	16-18	10-14	2-3	0.10

For the experimental tests, I utilized a pulsed laser system, specifically the Trumpf TruPulse 556, characterized by a peak pulse power of 10 kW and a wavelength of 1064 nm. The optical configuration was based on a Precitec YW50 coaxial welding head with a focal length of 150 mm, which was manipulated by a CLOOS 7-axis welding robot. To facilitate the positioning and secure clamping of the samples a specially designed table was employed, as illustrated in Figure 3.1. The Argon gas shielding was provided from the top and at the root of the weld bead in order to prevent any external contamination.

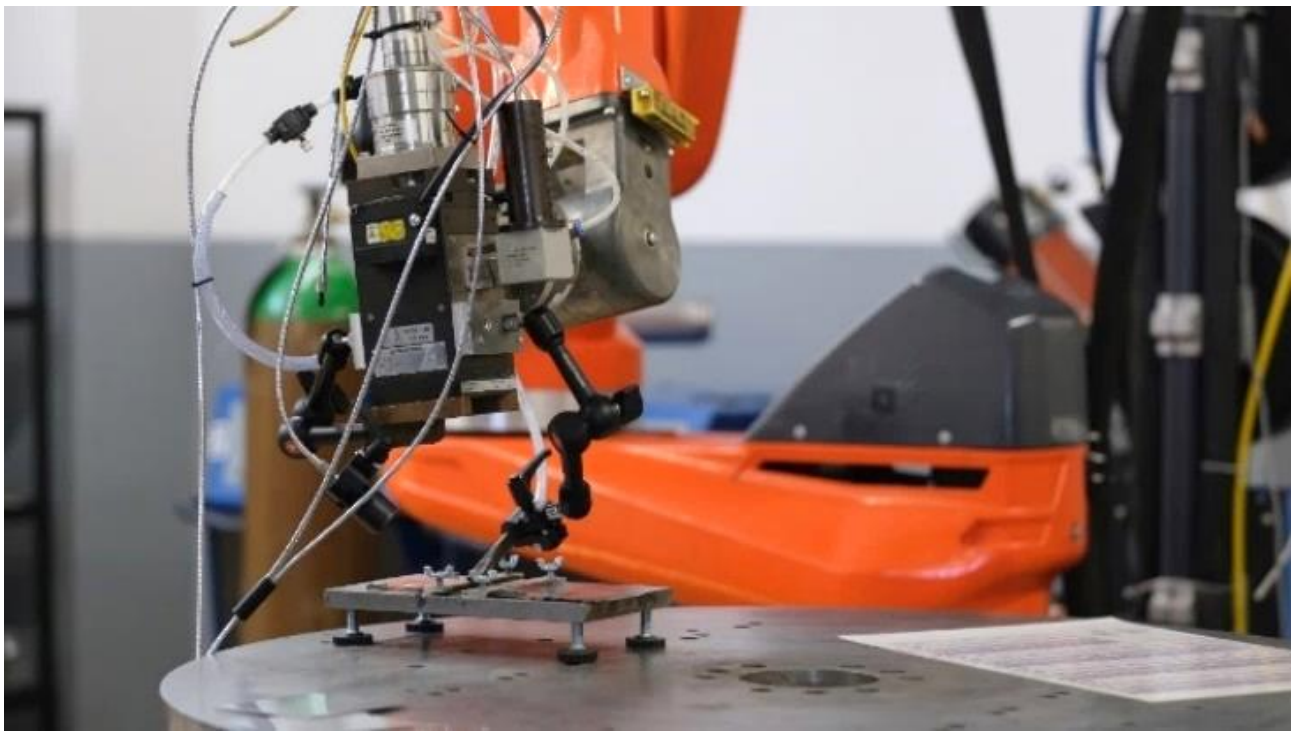

Figure 3.1. Details of the experimental frame [STA22]
"Advanced Welding Ecotechnology R&D Center" from Transilvania University of Brasov

The experimental tests were conducted using pulsed beam with 0.7 mm spot diameter in focal on the surface of the material. A total of 18 fusion lines and one welding were realised using a constant processing speed of 45 cm / min. The input variables were the laser power, pulse

duration and pulse repetition rate using one single factor at a time approach. The process parameters window was chosen based on preliminary tests.

The optimization of the laser welding process was made using a systematic approach, in which the laser power, pulse duration, and repetition rate were gradually increased. The parameters used for these incremental adjustments are presented in Table 3.2, 3.3, and 3.4.

Variation of the laser power Table 3.2.

Parameters / sample	1.1	1.2	1.3	1.4	1.5	1.6
Laser power [w]	900	1000	1100	1200	1300	1400
Pulse duration [ms]	7	7	7	7	7	7
Repetition rate [Hz]	40	40	40	40	40	40
Power density [J]	6.3	7	7.7	8.4	9.1	9.8
Welding speed [cm/min]	45	45	45	45	45	45

Variation of the laser pulse duration Table 3.3.

Parameters / sample	2.1	2.2	2.3	2.4	2.5	2.6
Laser power [w]	1300	1300	1300	1300	1300	1300
Pulse duration [ms]	5	5.5	6	6.5	7	7,5
Repetition rate [Hz]	40	40	40	40	40	40
Power density [J]	6.5	7.1	7.8	8.3	9.1	9.8
Welding speed [cm/min]	45	45	45	45	45	45

Variation of the laser repetition rate Table 3.4.

Parameters / sample	3.1	3.2	3.3	3.4	3.5	3.6
Laser power [w]	1300	1300	1300	1300	1300	1300
Pulse duration [ms]	7	7	7	7	7	7
Repetition rate [Hz]	15	20	25	30	35	40
Power density [J]	9.1	9.1	9.1	9.1	9.1	9.1
Welding speed [cm/min]	45	45	45	45	45	45

All of the samples were cross-sectionally examined in order to determine the ideal welding geometry. Standardised processes were used to cut and prepare the samples (polishing with sand paper from 180 to 2000 grit and polishing on velvet cloth with 0.3 μm Alumina

suspension). The samples were then electrochemically etched for 20 seconds at 5V and 500 mA using a 10% oxalic acid solution.

As with any welding, the goal was to achieve complete penetration and a minimum heat affected zone while utilizing the least amount of energy. The dimension of the heat affected zone of any laser processing is determined by energy and speed. Figure 3.2 shows the influence of the laser power and power density on the geometry of the weld bead. The macro pictures of the materials were obtained with a LEICA EZ4 stereo microscope, and the optical microstructures of the fusion lines and welding joints were examined with a LEICA DML inverted microscope.

The macrographs in figure 3.2, samples 1.1 to 1.6, show that melt depth increases virtually exponentially as laser power increases. It is a predictable result, and it is evident that complete penetration is reached only at 1400 W.

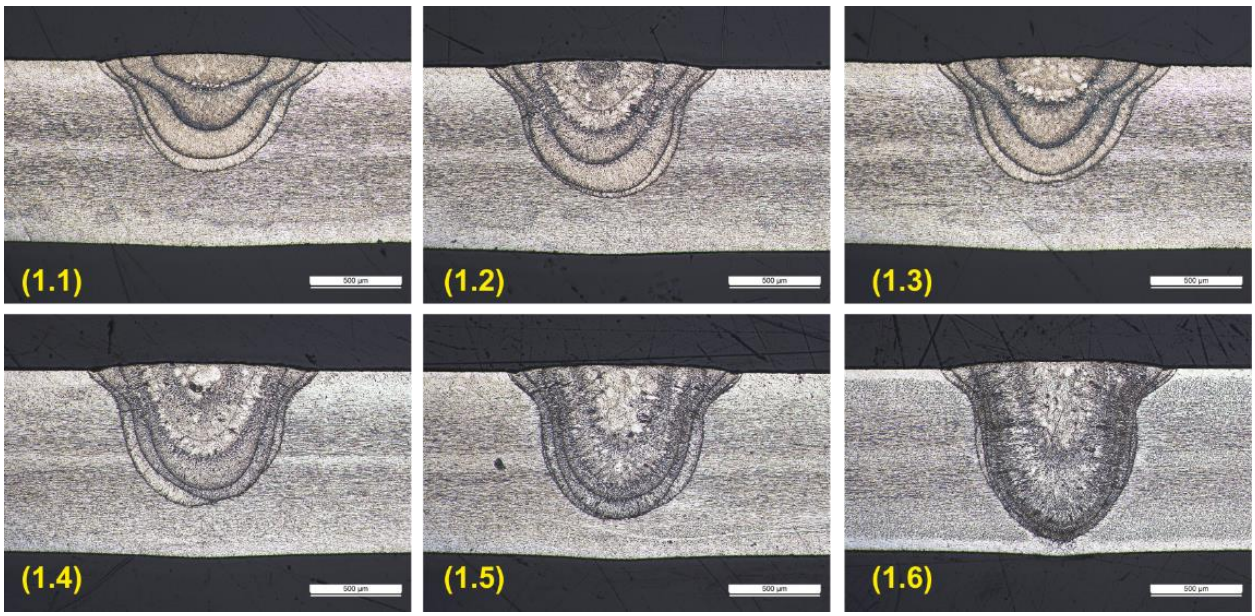

Figure 3.2. Laser power influence on the melt geometry. Cross section of samples 1.1 to 1.6 [STA22].

Regarding repetition rate and pulse length, comparable results were also observed. Figure 3.3 reveals that by increasing the pulse duration, a melt shape that is almost identical may be achieved. The penetration depth and melt width will both rise as the pulse duration and power density increase. The behaviour of the laser pulse's interaction with the material surface must be taken into account, even when the cross-section profile is almost identical. One of the most important variables in laser processing is the pulse energy [J], which is calculated as the average power * pulse time. Samples 1.6 and 2.6 were realized with the same laser energy but

different power and pulse duration, as shown in Tables 3.2 and 3.3. The results show that, even when the total pulse energy remains constant, the melt depth will increase at longer pulse duration (Figure 3.3).

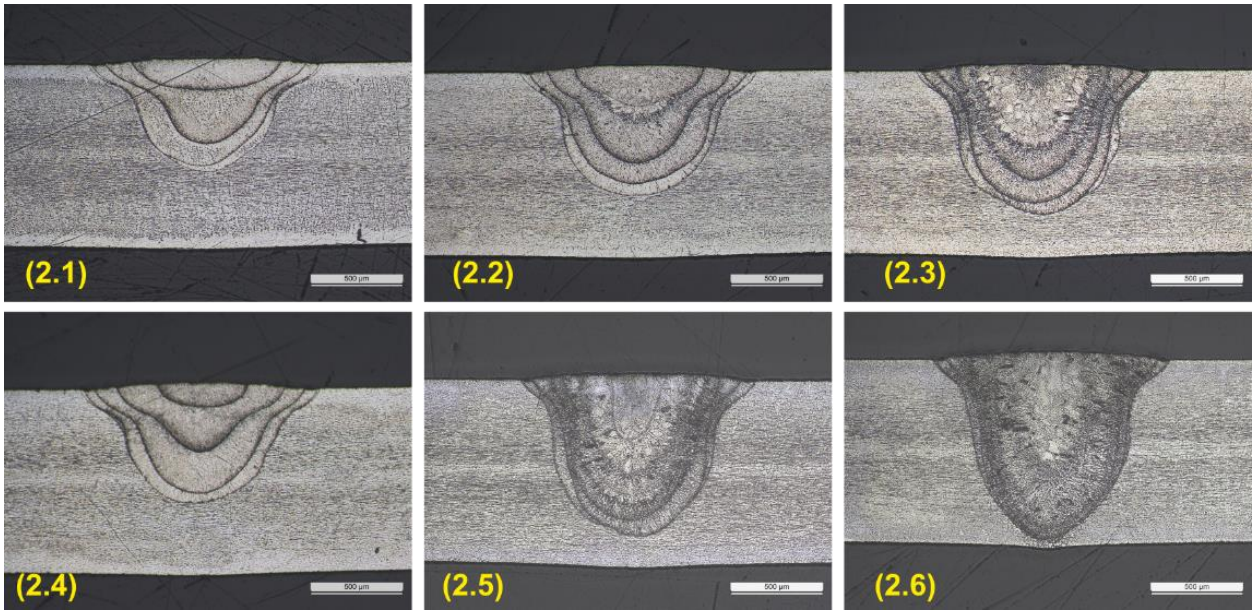

Figure 3.3 Pulse duration influence on the melt geometry. Cross section of samples 2.1 to 2.6

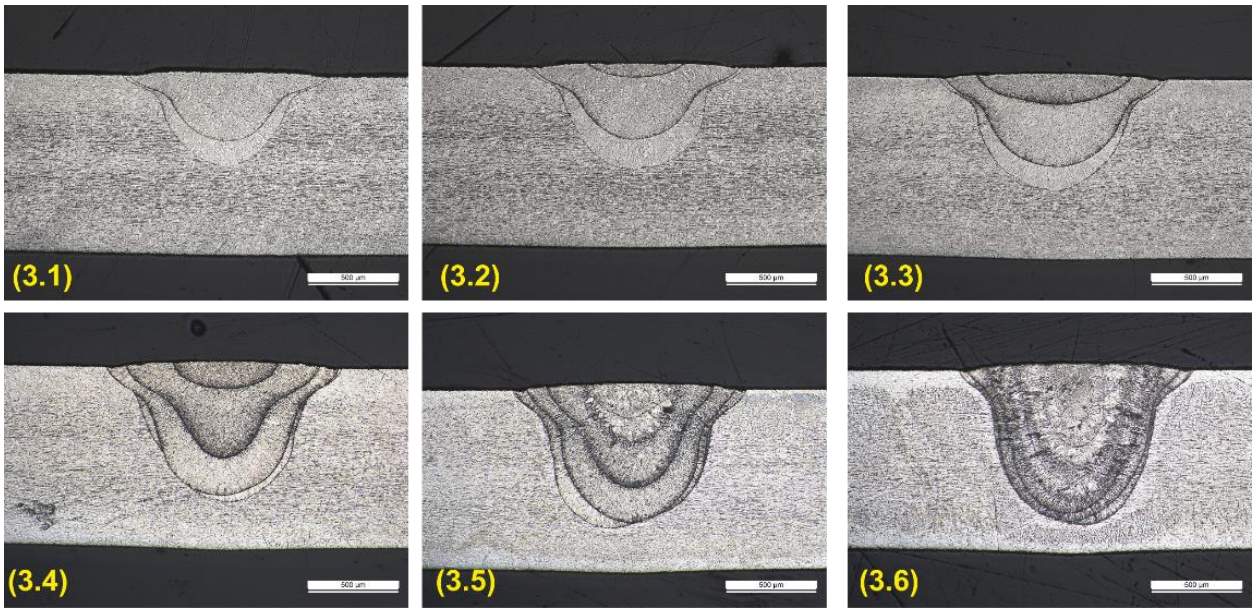

Figure 3.4. Laser repetition rate influence on the melt geometry. Cross section of samples 3.1 to 3.6 [STA22].

The pulse energy must be related to the repetition rate, as shown in Figures 3.5 e and f. The repetition rate influences the melt width and depth. Even though a high pulse energy of 9.1 J was used for the samples 3.1 to 3.6, the melt width and depth are minimal. Furthermore, the rate of laser repetition throughout the welding process must be proportional to the welding

speed. If the speed remains constant, it is evident that increasing the repetition rate would result in more pulses interacting with the same surface area. This test shows that increasing the repetition rate at constant speed allows us to achieve complete penetration.

The repetition rate is the most influential parameter on the microstructure of the melted region. A high repetition rate implies a higher laser energy per surface area.

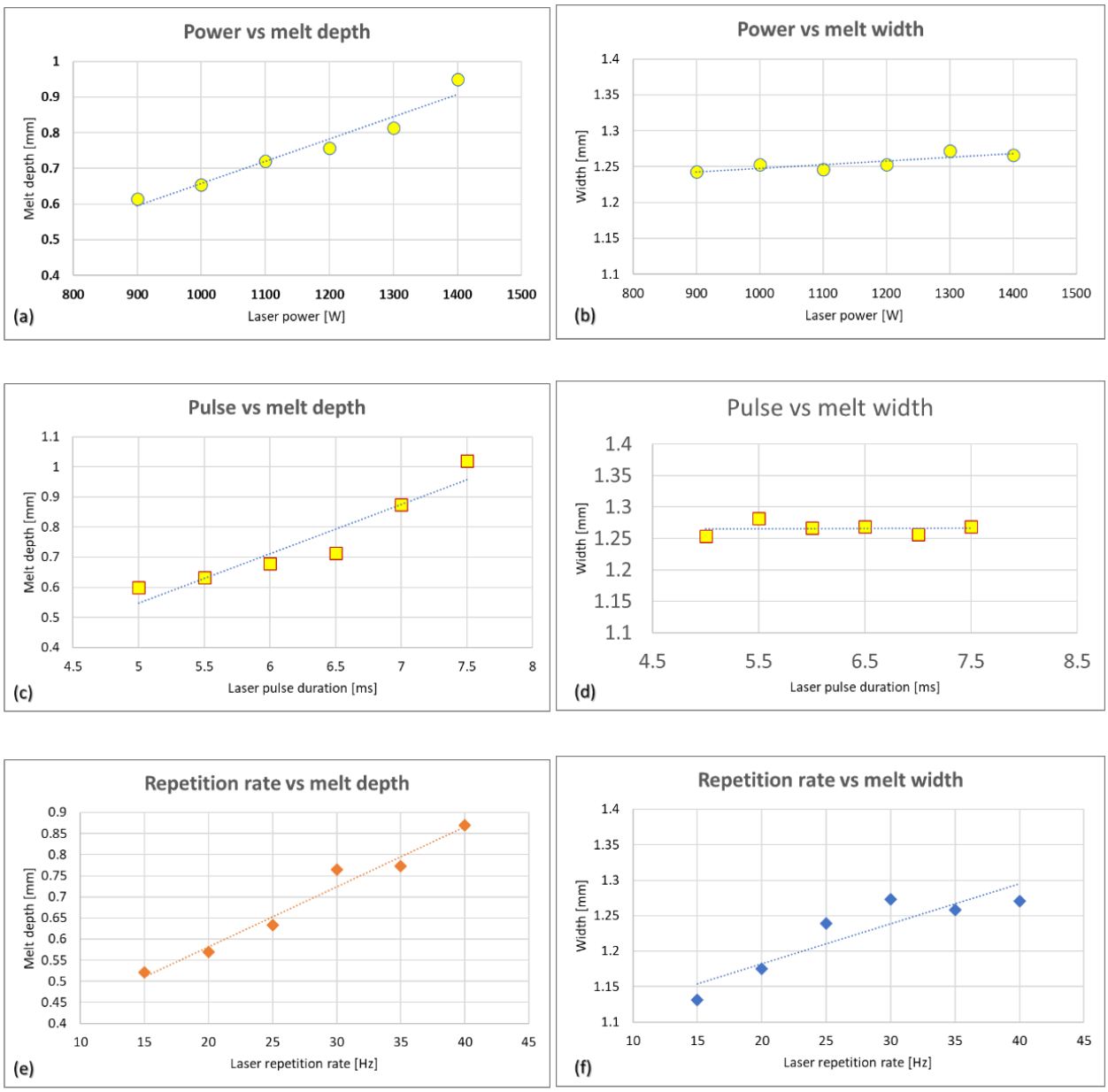

Figure 3.5. Graphical representation of the process parameters influence on the melt depth and width, and indication of linear trendline (a) Power vs melt depth, (b) laser power vs width, (c) pulse duration vs melt depth, (d) pulse duration vs width, (e) pulse repetition rate vs melt depth, (f) pulse repetition rate vs melt width [STA22].

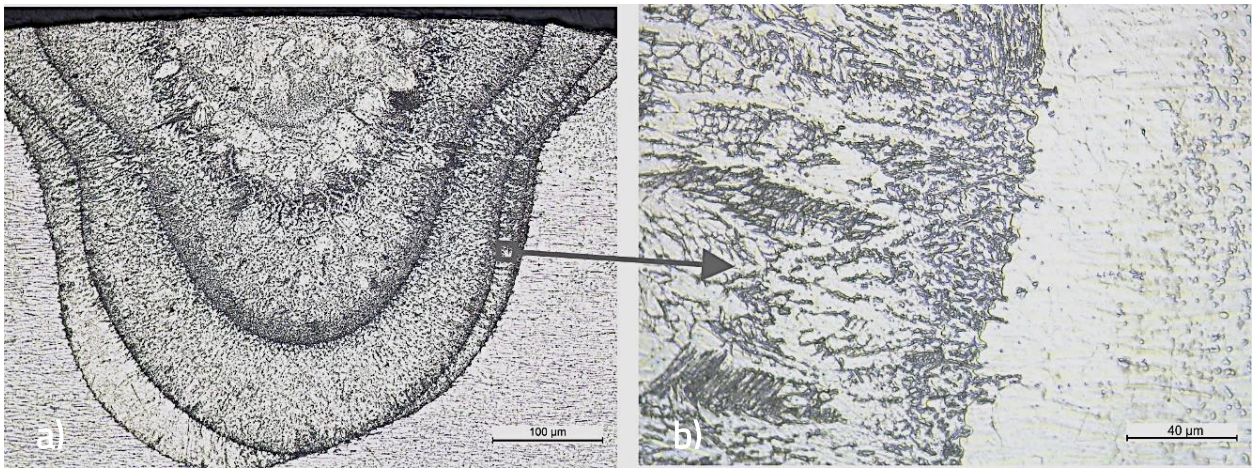

Figure 3.6. Macro (a) and microstructure (b) of the sample 3.5 [STA22].

Figure 3.6 shows the microstructure of sample 3.5, which was realized at a repetition rate of 35 Hz. The microstructure of SS 316L is characterized by a completely austenitic matrix with polyhedral grains. The rapid cooling that occurs during laser processing, along with the repeated interactions of the laser pulses with the material, results in the occurrence of multiple solidification patterns (Figure 3.6 a). Lathy and skeletal ferrite, noticeable as darker structures in Figure 3.6b, develop during the melting-solidifying and remelting process when laser pulses interact with the material [STA22].

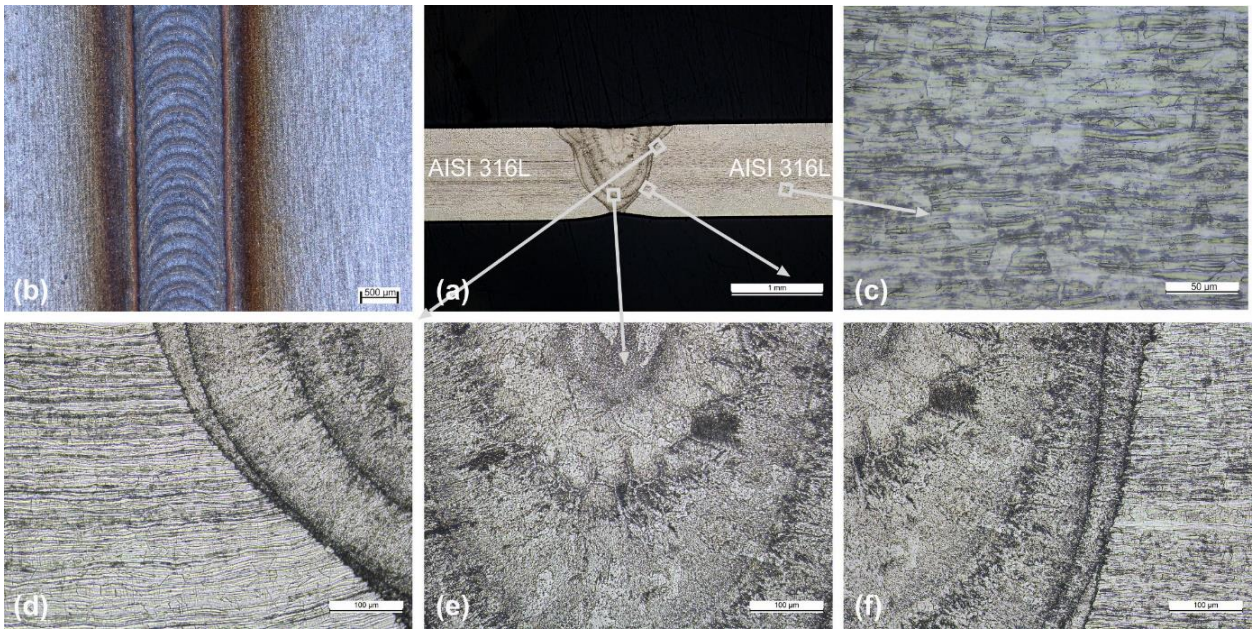

Figure 3.7. Pulsed laser welding of AISI 316L, a) weld bead profile, b) top view of the weld joint, c) base material, d) and f) detail of the weld bead – base material interface, e) detail of the weld area [STA22].

The optimal parameters for welding of AISI 316 L stainless steel have been determined using the graphical representation in Figure 3.5, respectively: laser power of 1300 W at 7ms pulse duration and 40 Hz repetition rate (Figure 3.7). For all of the experiments, a welding speed of 45 cm/min was utilized. The welding was protected at the top and bottom using pure argon gas. Although the butt weld geometry is simple, no-gap alignment between components is required for laser welding of thin sheets. To test the process repeatability, five welding joints were made.

Using the above-mentioned parameters, a defect-free welded joint was achieved. Figure 3.7 presents the overall look of the weld as well as details from the interface of the melt zone and base material. The weld joint has complete penetration and no obvious heat impacted zone.

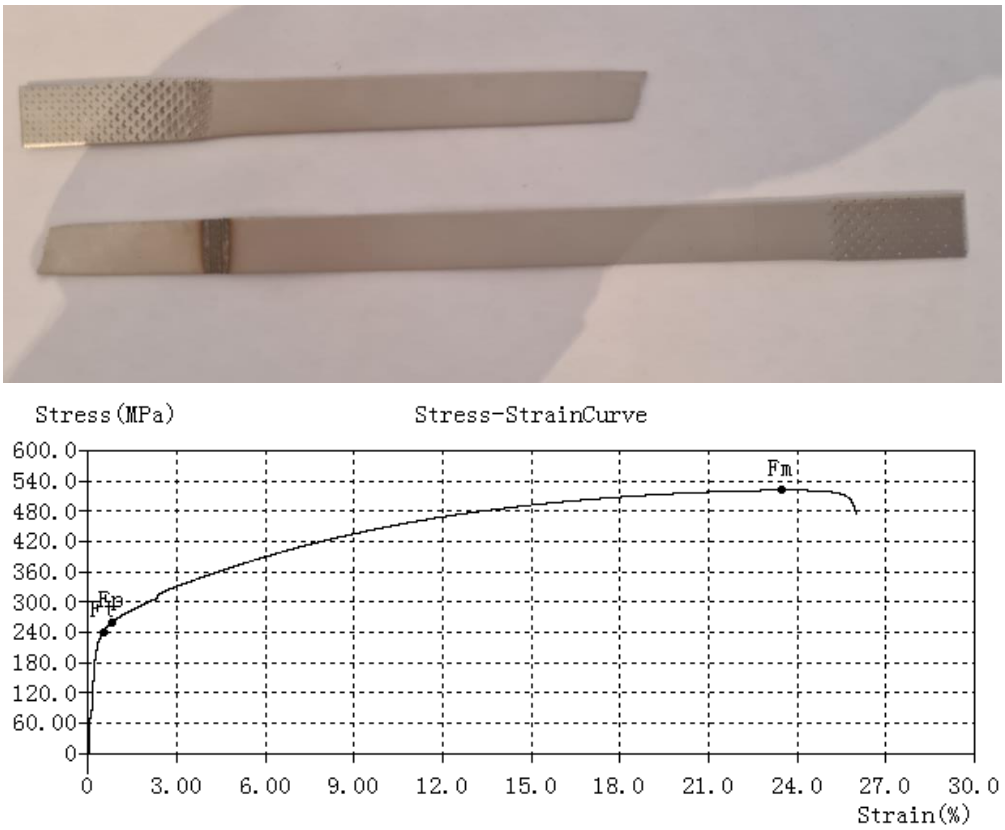

Figure 3.8. Fracture and stress-strain obtained on AISI 316 L laser welding [STA22].

The mechanical behaviour of the welded specimen was determined using an universal testing machine. Tensile testing of the welds was carried out on specimens 10 mm width and 200 mm long. The fracture of the samples occurred in the base material, at a considerable distance of the HAZ or weld bead, as can be observed in fig. 3.8. The welding mechanical behaviour is in accordance with Figure 3.8's stress strain curve.

Specifically, for AISI 316L stainless steel, the tests show that geometrical profile of the weld bead can be heavily influenced by the process parameters. Using the 18 tested samples I demonstrated that laser parameters have a major impact on the geometry and microstructure of the fusion lines and in order obtain a full penetration, a laser energy of at least 9.1 Joule is required. Laser power (1300W), pulse length (7ms), and repetition rate (40Hz) were found to be the best parameters for welding AISI 316L thin sheets, by using the lowest possible energy input into the process.

3.2 Dissimilar laser welding of stainless steel – carbon steel

Nowadays the laser welding of stainless steel is used as a conventional process in various industrial applications. Lots of stainless-steel grades have a good weldability and are employed in manufacturing of components that are exploited in corrosive environments.
In addition to the favourable performance characteristics exhibited by stainless steel, there exists a drawback that restricts its utilization, namely its cost.
One potential approach to reduce the manufacturing expenses of diverse items is the selective use of stainless steel just on the most vital surfaces that are prone to corrosion. To address this issue, the practice of combining stainless steel with other materials, such as carbon steel, emerged as a potential solution. However, this approach also posed challenges in achieving heterogeneous welding.

3.2.1 Key Concept

Up to present, due to the complexity of the domain, there are relatively few research covering physical and mechanical behaviour of stainless-steel welding in a dissimilar configuration.
Due to the many variables that affect weld quality, several steel combinations have not been investigated thoroughly. One example, is the AISI 321 stainless steel and AISI 1010 carbon steel combination that have multiple applications, mainly due to the nature of AISI 321 which been alloyed with titanium poses a good weldability and corrosion resistance.
Subsequently, materials compatibility and weld characteristics of heterogenous AISI 1010 – AISI 321 are presented, as an in-depth study conducted in the laboratory of ICDT, Transilvania University of Brasov [STA18].

3.2.2 Methodology, Resources, and Outcomes

Welding experiments were carried out using 50x100x0.5mm AISI1010 and AISI 321 commercial steel specimens. AISI 1010 (CS) steel is a low carbon steel that is widely used in the automotive and construction industries.

The AISI 321 (SS) austenitic stainless steel is a commercially stainless steel alloyed with titanium. The addition of Ti to the chemistry of AISI 321 is beneficial in providing excellent surface oxidation resistance of stainless-steel components, as well as reducing inter-granular corrosion and chromium carbide precipitation at the grain boundary during welding procedures. Table 3.5 shows the chemical composition of the materials utilized in the welding experiments.

The chemical elemental composition of the welded steel types Table 3.5

Material	Element wt. (%)								
	C %	Si %	Mn %	P %	S %	Cr %	Ni %	Mo %	Ti %
AISI 1010	0.099	0.168	0.51	0.0033	0.0069	0.043	0.041	0.0024	-
AISI 321	0.08	1	2	0.045	0.03	18	11	-	0.15

The heterogenous weldings were carried out with a Coherent F1000 diode laser operating at =975 nm with a peak power of 1000 W and a maximum divergence of 56 mm*mrad for the incident beam. As in the previous description, an CLOOS Quirox welding robot was employed to manipulate the welding head (Precitec YW 50).

The sheets were positioned and fastened using a specially constructed tool (see Fig. 3.9(b)). 4L/min argon has been purged through a specially designed channel machined at the bottom of the device in order to protect the weld bead root. The upper part of the melted metal bath was shielded trough the welding head with 99.98% vol. argon at a constant flow of 10 L/min. The laser welding process of the CS-SS materials was conducted without filler material. In order to protect the laser optics, a 5° inclination of the welding head was used in the direction of welding. The experimental setup used for the dissimilar laser welding is presented in Figure 3.9 a and 1b. Table 3.6 provides a summary of the process parameters used for the dissimilar welding of carbon steel and stainless steel (CS-SS). The input variable in the welding experiments was the welding speed. In order to highlight the impact of the factors on weld shape, a method involving a gradual increase in welding speed while keeping constant power was employed.

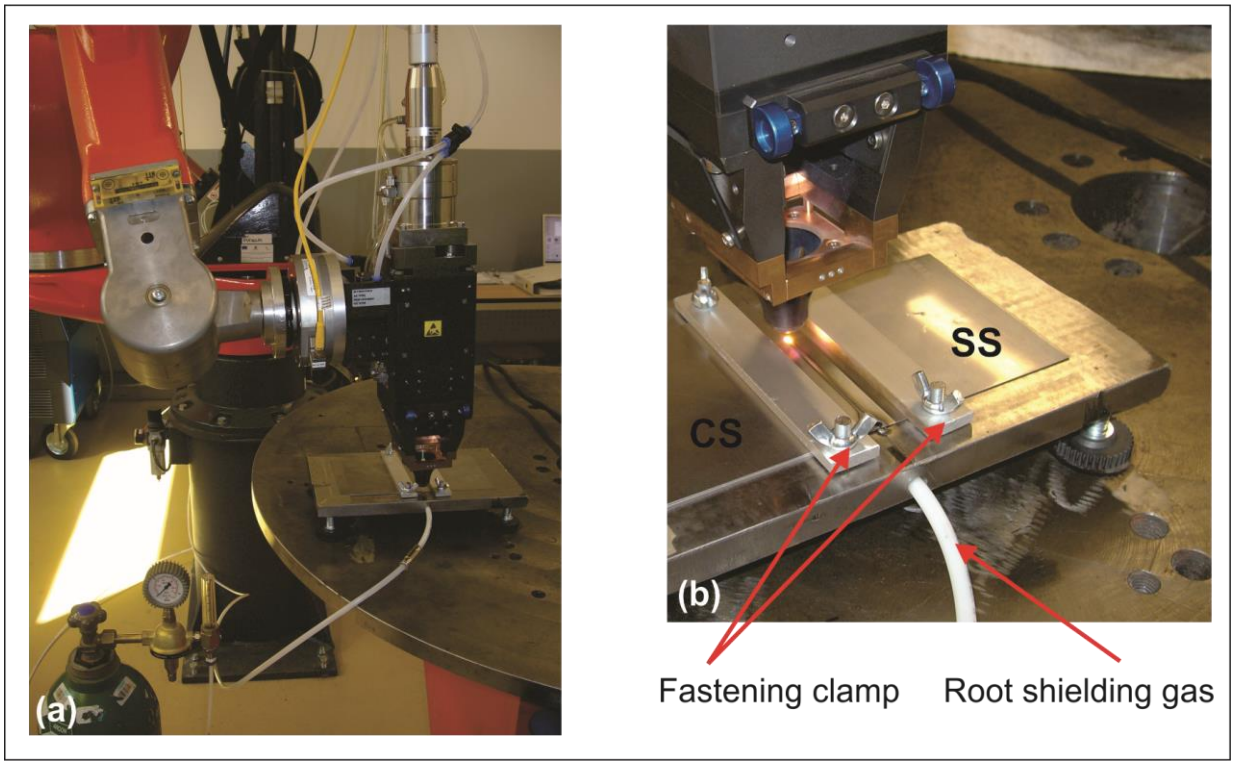

Figure 3.9 (a) Experimental set-up used for the laser welding tests, (b) close-up of positioning and fastening device. "Advanced Welding Ecotechnology R&D Center" from Transilvania University of Brasov [STA18].

Based on a series of first experimental trials, it has been determined that a laser power of 550W is the lowest threshold required to achieve full penetration within the welding speed range of 160-200 cm/min.

The positioning of the laser beam was primarily focused on the stainless steel plate rather than the carbon steel, owing to the stainless steel's comparatively lower heat conductivity and higher reflectivity.

Experimental conditions and response factors Table 3.6

Sample		3.1	3.2	3.3	3.4	3.5
Parameters						
Laser power	**[W]**	550	550	550	550	550
Power density	**[kW/cm²]**	143	143	143	143	143
Energy density	**[J/mm²]**	29.4	27.7	26.2	24.8	23.5
Welding speed	**[cm/min]**	160	170	180	190	200
Weld penetration	**[mm]**	0.51	0.50	0.51	0.37	0.30
Weld bead width	**[mm]**	1.19	1.14	1.09	1.07	1.05
		0.69	0.54	0.47	-	-
Weld bead area	**[mm²]**	0.41	0.36	0.33	0.25	0.19

The power density and the energy density are calculated as follows [PAS13]:

$$Pd = \frac{P}{A_s} \ [kW/cm^2] \tag{3.1}$$

$$Ed = \frac{P}{(v \cdot A_s)} \ [J/mm^2] \tag{3.2}$$

where: Pd is the laser power density, Ed is the laser energy density, P is the laser power, V is the welding speed and As is the laser spot area.

The welded samples were cut and processed according to a standard procedure before being electrochemically etched using a 10% solution of oxalic acid for the SS and Nital 1.5% reagent for the CS. For metallographic analyses, an Olympus GX51 optical microscope and a Quanta Inspect F electron microscope at 30 kV were used.

In the case of industrial applications of welded components, thorough penetration of thin sheets butt welds is necessary to get the optimal tensile behaviour while limiting the heat affected zone. In the case of CS-SS laser welding, full and partial penetration was attained, as illustrated in Figure 3.10. The geometrical profile of the weld bead demonstrates that full penetration requires a optimal corelation between welding speed and power density (samples 3.1, 3.2, 3.3).

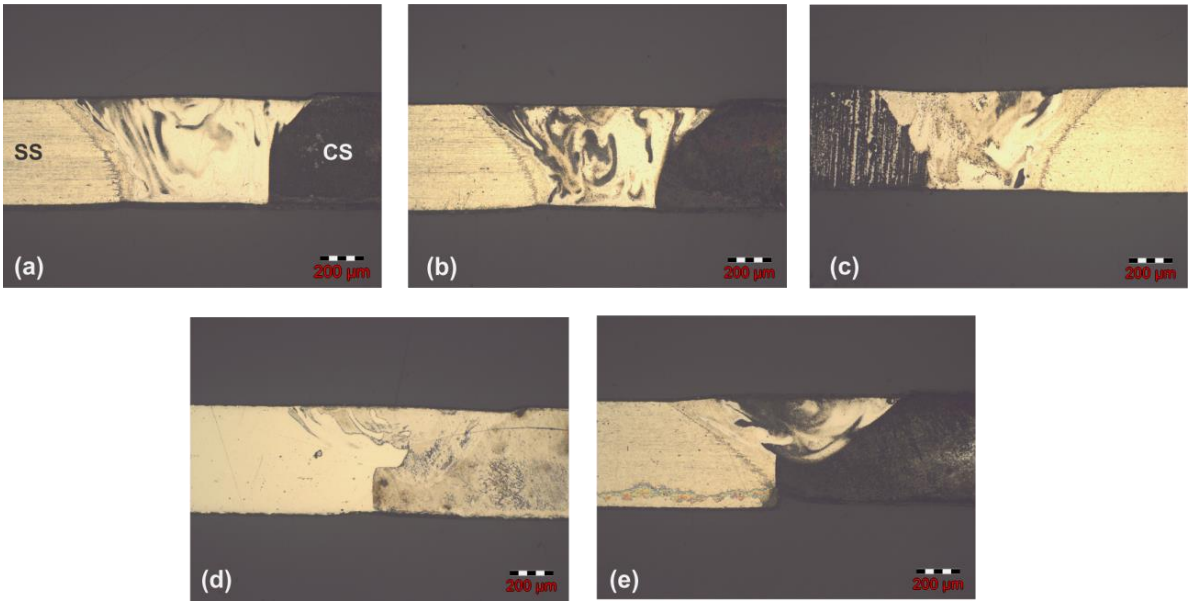

Figure 3.10 Low magnification cross-section of CS-SS laser welding; (a) sample 3.1, (b) sample 3.2, (c) sample 3.3, (d) sample 3.4, (e) sample 3.5 [STA18].

The minimal laser energy required for a proper weld bead profile was determined by keeping the same laser power while increasing the welding speed by about 6%. Figure 3.11 shows the

relationship between welding speed and weld bead width and area, illustrating that weld bead area reduces significantly over 180 cm/min.

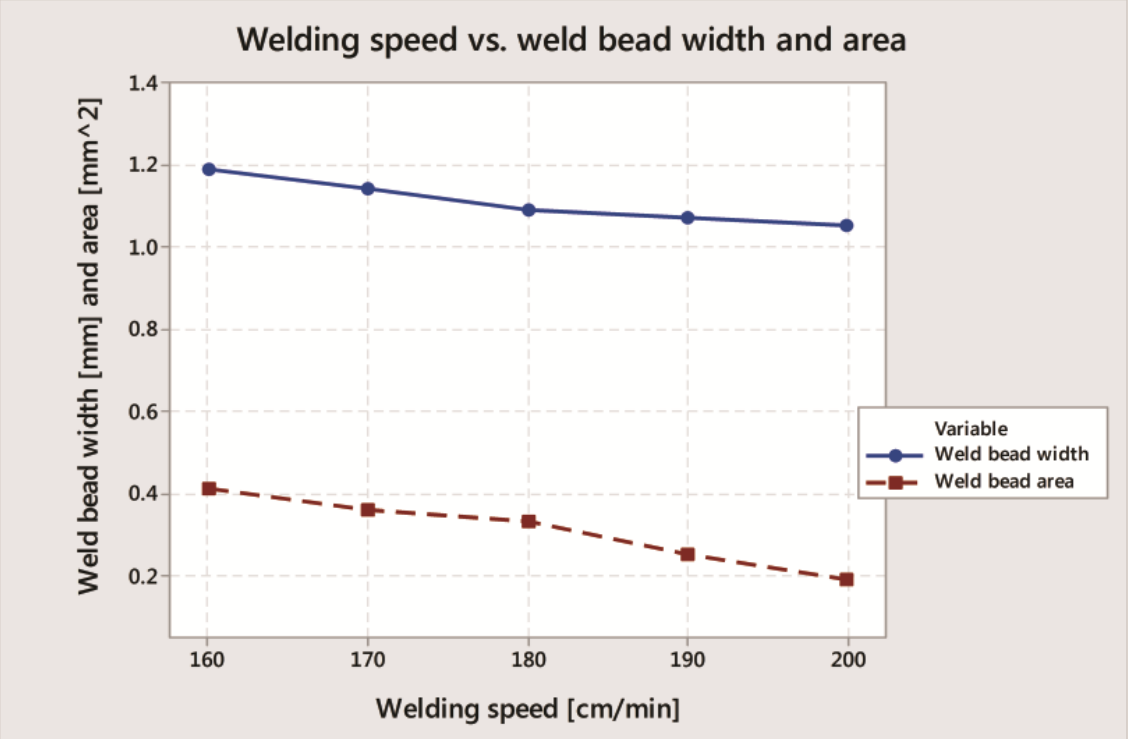

Figure 3.11 Relationship between the welding speed and the weld bead profile [STA18].

According to this, a minimum energy of 26 J/mm^2 is required for complete penetration welding of 0.5 mm dissimilar sheets. The heterogeneous structure created in the weld bead could be seen in the micrographs from Figures 3.12 and 3.13. The weld bead microstructure is composed by mixed and unmixed regions due to the high cooling rate of the weld zone. Strong non homogeneity regions with distinct areas rich in ferrite alternating with areas of mixed austenitic-martensitic-ferrite microstructures are revealed in Figure 3.12a.

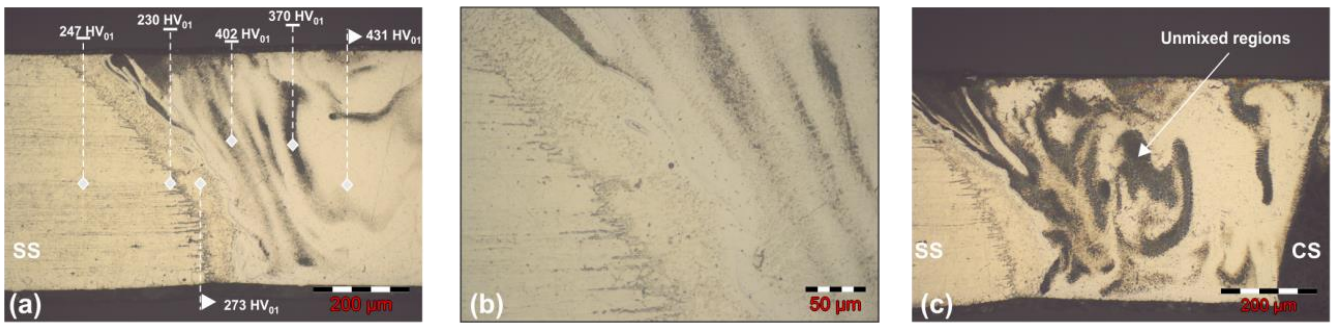

Figure 3.12 Optical micrograph at the interface of stainless steel – weld bead and hardness distribution at the interface with the SS [STA18].

The overall microstructure of the dissimilar joints is defined by the stainless steel, which is characterized by an austenitic twin grains structures with ferrite particles precipitated on grain boundaries and carbon steel with ferrite - pearlite structure. There is a boundary fusion zone (unmixed zone, partially mixed zone, intermediate mixed zone, or non-interference zone, as defined by reference literature studies [NAF09]) at the interface with the base materials that varies in structure and dimension depending on its location (near the carbon steel or near the stainless-steel side). In all circumstances, the fusion boundary is structurally distinct from the weld region and the base materials. Figures 3.10b and 3.12a show that a substantial amount of carbon steel elements (darker region) are present at the border with the stainless steel and a bigger area rich in Cr and Ni is present near the interface with the carbon steel. In proximity of the carbon steel is a ferrite structure mixed with pearlite [STA18].

The boundary zone near the AISI 321 is formed by a needle-like epitaxial growth area with an austenite-ferrite twin structure, as shown in Figure 3.12. The identification of an unmixed zone with a high iron level in this location is an unexpected result. The epitaxial growth suggests that the mixing of the different components did not occur during the melting-solidification process, solidification being facilitated in this case by the high cooling rate increased by the shielding gas given at the weld's root.

Figures 3.13a and 3.13b show the solidification pattern determined by columnar development from the weld zone perpendicular to the stainless-steel base material. The lamellar ferrite stringers that resist austenite transformation during cooling may be seen in this boundary zone between the welding zone and the stainless steel.

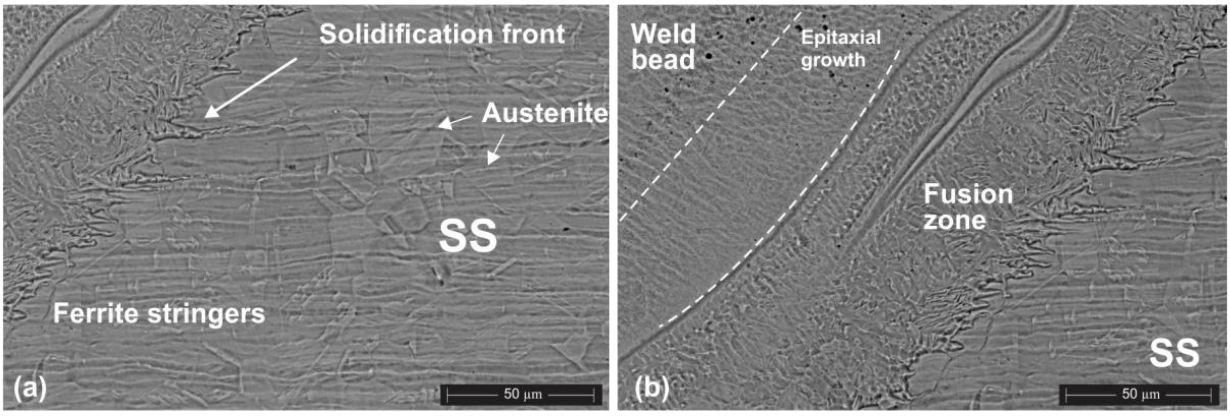

Figure 3.13 SEM microscopy of the fusion zone on the stainless steel side [STA18].

The high magnification micrograph from Figure 3.14d illustrates the ferrite branches that are surrounded by the austenite matrix. The microstructure of the weld zone is characterized by

an austenitic matrix, along with residual δ-ferrite and partial development of widmanstatten austenite.

The regions that have not undergone mixing are observed as discrete areas (islands) consisting of a high concentration of ferrite in carbon steel. These areas were subjected to melting and subsequent solidification within the entirety of the weld zone, either with or without limited dilution from the matrix of the weld bead. The presence of these distinct zones is particularly evident in close proximity to the base materials. Figure 3.14c shows visible darker sections, signifying a substantial presence of iron originating from the carbon steel. Additionally, there are lighter areas characterized by a notable concentration of nickel-chromium. The chemical analysis conducted on the microzones depicted in Figure 3.15a highlights the distribution of the primary alloying elements over the cross-sectional area of the weld bead. Due to the significant heterogeneity of the weld bead, the local chemical analysis was repeated three times, and the resulting average data values were taken into consideration.

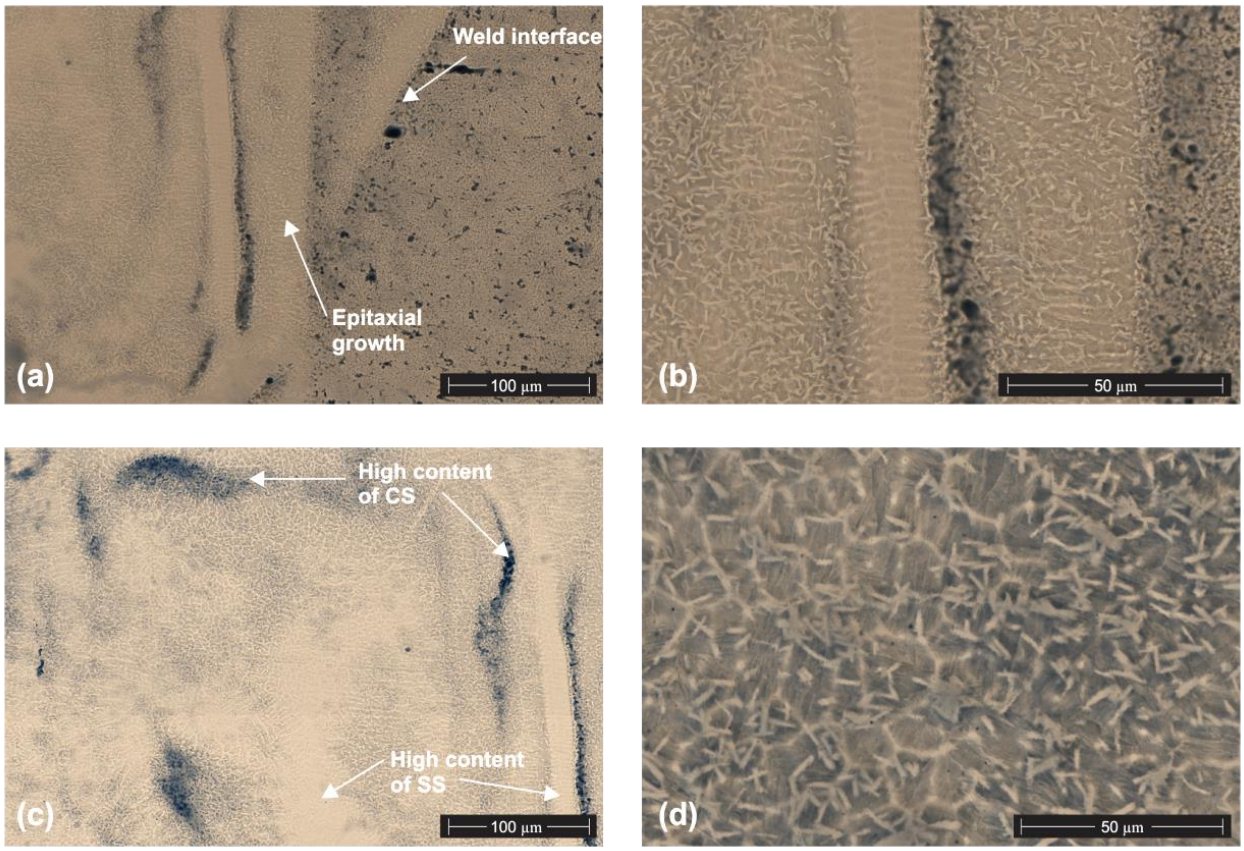

Figure 3.14 SEM microscopy of the sample 3.2 cross-section, (a) weld interface at CS side, (b) higher magnification of weld interface at CS side, (c) distinct regions with higher content of CS and SS, (d) details of the ferrite branches in austenite matrix [STA18].

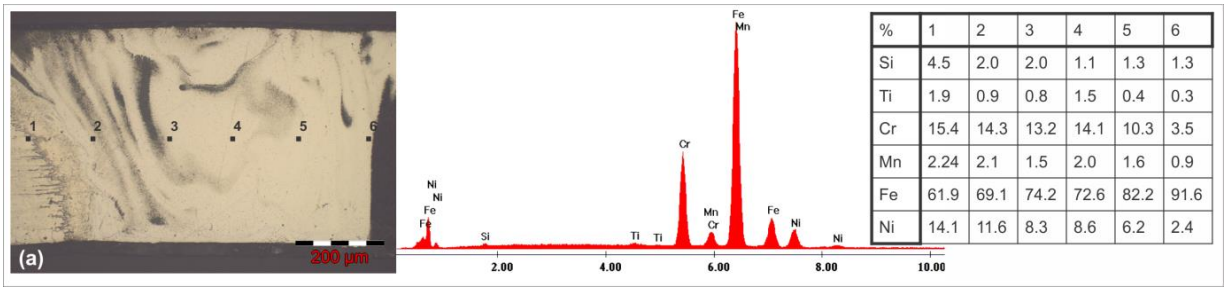

%	1	2	3	4	5	6
Si	4.5	2.0	2.0	1.1	1.3	1.3
Ti	1.9	0.9	0.8	1.5	0.4	0.3
Cr	15.4	14.3	13.2	14.1	10.3	3.5
Mn	2.24	2.1	1.5	2.0	1.6	0.9
Fe	61.9	69.1	74.2	72.6	82.2	91.6
Ni	14.1	11.6	8.3	8.6	6.2	2.4

Figure 3.15 (a) Distribution of the 6 microzones punctually analysed on the cross-section of the 3.1 sample, (b) Energy-Dispersive X-ray spectrum EDS of sample 3.1 microzone 2 [STA18].

The temperature-induced diffusion phenomenon causes a change in the composition of the weld bead as can be observed in the areas closer to the boundary with the base material. This alteration is attributed to the diffusion mechanisms that are enhanced by the temperature. The phenomenon of diffusion is evident in the migration of alloying elements such as chromium (Cr), nickel (Ni), and titanium (Ti) from stainless steel into the weld bead. Additionally, a notable diffusion of iron (Fe) occurs from carbon steel (CS) towards the whole of the weld joint. A noticeable trend of decreasing nickel (Ni) and chromium (Cr) concentrations can be noticed in the region, that are in close proximity to the low alloy steel. The date obtained from the Energy Dispersive Spectroscopy (EDS) analysis indicate that the extent of iron diffusion within the weld bead was less prominent in samples 3.3 and 3.4, which were welded using a lower energy density, compared to samples 3.1 and 3.2.

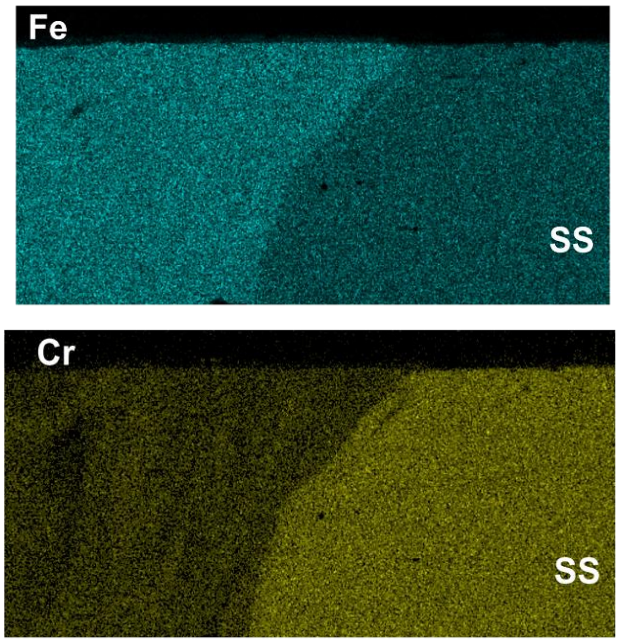

Figure 3.16 EDS mapping of iron and chromium content on the sample 3.1 at the interface with the SS [STA18].

The distribution of iron and chromium on the cross-section profile of the 3.1 sample is highlighted by the chromatic contrast seen in Figure 3.16. The energy-dispersive X-ray spectroscopy (EDS) mapping technique provides a visualization of the spatial distribution of chemical elements present at the weld interface with the stainless steel. The weld zone has high iron concentration as compared to the SS, along with a corresponding drop in chromium levels.

The fast-cooling condition during the laser welding can cause hardening of the welding zone or of the heat affected zone. This phenomenon is potentiated by the fact that no filler material is used, so no beneficial chemical elements can be added into the welding.

The microhardness testing of the welded joints was conducted using a Future-Tech FM-700 tester. The experimental procedure involved applying a load of 100gf and maintaining it for a duration of 10 seconds. Four indentations have been made on every specific region of the weld joint. The hardness investigation was conducted twice in each location due to the significant non-homogeneity of the weld bead.

The microhardness profile of samples 3.1, 3.2, and 3.3 is illustrated in the diagram shown in Figure 3.17. The graphical representation illustrates that both the weld zone and heat affected zone exhibit an higher hardness in comparison to the base materials. It is evident that the heat affected zone near to the carbon steel exhibits a greater level of hardness in comparison to the corresponding zone on the stainless steel side.

The observed outcome is surprising when considering the relative hardness values of stainless steel (248 HV01) and carbon steel (160 HV01). Furthermore, a significant reduction in hardness (250 HV01) was seen in the fusion zone of the stainless steel side. The observed decrease in hardness within the fusion zone (Figure 5b) can be attributed to the rapid cooling rates experienced, which resulted in the transformation of the austenite phase into a ferrite-austenite microstructure characterized by lower hardness values. Mousavi [AKB09] reported comparable results. The increase in hardness observed in the heat-affected zone (HAZ) of carbon steel can be attributed to the transition of the ferrite-pearlite microstructure into a martensite structure, which is facilitated by the significant temperature gradient experienced during the welding process [STA18].

The presence of iron enrichment in the fusion zone next to the carbon steel side, together with a significant concentration of nickel (Ni) and chromium (Cr), has the potential to result in the production of hard FeNi/CrNiFe phases. This is supported by the observation of increased hardness in this particular region.

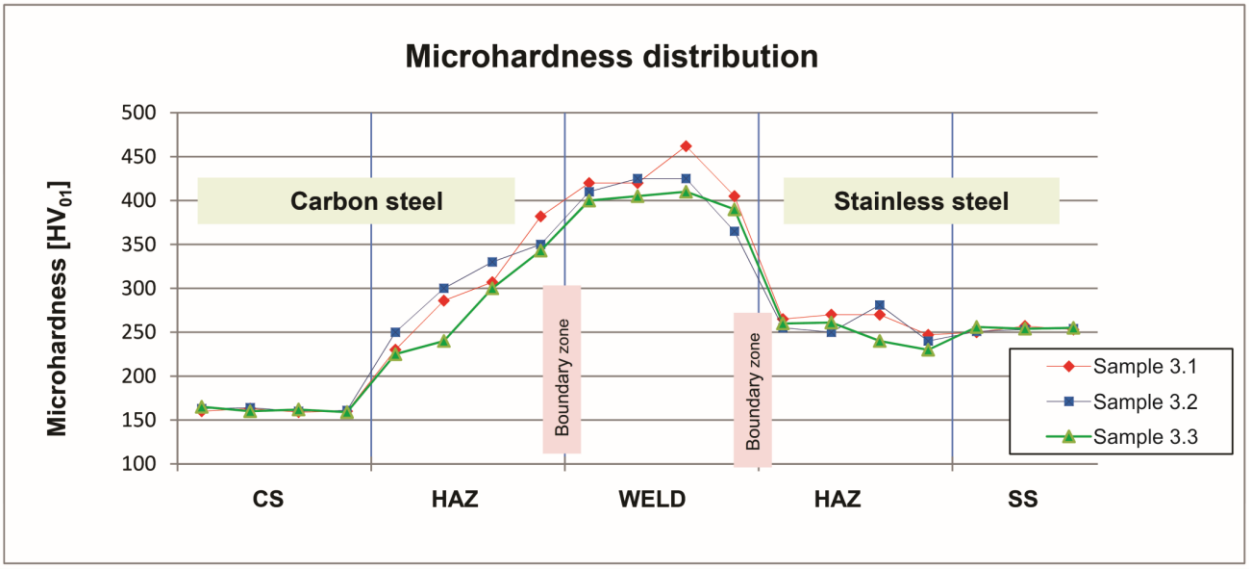

Figure 3.17 Microhardness distribution on the cross-section of the dissimilar butt welding of AISI 1010 and AISI 321 [STA18].

It is worth noting that the hardness profile of all the samples analyzed has a similar trend, as seen in Figure 3.17. A slight reduction in micro-hardness is evident in sample 3.3. Based on the process parameters employed, it can be concluded that the hardness profile is subject to the effect of the energy density, given that the sample was welded using the minimum heat input.

The tensile properties of the heterogenous welds were assessed using a servo-hydraulic universal testing equipment operating at a crosshead speed of 10mm/s under ambient conditions. The transverse tensile tests were conducted on specimens with a width of 15 mm and a length of 120 mm. The fractures of all the tensile testing samples occurred on the carbon steel side, at a significant distance from the heat-affected zone (HAZ) or the welded joint. The specimens experienced fracture when subjected to a force of 3.1 kN and an elongation of 15%.

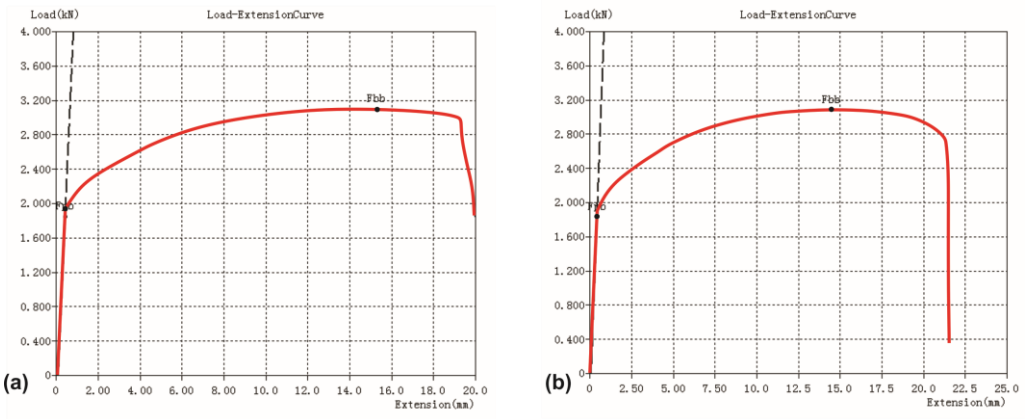

Figure 3.18 Stress-strain curves of dissimilar welded samples 3.1(a) and 3.4(b) [STA18].

Figure 3.18 shows the stress-strain curve acquired from specimens 3.1 and 3.4. In both instances, an acceptable tensile response was achieved, despite the fact that sample 3.4 (as seen in Figure 3.18b) exhibits only partial penetration.

Good results were obtained within the present study of heterogenous laser welding of AISI 1010 – AISI 321 demonstrating that this configuration can be used for various industrial applications. Attention should be paid to mitigation of non-homogeneous regions and on diffusion of iron from the carbon steel into the weld bead. As demonstrated, the laser energy or the total energy introduced into the process can influence the overall composition of the weld bead. As the energy level diminishes, there is a corresponding reduction in the extent of the non-homogeneous region.

Moreover, the hardness profile in the dissimilar welding of AISI 1010 and AISI 321 is also influenced by the diffusion of iron from the carbon steel. This diffusion process can result in the formation of intermetallic phases with the alloying elements, ultimately leading to an overall elevation in hardness. The presence of elevated iron content leads to an increase in hardness, mostly attributed to the production of hard phases such as FeNi/CrNiFe.

3.3 Dissimilar laser welding of stainless steel and carbon steel with active flux

It becomes obvious that controlling the input energy in the laser welding process is crucial to mitigating most of the drawbacks associated with laser processing. It is recommended to avoid the risk of material overheating and the use of excessive cooling rates in welding processes.

One method is to restrict the energy employed in laser processing; nevertheless, it should be noted that there is a minimum threshold below which the energy supplied will not be enough to cause material melting.

In order to reduce laser energy, it is important to enhance the capacity of the materials to absorb the laser radiation. By doing so, a lower amount of energy will be required for melting or processing the materials.

3.3.1. Concept Overview

There are two methods for reducing the input of the laser energy.

1. By using a pulsed laser

2. By increasing the absorbance of the materials surface. Both solutions can be used for laser welding processes.

Assuming that, I have used a pulsed laser to obtain heterogenous welding between AISI 321 and S235 carbon steel and also, I used an active flux for fine tuning the weld bead composition [STA19].

By using the active flux (SiO_2 + Poly (vinyl alcohol)) I aimed to increase the laser absorption and also to promote the formation of ferrite during the solidification of the weld bead. A less plasma plume and a narrower weld bead profile is also aimed by using the SiO_2 active flux.

3.3.2 Methodology, Resources, and Outcomes

As described in the introduction of this chapter, pulsed lasers provide advantages in terms of reduced energy input and the potential for modulating the shape of the laser pulse. Despite a reduced energy, the characteristics of the molten bath exhibit variations when compared to those achieved with continuous lasers, mostly due to the generation of shock waves induced by each individual pulse. Because of that, the weld zone is susceptible to the phenomenon of hardening and the formation of regions with incomplete mixing.

To further research and improve the heterogenous laser welding process I have been used a pulsed laser, namely TRUMPH TruePulse 556 and a welding module PRECITEC YW 50 at 200 mm focal distance to fabricate fusion lines and welding samples with and without active flux. Experimental tests were performed on plain sheets of carbon steel (S235) and stainless steel AISI 321, with dimensions of 50x100x0.5. The chemical composition of both materials is presented in Table 3.7.

Chemical composition of the carbon steel and stainless-steel Table 3.7.

Material	Element wt. (%)								
	C %	Si %	Mn %	P %	S %	Cr %	Ni %	Mo %	Ti %
S235	0.099	0.168	0.51	0.003	0.006	0.043	0.041	0.002	-
AISI 321	0.08	1	2	0.045	0.03	18	11	-	0.15

The active flux was produced by combining SiO_2 and Polyvinyl alcohol in a proportion of 15%.

Each plate was submerged in the active flux solution, ensuring that both sides were covered, and after that allowed to air dry at room temperature for a duration of 2 hours.

The experimental tests were conducted in the same laboratory as the previous ones, employing the CLOOS 7-axis robot for the manipulation of the PRECITEC YW 50 welding module.

The same clamping system was used to position and fix the test plates in a butt joint configuration. Argon gas, with a purity level of 99.99%, was used to provide shielding for both the top and root parts of the weld bead. The shielding of the weld bead root was achieved via a channel that was machined into the clamping device, as seen in Figure 3.19a. Before performing the welding tests, a series of fusion lines were made on a 1.5 mm AISI 321 stainless steel sample. The goal was to determine the effect of the SiO_2 mixing ratio and the range of process parameters on the welding results. The initial experimental results indicate that the laser power may be adjusted within the range of 2000 to 2500 W while maintaining a constant frequency of 150 Hz.

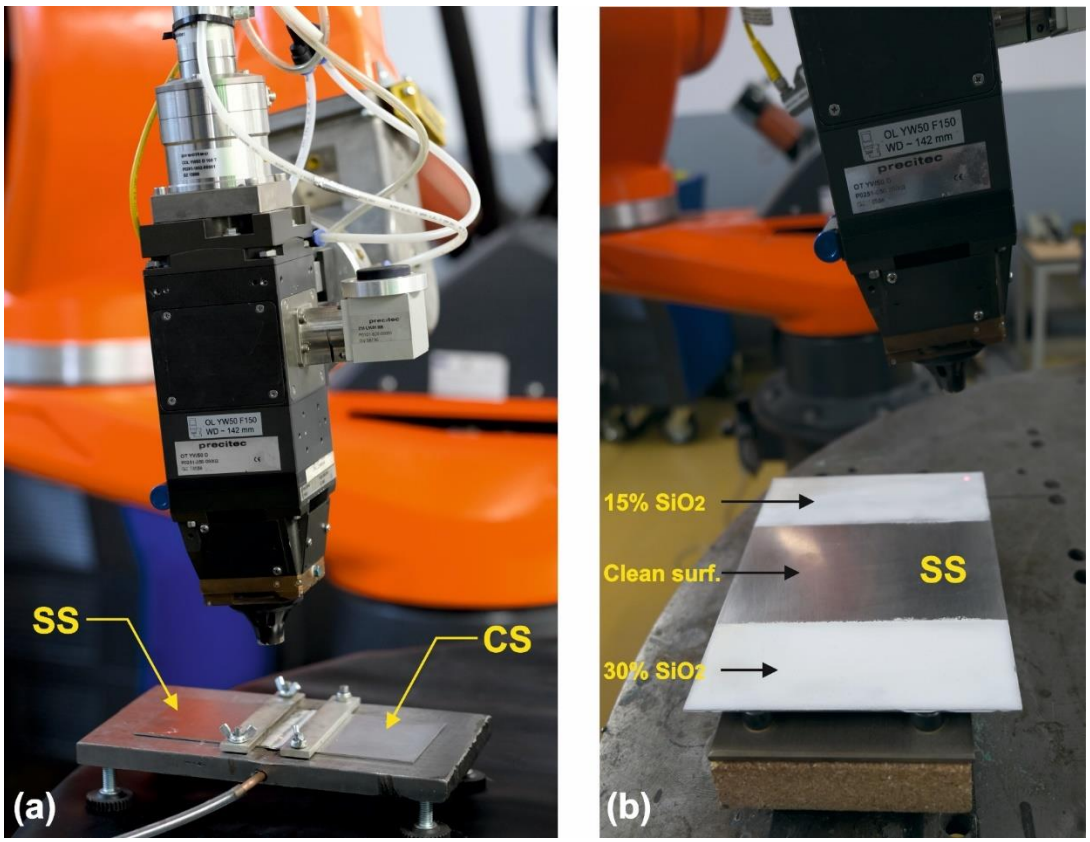

Fig. 3.19 Set-up used for the experimental tests, a) fastening device for welding of carbon steel - stainless steel, b) stainless steel plate with 15 % SiO_2 and 30% SiO_2 active fluxes. "Advanced Welding Ecotechnology R&D Center" from Transilvania University of Brasov [STA19].

The parameters summarized in the table 3.8 have been chosen for the final tests in order to emphasize the influence of the active flux. Increasing of the welding speed was necessary to not over-melt the weld bead.

Laser welding parameters Table 3.8

PARAMETERS	UNITS	SAMPLE	
		1 – without active flux	2 – with SiO_2 active flux
Laser power	W	2300	2000
Frequency	Hz	150	150
Pulse duration	ms	1	1
Welding speed	cm/min	73	90

The samples were cut using a hydraulic machine and then prepared for analysis by polishing and electrochemical etching in a solution consisting of 10% oxalic acid in water. The specimens were analysed using an LEICA DM ILM LED inverted optical microscope and a scanning electron microscope (SEM) model Quanta FEG 250, manufactured by FEI in the Netherlands, operating at 30 kilovolts (kV).

Silicon dioxide (SiO_2) functions as an oxidizing flux and acts as an acceptor of free oxide ions (O^{2-}). The activator flux facilitates the introduction of increased concentrations of oxygen and silicon into the weld bead. A certain quantity of oxygen can lead to the development of oxide particles, which in response can enhance the creation of acicular ferrite, resulting in improved welding toughness [SIN03]. However, excessive oxygen content has several negative effects on the mechanical properties and susceptibility to cracking of the weld bead.

Excessive silicon content in the weld bead can lead to the hardening of the metal matrix, hence reducing the toughness of the welded junction. The decomposition of SiO_2 occurs as a result of the elevated temperatures achieved during laser welding, as stated in reference [SIN03].

$$SiO_2 = SiO(g) + 1/2\ O_2\ (g) \qquad (3.3)$$

The equation (3.3) represents the reaction in which SiO_2 decomposes into SiO gas and half of an O_2 gas molecule.

Two different mixing ratios of SiO_2 to polyvinyl alcohol (15% and 30% by weight of SiO_2) were used in order to determine the most favourable composition for the activator flux. The objective is to enhance the depth of penetration while avoiding excessive saturation of the

molten bath with oxidizing agents. Moreover, the quality of the welding is significantly affected by the stability of both the welding process and the plasma plume. Consequently, first experiments were conducted on a stainless-steel plate with a thickness of 1.5 mm. The plate was coated with active flux containing 15% and 30% SiO_2. After that, five fusion lines were created to determine the impact of the active flux, as seen in Figure 3.20. The fusion lines were created using a constant speed of 80 cm/min, pulse length of 1 ms, and frequency of 120 Hz. The power was gradually raised from 1500 to 3500 W in increments of 500 W, with each line representing a different power level (line 1 - 1500 W, line 2 - 2000 W, line 3 - 2500 W, line 4 - 3000 W, and line 5 - 3500 W) [STA19].

Lines/samples 1 and 2 will not be further elaborated upon as they exhibit a lack of surface melting or absence of melting altogether.

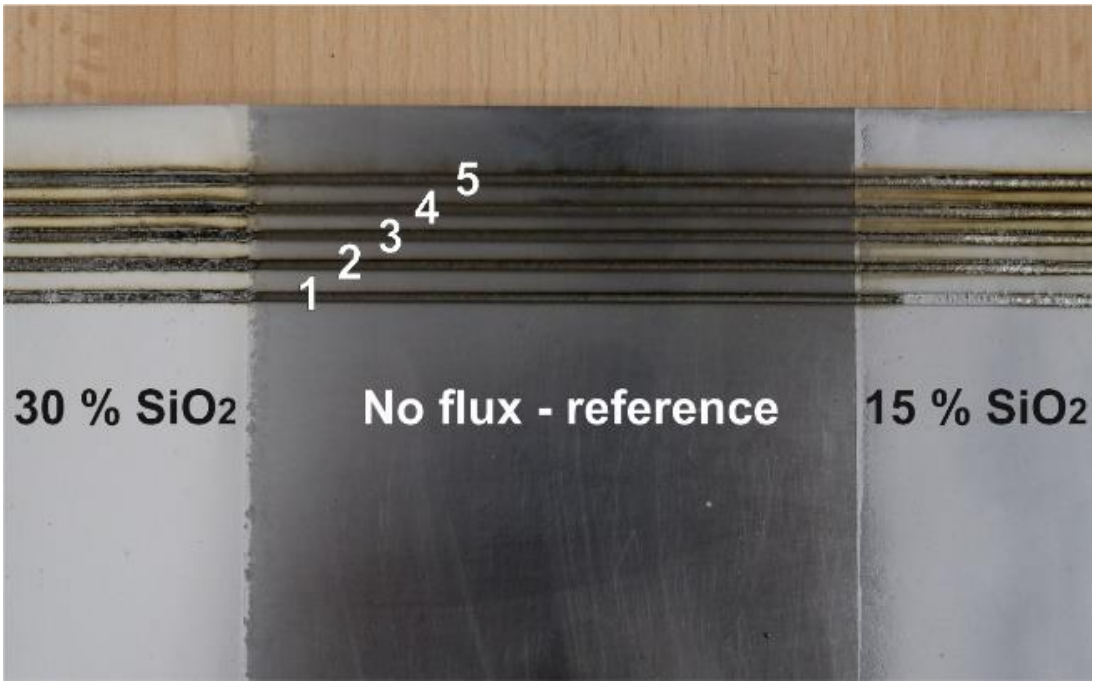

Figure 3.20 Fusion lines realized on stainless steel plate with different content of the SiO_2 flux [STA19].

The impact of active flux on the geometrical profile and microstructure of the melt region it can be seen in figure 3.21 The utilization of an active flux enhances the laser absorption process and results in the formation of a more pronounced key-hole profile of the melt zone, despite the fact that the depth of the melt is comparatively less in relation to the reference samples. At the same time the presence of SiO_2 influences the solidification pattern and facilitates the production of ferrite phase (as seen in Figure 3.22b), characterized by the presence of vermicular and lathy ferrite, rather than austenite phase.

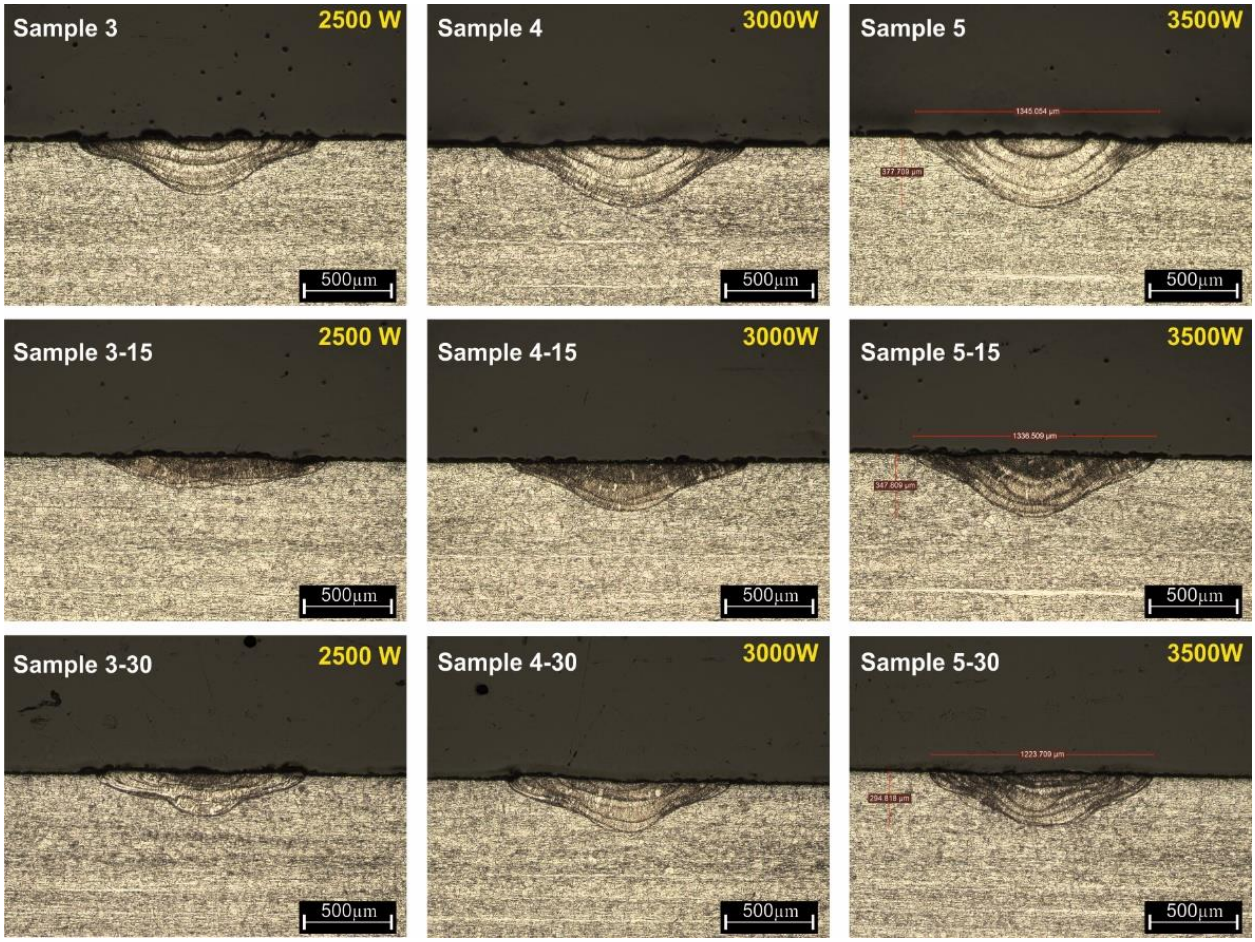

Fig. 3.21 Cross-section of the fusion lines realized with 15% and 30% SiO_2 flux (3, 4 and 5 reference sample without flux, sample 3-15, 4-14 and 5-15 with 15% SiO_2, sample 3-30, 4-30 and 5-30 with 30% SiO_2) [STA19].

The fusion zone observed in the reference sample (as shown in Figure 3.22a) has an austenitic shape, wherein the development of austenite grains can be observed originating from the unmelted austenite grains present in the substrate. The orientation of growth is parallel to the temperature gradient generated by the laser. The fusion zones generated with the addition of SiO_2 show a microstructure characterized by a mixture of lathy and skeletal ferrite morphologies. These morphologies are clearly visible as darker structures in figure 3.22b. The presence of acicular ferrite is advantageous in the context of welding stainless steel, whether in similar or dissimilar joint configurations, since it enhances toughness.

The analysis of the data shown in Figure 3 indicates that an increased concentration of SiO_2 has the potential to decrease the depth of the fusion line. Hence, the utilization of an active flux containing 15% SiO_2 exhibits superior results in relation to weld depth and the development of microstructure.

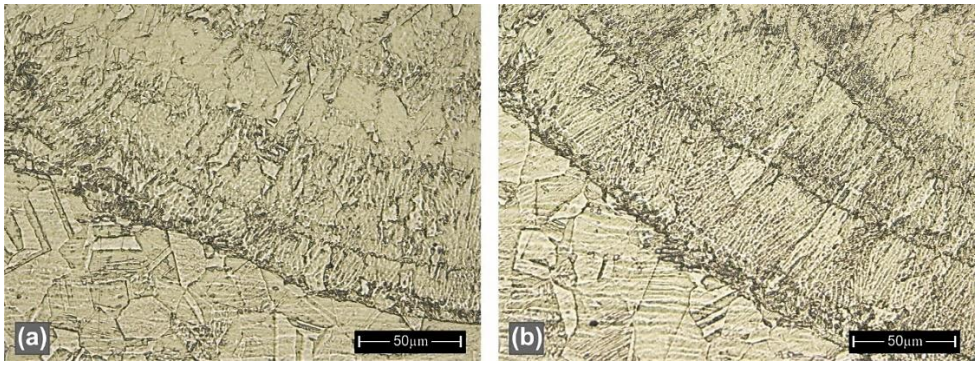

Fig. 3.22 Image of the reference fusion line (sample 5) and the fusion line with 15% SiO_2 addition (sample 5-15) [STA19].

Table 3.8 shows the optimal settings for heterogenous welding of stainless-steel carbon steel based on the obtained data. Figure 3.23 show the laser welding joints with and without active flux. In the case of the sample welded with 15% SiO2 active flux, the weld bead and heat affected zone are smaller.

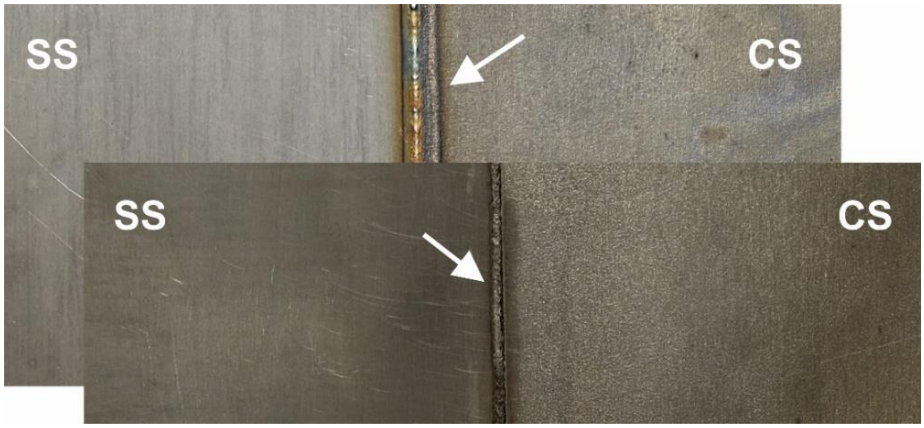

Fig. 3.23 Image of the dissimilar laser welding with and without the SiO_2 flux; SS-stainless steel, CS-carbon steel [STA19].

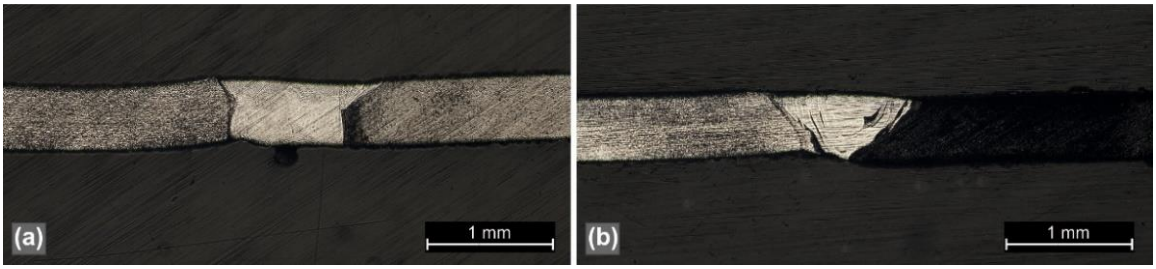

Fig. 3.24 Macro image of the weld bead cross-section; a) reference sample, b) sample obtained with the addition of SiO_2 flux [STA19].

In order to achieve good tensile properties, it is necessary to have full penetration in butt welds of thin sheets. Figure 3.24 shows that complete penetration was attained in the case of CS-SS laser welding with and without the inclusion of SiO_2. The geometrical profile of the weld bead analysis reveals that SiO_2 flux reduces the heat affected zone of the weld joint on the

stainless steel - carbon steel side. Furthermore, by employing the 15% SiO_2 flux, the laser power may be reduced by about 18%. In the case of SiO_2 active flux addition, full penetration welding with narrower with and smaller heat affected zone was produced.

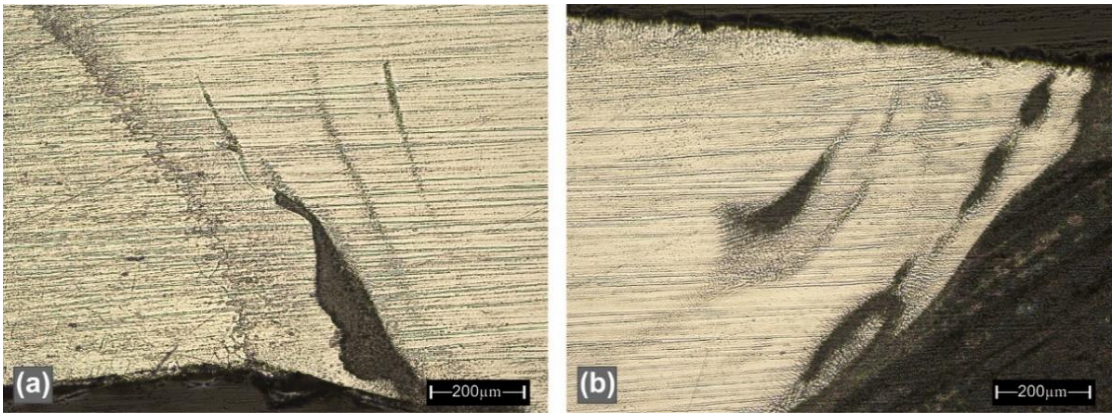

Fig. 3.25 Macro image of the weld bead sample with the addition of SiO_2 flux [STA19].

Figure 3.25b shows visible darker areas that indicate a significant presence of ferrite diffused from the carbon steel. Additionally, there are lighter areas with a notable concentration of nickel-chromium. Figure 3.26 displays a high magnification scanning electron microscopy (SEM) image highlighting the ferrite branches that are surrounded by the austenite matrix. The microstructural transformation within the weld bead is characterized by a transition from a fine equiaxed ferrite structure to an orientated skeletal ferrite morphology at the contact with the carbon steel.

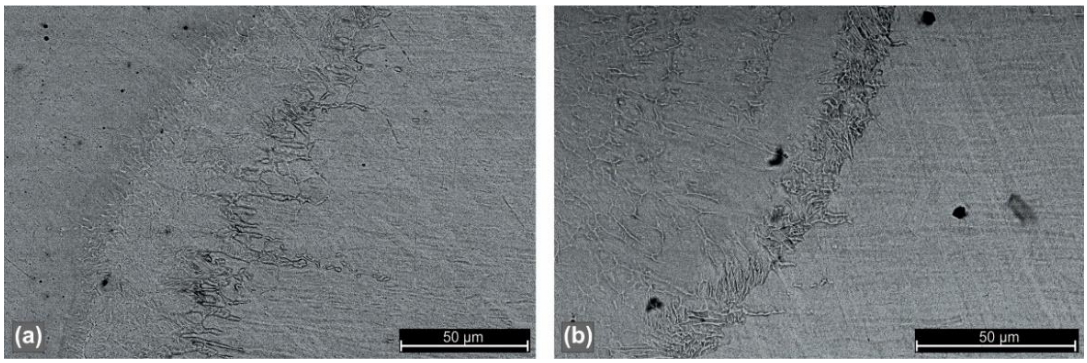

Fig. 3.26 Electron microscopy of the weld bead near the stainless-steel side, with (a) and without SiO_2 (b) [STA19].

As shown, the utilization of a 15% SiO_2 active flux in heterogenous laser welding of AISI 321 – S235 steel has been shown to result in a significant decrease of laser power, approaching around 18%. Achieving an appropriate balance between laser power and welding speed is crucial in order to obtain a defect-free dissimilar joint.

CHAPTER 4. LASER PROCESSING OF ADVANCED MATERIALS

4.1 FeCrAl alloys

FeCrAl alloys are known for their superior high-temperature oxidation resistance, mechanical strength, and corrosion resistance. These alloys are integral in aerospace, automotive, and energy sectors, enduring elevated temperatures and aggressive environments. Comprising mainly iron (Fe), chromium (Cr), and aluminum (Al), FeCrAl alloys can be further alloyed with elements like yttrium (Y) and silicon (Si) to enhance specific properties. The composition is finely tuned to obtain an optimal balance between oxidation resistance and mechanical strength. The microstructure of FeCrAl alloys is characterized by a fine-grained, homogeneous distribution of constituent elements. Chromium forms a protective oxide layer (Cr_2O_3) on the alloy surface, preventing further oxidation and ensuring long-term stability at high temperatures. Aluminum enhances oxide layer adhesion and thickness, contributing significantly to the alloys' exceptional corrosion resistance.

The FeCrAl alloys exhibit increased resistance to oxidation at elevated temperatures, as result of the protective chromium oxide layer formation when exposed to oxidizing environments. This oxide layer acts as a barrier, preserving the material's structural integrity even at temperatures exceeding 1000°C [KEV17].

The FeCrAl alloys are mainly used in the manufacturing of heating elements, industrial furnaces, electric ovens, and in various components within automotive and aerospace industry that involve combustion or exhaust systems. Also, the alloys can be used in nuclear power plants due to their good resistance to neutron irradiation, which is a critical factor in nuclear applications.

Lately, the FeCrAl alloys have gained significant attention in the context of modern 4R (Robust, Resilient, Reliable, and Resource-Efficient) nuclear reactors due to their mechanical and chemical properties that make them suitable for hardest exploitation conditions within these reactors that use water and liquid metal coolants like lead (Pb), lead-bismuth eutectic (Pb-Bi), and tin (Sn).

As principal investigator in the project Advanced Metallic Materials for New Generation Nuclear Power Plants, 4R, NUCLEARMAT I have been involved in designing the technology for laser surface treatment of innovative FeCrAl alloys to increase the corrosion resistance in melted lead cooling media.

4.1.1 Theoretical Basis

One of the major challenges of the modern nuclear reactors is the cooling media used for controlling the temperature. Lead has a high boiling point of 1749°C (3180°F), which allows it to remain in a liquid state at very high temperatures preventing boiling and thus ensuring stable operation under extreme conditions. Moreover, lead is chemically stable and has low reactivity with air and water at high temperatures, reducing the risk of corrosion and chemical reactions with reactor materials. Besides all the advantages and low reactivity of lead in normal conditions, at high temperatures, lead can react with the surface of FeCrAl alloys, potentially leading to corrosion.

The common FeCrAl alloys have approximately 70-72% iron (Fe), 20-22% chromium (Cr), 4-6% aluminum (Al) in which the chromium is the key element responsible for the corrosion resistance. Chromium oxide (Cr_2O_3) is highly stable and possesses excellent corrosion resistance properties, even at high temperatures and in conjunction with Aluminium oxide (Al2O3) form a stable oxide layer that leads to passivation, a phenomenon where the material becomes resistant to further corrosion. For nuclear application the protective oxide layer should be continuous and sufficiently thick, in order to effectively isolate the alloy from the corrosive medium.

To enhance oxidation resistance and prevent exfoliation, the FeCrAl alloys can be alloyed with reactive elements like Y, Hf, Zr, Ti, Ce, and La, which form stable sulphides improving the adhesion of the protective layer. Related to this, I have collaborated with the research members of the ERAMET and LAMET laboratory for designing new types of FeCrAl fine alloyed with Yttrium Titanium and Zirconium and good results have been obtained in term of enhance the oxidation resistance at elevated temperatures. Moreover, superior adhesion of the oxide layer to the substrate was obtained by varying the type and concertation of the alloying elements.

However, challenges arise due to surface roughness influenced by factors like temperature and working medium nature [GEA20, VOI18]. FeCrAl alloys, used in 4R generation nuclear power plants with new efficient cooling media such as Lead and Bismuth, require strict control of oxygen content. Surface processing techniques like alumina-rich layer deposition and laser surface remelting are currently researched for increasing the corrosion resistance.

Laser surface engineering enables precise modifications in surface texture, roughness, and microhardness, promoting grain refinement and increasing of the oxide's layers.

4.1.2 Key concept

Based on the experience gained in the laser technology, I applied the laser surface melting to refine the subsurface microstructure grains of the FeCrAl aiming a better compactness necessary to increase the resistance to dissolution of the alloy in the high-temperature working environment [GEA20]. Special designed alloys with various concentrations of Cr and Al have been subjected to laser processing in order to determine the influence of the Cr and Al on the corrosion resistance of the alloy.

4.1.3 Methodology, Resources, and Outcomes

The FeCrAl alloys were realised at Eramet laboratory within UPB Romania (Politehnica University of Bucharest). The new FeCrAl alloys with tailored designs were developed under the project Advanced Metallic Materials for New Generation Nuclear Power Plants, 4R, NUCLEARMAT [GEA20]. The production of the alloys was carried out using the vacuum arc remelting technique inside an argon protective environment, as described in the previous studies [GEA19]. The raw materials employed for obtaining the FeCrAl exhibited a high level of purity. Specifically, the steel utilized was of the MK3 brand, that is known for its exceptional softness.

The composition of the steel was as follows: carbon (C) content of 0.02%, silicon (Si) content of 0.04%, manganese (Mn) content of 0.21%, sulphur (S) content of 0.02%, phosphorus (P) content of 0.015%, nickel (Ni) content of 0.2%, chromium (Cr) content of 0.15%, molybdenum (Mo) content of 0.07%, copper (Cu) content of 0.14%, aluminium (Al) content of 0.12%, with iron (Fe) constituting the remaining balance. Furthermore, to complete the alloy was used metallic chromium, with a minimum purity of 99% (Cr), and electrolytic aluminium, with a minimum purity of 99.5% (Al).

Chemical composition of FeCrAl alloys Table 4.1.

Sample	Chemical composition, wt.%			
	Cr	Al	Fe	Other elements*
S1	8.3	6.2	80.9	4.5
S2	10.7	5.1	83.1	1.1
S3	13.9	4.1	81.1	0.9
S4	16.2	4.1	78.8	0.9

*The designed alloys are in ongoing patent procedure

In order to obtain a uniform composition of the alloy, every sample underwent a process of rotation and melting, repeated three times on both sides. The FeCrAl alloy samples, labelled as S1 to S4, were subjected to chemical analysis using a Spark Optical Emission Spectrometer - SPECTROMAXx M. The composition of these samples is provided in Table 5.1. The obtained alloys were machined prior to laser processing as depicted in figure 4.2.

The surface processing and remelting of FeCrAl samples was conducted using a 1kW continuous wave diode laser manufactured by Coherent. This laser emits near-infrared light at a wavelength of 975 nm with a maximum divergence of 56 mm*mrad. A six-axis CLOOS robot, equipped with a YW50 Precitec laser processing head, was utilized for precise processing. In order to ensure the protection of the laser optical system, the processing head was inclined at a minimum inclination of 4°.

The melted bath was protected by coaxially supplying Argon gas within the laser beam at a flow rate of 6 l/min. Negative defocusing, as depicted in Figure 5.1, was achieved by adjusting the distance between the processing head and the material's top surface. A consistent stand-off distance of 6mm was maintained for all experimental tests. The key parameters of the laser processing regimen are detailed in Table 4.2.

The investigation focused on determine the effects of laser irradiation on the characteristics of the remelted region. Two different processing parameters, or regimes, were employed for each sample in order to analyze their respective impacts.

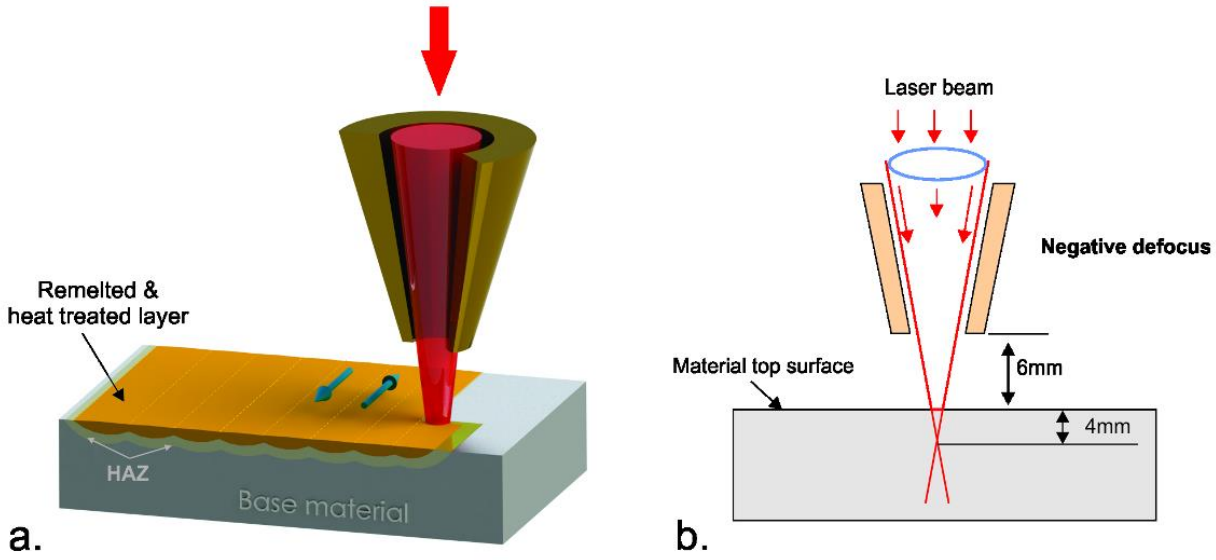

Figure 4.1. Schematic of the laser processing/remelting process: a) laser system movement for surface remelting; (b) positioning the laser head and focus point in relation to the metal surface [GEA20].

Laser processing parameters Table 4.2.

Parameters / Regime	Power [W]	Processing speed [cm/min]	Spot diameter [mm]	Gas flow (Ar) [l/min]	Stand-off distance [mm]
1	320	80	1.1	7	6
2	500	80	1.1	7	6

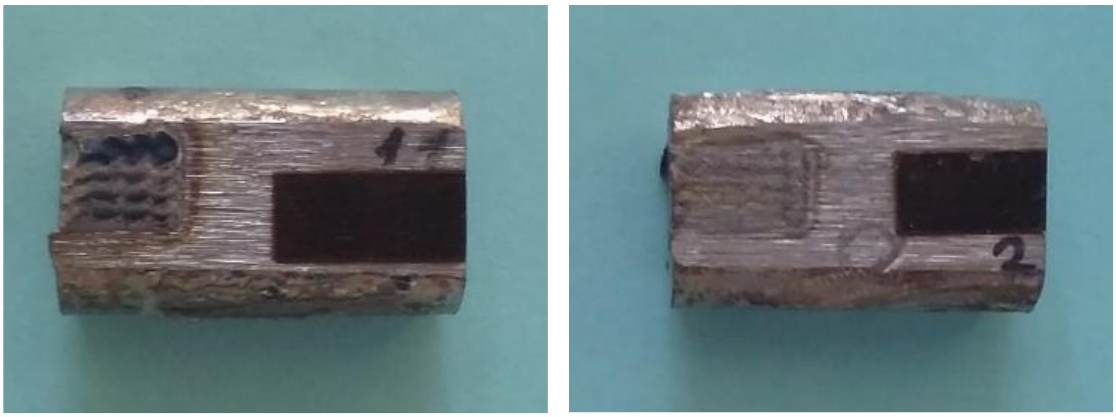

Figure 4.2. Surface of the processed samples with laser; a) regime 1; b) regime 2 [GEA20].

After laser processing, the specimens were prepared for microstructural investigation by cutting with high-precision discs using the IsoMet 4000 cutting machine. Then were immersed in phenolic resin and sanded using metallographic paper with grit levels ranging from 360 to 1200, before polishing with alpha alumina powder (Topol1-3, particle diameters varying from 3 to 0.1 microns). An electrochemical etching in a solution of 10% oxalic acid in distilled water was used for 15 seconds to highlight the microstructure of the remelted areas and to evaluate the penetration depth. The metallographic study was carried using an Olympus GX51 optical microscope assisted by a study image processing software. Further in-depth analyses were performed utilizing an FEI SEM Inspect S electron microscope equipped with a Z2e EDAX analyser.

The as-cast microstructure was revealed by analysing of the test samples, which was characterized by coarse polyhedral grains of heavily alloyed ferrite. The microstructure is characterized by fine dendrites oriented in the direction of heat flow in sections remelted with a laser, keeping the original grain boundaries of the base material (Figure 4.3, optical microscopy - OM). The impact of laser processing on FeCrAl alloys was assessed using scanning electron microscopy (SEM) and energy-dispersive X-ray spectroscopy (EDAX) analysis to determine the chemical compositions of the laser remelted regions and their surrounding areas.

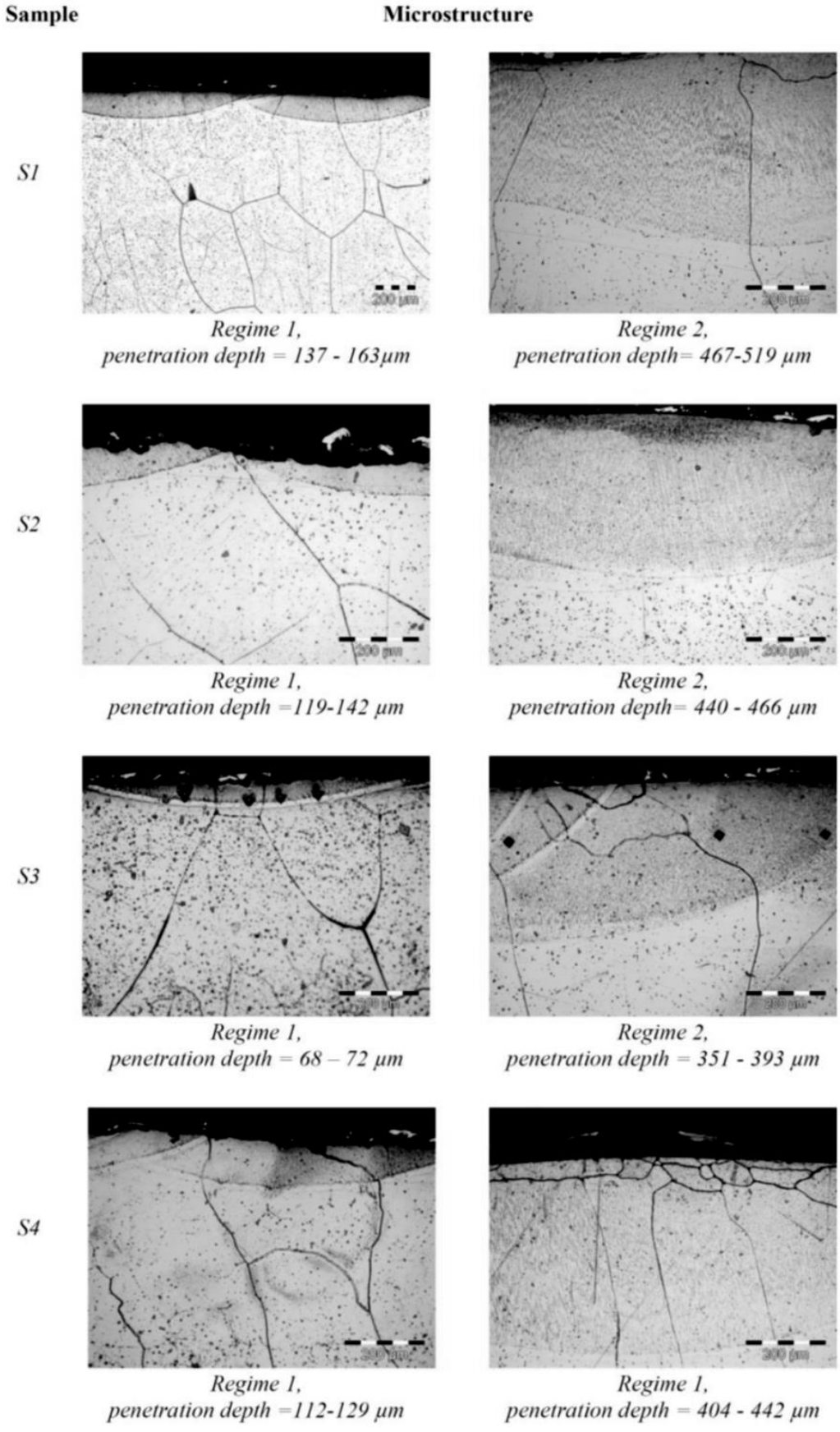

Fig. 4.3. Cross-section profiles of laser-processed regions of FeCrAl alloys using optical microscopy (OM) [GEA20].

Laser melting depth measurements were performed with the same magnification (200x) to permit comparisons between the results obtained. The chromium concentration in the examined samples rose from 8.3 wt.% to 16.2 wt.% Cr, whereas the aluminium concentration declined from 6.2 wt.% to 4.1 wt.% Al.

Laser surface processing of samples S1–S4 resulted in different thicknesses of melted layers depending on laser power and alloy chemical composition. Melting depths ranged from 68 μm (sample 3) to a maximum of 163 μm (sample 1) when a laser power of 320W was used. When the laser power was increased to 500W, the melting depth increased from 393 μm (sample 3) to 519 μm (sample 1). The melting depth is mostly determined by the chromium concentration, a refractory metal that reduces the alloy's heat transfer coefficient [GEA20].

Furthermore, by dissolving in iron (producing highly alloyed ferrite) and encouraging the development of complex carbides, chromium adds to the increase in hardness. The microstructure of laser-remelted layers is characterised by fine and uniform dendritic structures.

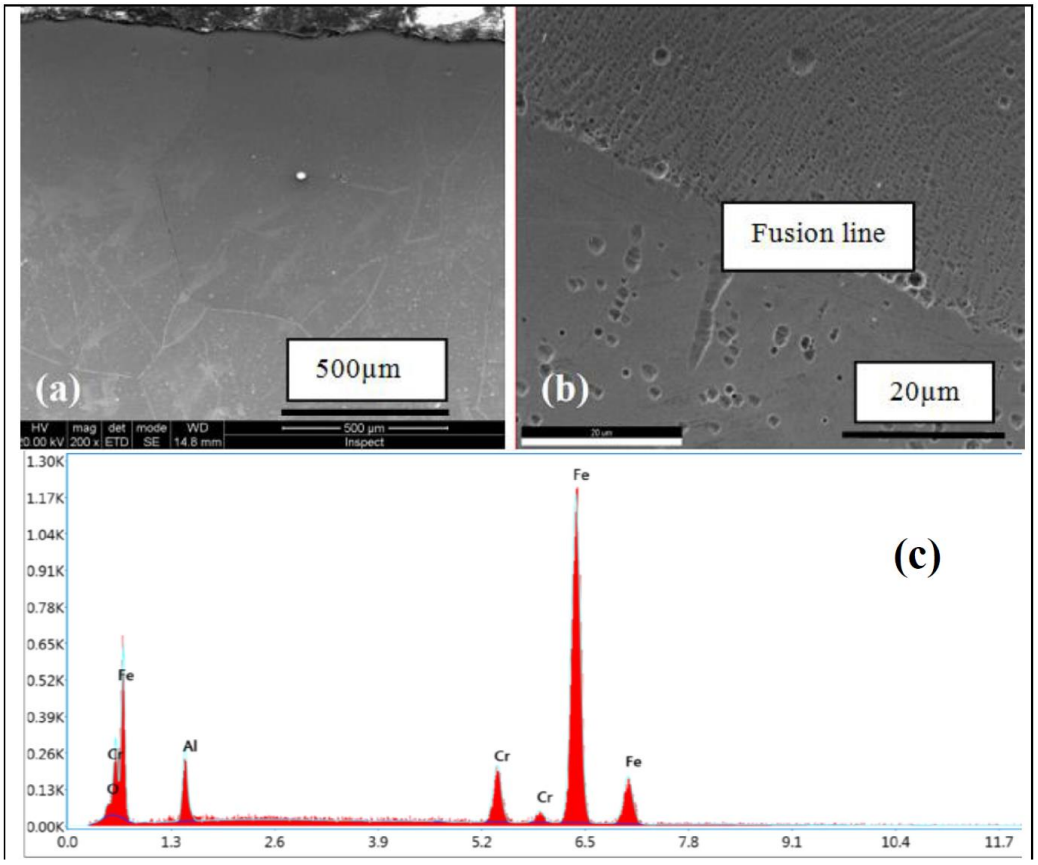

Fig. 4.4 Laser processed area analysis of S1 cross sections: a) the laser-processed region, b) information on the interface between the remelted area (top) and the unprocessed base material (bottom), c) EDS spectrum of the components found in the laser-processed area [GEA20].

At 320 W the surface profile is more irregular compared with the surface appearance obtained with a power of 500 W. In the case of Sample 1 (Figure 5.4), there is a minor increase noticed in the Cr concentration (from 9.7 to 9.92 wt.%) and Al concentration (from 6.54 to 6.93 wt.%).

Chemical compositions on micro-zones determined by EDAX analysis for the laser remelted area

Table 4.3.

ELEMENT	WEIGHT %	ATOMIC %	ERROR %
O K	0.46	1.49	37.98
AL K	6.54	12.44	10.66
CR K	9.7	9.57	5.44
FE K	83.29	76.51	2.45

Chemical compositions on micro-zones determined by EDAX analysis for the base material

Table 4.4.

ELEMENT	WEIGHT %	ATOMIC %	ERROR %
O K	0.27	0.86	75.98
AL K	6.72	12.81	10.51
CR K	9.58	9.48	5.42
FE K	83.43	76.84	2.43

A reduction in grain size has been noticed in the laser remelted regions, resulting in a refinement of grains by a factor of two (from an average diameter of 400 μm to around 200 μm). The observed spike in oxygen concentration in the remelted region proof that the surface layer had an addition of oxygen during laser processing. This addition of oxygen has positive effects on improving the material's capacity to withstand elevated temperatures in corrosive-erosive metallic conditions.

The development of chemical concentration stays in the same domain when a laser power of 500W is used, with a steady drop of Cr (9.35 wt.%) and Al (6.52 wt.%). A similar microstructure and chemical composition development was found in Sample 2 (Fig. 4.5). The concentrations of chromium and aluminum in the laser remelted layer were: Cr (10.93 wt.% to 11.01 wt.%); Al (5.68 wt.% to 5.78 wt.%), which were near to the concentrations measured in the transition zone via base material, i.e. Cr (10.95 wt.% to 11.11wt.%) and Al (5.7 wt.% to 5.72 wt.%). The oxygen content in the laser-remelted layer was 0.39 weight percent O. These chemical concentrations are all equivalent to the base material (Table 4.1) [GEA20].

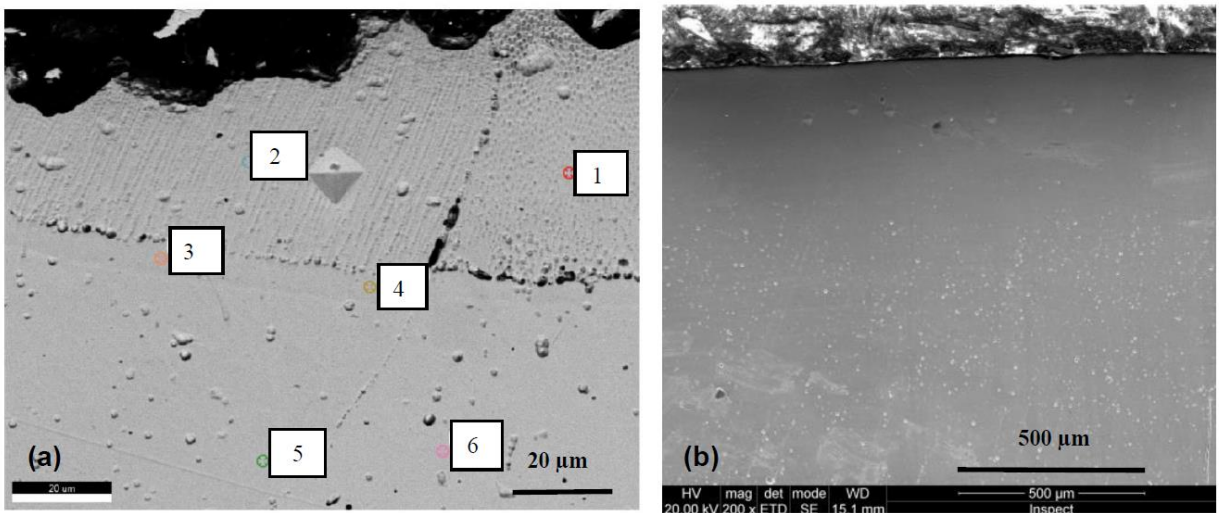

Figuure 4.5. Cross sections of the laser processed layers of Sample 2: a) regime 1, b) regime 2

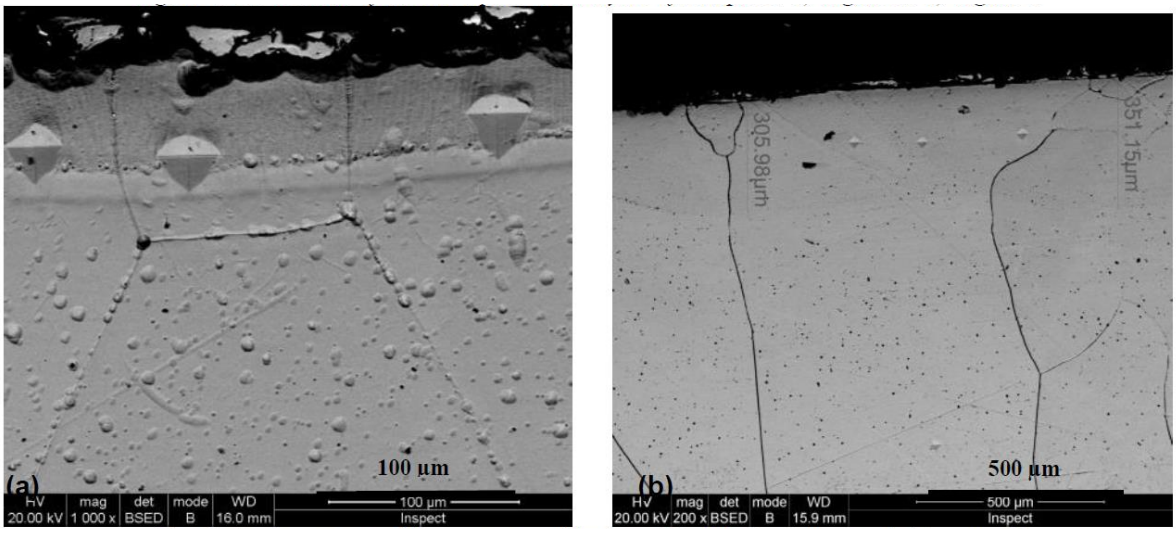

Figure 4.6. Cross sections of laser processed layers of Sample 3: a) regime 1, b) regime 2

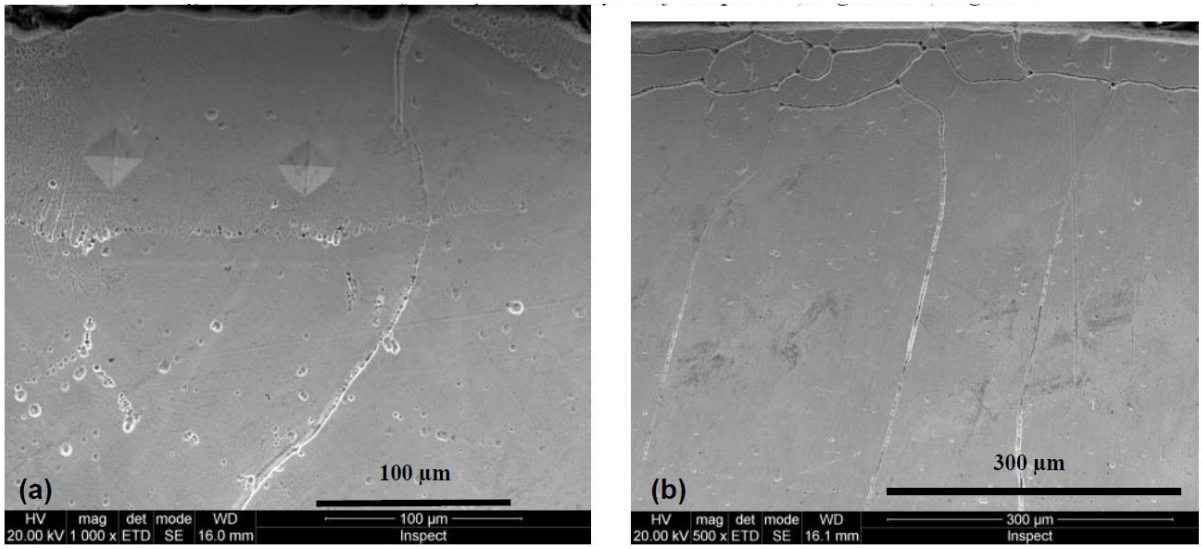

Figure 4.7. Cross sections of laser processed layers of Sample 4: a) regime 1, b) regime 2 [GEA20].

The difference in the smoothness of the cross section profile is clearly obvious for both Samples 2 and 3 (S2 and S3) (Fig. 4.6), for various levels of processing laser intensity. The variation is caused by the melted metal's surface tension, which is affected by temperature and cooling speed. A smoother surface was obtained with a higher temperature and a longer maintaining time.

The concentrations of the main chemical elements in Sample 3 were: Cr (15.86 wt.% - 16.17 wt.%); Al (4.67 wt.% - 4.75 wt.%). The oxygen content in the laser remelted layer was 0.61 weight percent O. Pores, situated at the grain boundary or in the remelted region, were found as an unfavorable result in both samples 2 and 3. Sample 4's microstructure indicated a recrystallization effect (small grain formation) in the laser remelted zone (Figs. 7 and 8). This effect was seen in Sample 3 as well, albeit only in a limited region (Fig. 4.3, Sample 3, regime 2).

The surface profile was smooth in both regimes 1 and 2. The concentrations of the main chemical components in this situation were as follows: Cr (17.71 wt% for regime 1 and 18.28 to 18.55 wt% for regime 2); Al (4.12 wt% for regime 1 and 3.85-4.15wt% for regime 2). The oxygen content in the laser remelted layer was 0.64 weight percent O.

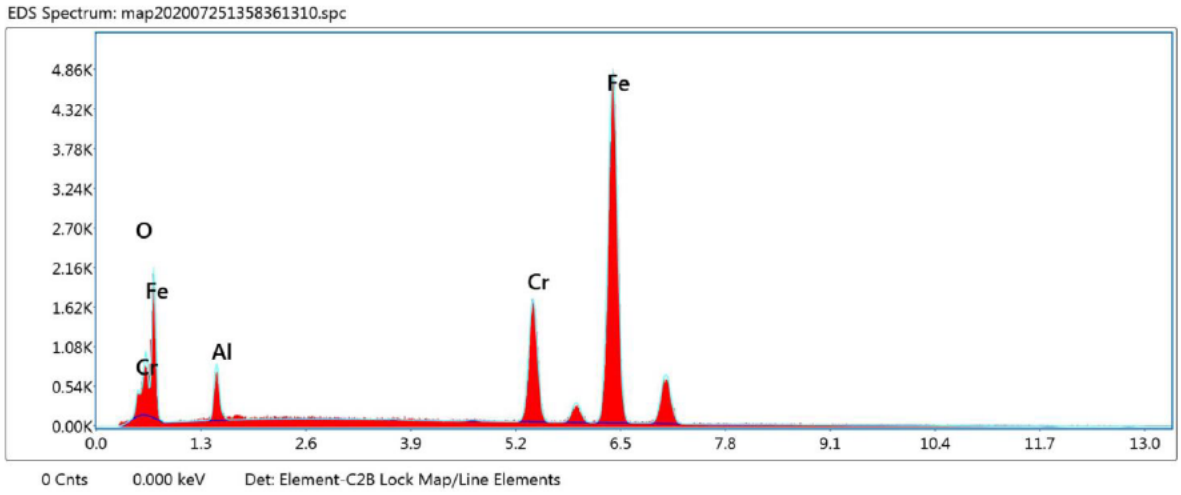

Figure 4.8. EDS spectrum of the elements identified in the laser processed area of Sample 4 [GEA20]

Microhardness measurements were conducted on both the base material and the laser treated layers using a Shimadzu HMV 2T microhardness tester. Five distinct measurements were conducted for each zone, applying a pressing force of 98mN and an indentation time of 15 seconds (Table 4.5).

Average values of HV0.1 microhardness measured on laser processed areas of FeCrAl alloys

Table 4.5.

Sample	Regime 1	Regime 2	Base materials
S1	265	245	228
S2	255	249	213
S3	238	221	223
S4	242	240	231

As presented, the results show the capability of laser surface processing to enhance both the mechanical and chemical properties of alloys with special designation. Utilizing laser surface melting and remelting techniques in Argon environment, FeCrAl alloys exhibited the formation of uniform, compact layers, effectively dissolving intermetallic precipitates from the base matrix. Penetration depths ranging from 68 μm to 519 μm were achieved under various laser power parameters. The resulted fine, dendritic microstructure have a flawless surface, with the exception of minor pores observed in samples containing higher chromium content. Notably, no oxidation effects were observed, indicating the efficiency of the protective atmosphere. Trough specific processing parameters the microhardness was enhanced, mainly due to rapid cooling, particularly in samples with high aluminum content.

All the results presented in this chapter were realised in direct collaboration with ERAMET and the LAMET laboratory at Politehnica University of Bucharest. This research was financially supported by the Romanian National Program for Research under Project No. PCCA 243/2014, focusing on Advanced Metallic Materials for New Generation Nuclear Power Plants (4R – NUCLEARMAT).

Ther results of laser surface melting are important but, as presented in the next chapter, further improvement of the process can be achieved by laser surface treatment in liquid media that aims to limit the heat-affected zone while providing mechanical treatment to the surface.

CHAPTER 5. ADVANCED LASER SURFACE PROCESSING IN LIQUID MEDIA

In any laser-based thermal process, a primary concern is the significant thermal gradient that is induced to the material. The proposed solution for reduction of the heat affected zone and thermal distortion of materials during laser processing is to submerge the material in water or in other liquid media. By using a liquid media during laser processing is possible to enhance the laser quenching process due to the rapid cooling provided by water immersion that allows for efficient transformation hardening and thus improving the surface hardness and wear resistance of the material. Moreover, in case of laser surface melting, the cooling effect of water can lead to a smoother surface finish after laser processing.
Whitin this chapter is presented a novel laser processing technique in a liquid media that aims to enhance the surface mechanical properties of the material, by thermal impact and micro-alloying at the subsurface level [STA23].

5.1 Concept Overview

As described in chapter 3, subchapter 2.33 and 2.4, numerous advantages in term of subsurface microstructure and surface mechanical proprieties can be obtained by laser heat treatment, laser shock processing and laser surface melting. Nevertheless, all the laser processing technique rise provocations in maintain the low thermal input and in the same time to massively chance the material structure and behaviour.
As solution to this, I have designed a novel laser processing technique [STA23] that micro-alloy the material surface corroborated with a thermal and shock treatment of the surface. To obtain that I have used a millisecond-pulsed laser to process the material surface during the immersion in an aqueous nickel acetate solution, aiming to improve the surface properties of a C45 mild steel (hardness, wear and corrosion resistance).
Laser processing in liquid environments gives rise to a complex array of phenomena, particularly evident in the case of laser processing of samples submerged in nickel acetate solution. The key phenomena characterizing this process include (i) nickel deposition on the sample's surface, facilitated by the lower reduction potential of Ni^{2+} ions, (ii) nickel diffusion into a thin material layer, and (iii) the in-situ quenching of the material leading to martensite formation. While limited research exists on laser processing in liquids, often aimed at achieving uniform heating, cooling, or surface ablation while avoiding undesired solid-phase

transformations, no studies have delved into the realm of metal alloy processing within aqueous salt environments. Such settings offer the potential for more uniform material processing, creating a diffusionally enriched environment conducive to nickel diffusion.

Nickel plays a key role in enhancing the material's properties through multiple mechanisms. Firstly, it increases the material's hardness via the solid solution hardening effect. Furthermore, nickel's presence leads to an improvement in the material's elastic moduli, enhancing its structural integrity. Additionally, nickel contributes to a reduction in the corrosion rate through a surface passivation effect, enhancing the material's resistance to corrosive environments. The primary objective of this study was to determine the surface structural changes during aqueous processing without inducing melting, ablation, or, at the very least, continuous stable surface melting—where melting occurs without splashing of melted metal, inclusions or oxide bifilms. To achieve this, laser parameters such as pulse energy, pulse duration, and repetition rate, in conjunction with liquid height, were systematically varied. Subsequently, the material surface was in depth examined for any signs of ablation or uneven melting traces following the application of 60 consecutive laser pulses. This approach aimed to gain insights into the dependence between laser parameters, liquid medium properties, and the surface structural modifications.

5.2 Methodology, Resources, and Outcomes

All the experimental test were conducted at the Center for Advanced Eco-Technologies at UNITBV Research Facilities, being respected all the safety regulation for using Nickel acetate salts.

The material used as substrate was C45E steel (EN 10083-2) with the chemical composition shown in Table 5.1. C45E belongs to the category of medium carbon steels that may be toughened by quenching and subsequent tempering, with excellent machinability and moderate weldability. It is frequently utilized in automotive manufacturing for producing shafts, axes, and gears.

Chemical composition of the steel* (C 45E | EN 10083-2) Table 5.1

Material	Wt.%								
	C %	Mn%	Cr%	Ni%	Si%	P%	Mo	S%	Fe%
C45 E	0.46	0.80	0.38	0.12	0.09	0.01	0.06	0.03	98.05

*Analysed by SPECTROMAXx Arc/Spark Optical Emission Spectrometry

In order to obtain the test specimens, a cylindrical bar of C45E steel was cut into round slices with dimensions of 24x4 mm (diameter x thickness). Before the laser processing, the surfaces of the specimens were mechanically polished to achieve a final roughness of Ra = 0.4 μm.
The liquid medium was an aqueous solution of nickel acetate (15% wt., near to its solubility limit at ambient temperature). The Chemical Company, Iasi, Romania, supplied nickel (II) acetate tetrahydrate Ni (CH3COO)24 H2O with a purity of >99.5%wt. The steel samples have been processed with a Nd:YAG TRUMPH Truepulse 556 laser system (max=1064 nm) and a PRECITEC (WC50) welding optical module at 200 mm focal length. To protect the optical system from vapours and splashes, a strong cross flow of compressed air was employed. Figure 5.1 shows the experimental setup along with images of the liquid surface and the steel sample acquired during the laser processing.

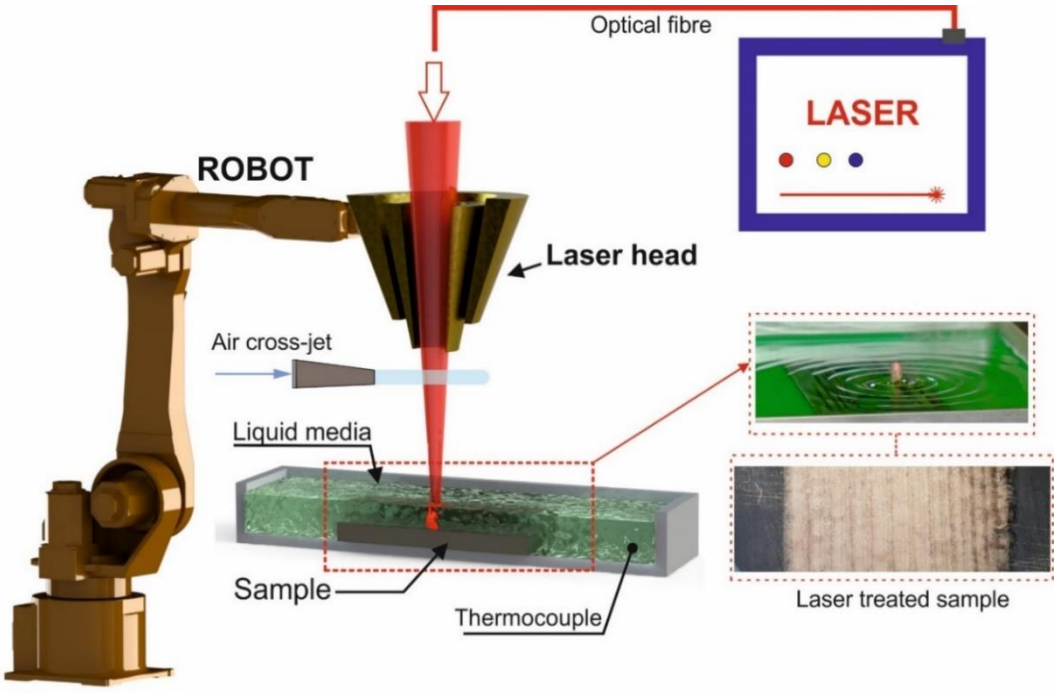

Figure 5.1. Schematic explaining of the laser heat treatment in liquid nickel acetate [STA23].

The shock processing of the substrate is dependent on the formation of plasma during the laser-material interaction. In most cases, the creation of plasma plumes in distilled water at a wavelength of 1064 nm (laser-induced breakdown) is determined by laser irradiance values exceeding 10^{10} W/cm^2 [VOG01]. Irradiance values of such magnitude are not typical for NIR lasers with pulse duration in the microsecond or millisecond intervals. However, when "impurities" (nickel and acetate ions produced by dissociation of the salt in this instance) are present, this threshold value can be significantly decreased by at least 50%. This is because it is easier to reach the critical free electron density required for avalanche ionization and

multiphoton absorption. As example, the threshold irradiance values for tap water can be diminished by a factor of seven in comparison to those of distilled water [36].

By realising several experimental tests, I have concluded that the best parameters setting for achieving a minimal surface ablation (with the exception of 1-2 μm surface scattering caused by plasma formation) is 380 mJ/pulse at 480 Hz repetition rate. Using the determined parameters, an irradiance of $2.3 \cdot 10^5$ W/cm^2 can be obtained, which is enough to stimulate plasma formation in liquid environment when dissolved nickel acetate and iron oxide are present. The level of the liquid is another important factor. This refers to where the cavitation bubble is in relation to the open surface of the solution (the air-liquid interface). If the bubble grows until it hits the free surface, it will burst, sending a jet of liquid into the air. If the bubble reaches its largest diameter and then bursts before it touches the boundary between the liquid and the air, it will send a shock wave toward the steel sample. If and only if the bubble gets close enough to the surface to hit the critical radius, the liquid surface rises, making a dome-shaped liquid. A thin layer of liquid (1–2 mm) will make the process unstable, with liquid blasts and splashes being caused by the explosive bubble sticking out into the liquid-air contact. During processing, the sample becomes almost "dry," and there is a large area of heat-affected zone on its surface with clear melted spots (fig. 5.2b, 5.2c) or serious melting (fig. 5.2d). When the liquid level is higher (5 to 6 mm), the cavitation bubble can't touch the free surface. This keeps the process steady, but a higher percent of the laser energy is lost. Several experiments were done to find the best level of nickel acetate solution. The best level was found to be 4 mm above the top of the sample. The processing speed was set to 8 mm/s, which is below which the surface will melt. It should be mentioned that a surface will melt if subjected to more than 60 laser pulses per mm^2, as the liquid medium does not efficiently conduct heat.

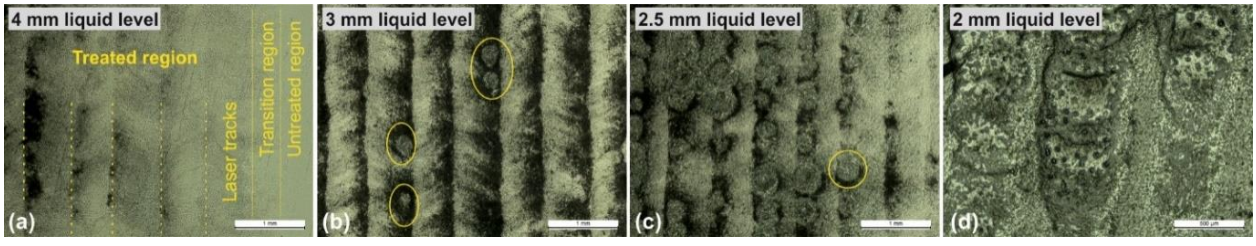

Figure 5.2 OM macros showing the effect of laser tracks at various nickel acetate liquid levels; (a) processed region with no visible surface damage, (b) top-surface with melted spots, (c) top-surface with several melted spots, and (d) significant melting of the surface. Parameters: Laser power 500W, laser energy 0.38 J, pulse length 0.7ms, repetition rate 480 Hz [STA23].

Water has an absorption coefficient of 60 m^{-1} at 1064 nm [SEN20], meaning that 4 mm of water will absorb around 30% of the pulse energy. The NIR domain laser beam is more readily absorbed by the 15% weight-weight aqueous solution of nickel acetate than by water. Every water-soluble nickel salt exhibits a wide absorption peak in the 850–1200 nm range, which coincides with the wavelength at which lasers produce light (1064 nm) [ZHA15]. Moreover, foaming of the liquid media may happen if the liquid is heated and associated with the wave propagation action. This is an unwanted effect as the foam can chance the absorption rate of the liquid. Using an increased pulse repetition rate meant that the foam would dissipate close to the treated region, mitigating this unwanted effect. Using the processing parameters listed in Table 5.2 were produced 25 partly overlapped tracks on the samples surface.

Laser processing parameters Table 5.2

Laser power [W]	Spot diameter [mm]	Laser Energy [J]	Pulse duration [ms]	Frequency [Hz]	Speed [mm/s]	Overlap degree [%]
~ 184	1	0.38	0.7	480	8	20

To ensure that the process was stable and repeatable, the tests were repeated until ten identical samples were produced. For the laser processing tests, a fresh amount of nickel acetate aqueous solution was utilized each time. The liquid medium was maintained at or below 50 °C.The samples that underwent laser processing were prepared for microstructural examination by conventional techniques consisting of cutting, polishing, and chemical etching (with 2% concentration of Nital reagent).

The influence of micro-alloying and phase transformation on morphology was investigated using optical and scanning electron microscopy. Structural evolution and chemical composition were studied through X-ray diffraction and energy dispersive spectroscopy, respectively. The 3D surface profile of the samples was analyzed with a Hirox KH-8700 digital microscope.

For the evaluation of crystallinity and phases, a Bruker D8 Discover X-ray Diffractometer (CuK1 = 1.5406) was employed, utilizing a locked-couple method, a step size of 0.02, a scan speed of 3 s/step, and a 2θ range from 20 to 80°. The general microhardness of the laser-treated material was determined using a MICROMET - 5124VD Buehler microhardness tester, capable of applying loads ranging from 0.5 gf to 2000 gf. Five indentations were made per sample,

with a 0.5 gf applied load and a 10 s dwell time (to reduce creep). The standard deviation was calculated after averaging the results. Furthermore, the subsurface mechanical response of both the laser-processed and reference samples was meticulously assessed using an NHT2 nanoindenter module from CSM Instruments/Anton Paar (Switzerland). This instrument employed a three-sided pyramidal diamond Berkovich tip with a radius of 100 nm for the measurements. Indentation loads from 1mN to 500mN were used to measure the depth of the structurally changed material, which translated into numerous penetration depths. To reduce the standard deviation, a matrix of at least 10 indentations was used for each load. The indentation procedure was as follows: approach speed of 2000 nm/min, loading duration of 30 seconds, rest time of 5 seconds (to reduce creep effect), and unloading period of 30 seconds. The Oliver and Pharr model was used to process the loading/unloading curves. The fluctuation in indentation hardness and elastic modulus as a function of penetration depth was of particular interest. The corrosion rate of laser-treated samples was determined using an SP-150 potentiostat/galvanostrat and EC-Lab software. The samples were considered as working electrodes (laser treated and reference), a platinum grid as counter electrode, and a saturated calomel Hg/Hg_2Cl_2, KCl sat. as reference electrode in a standard three-electrode electrochemical cell. The electrolyte was a 9% NaCl solution, and the tested area was 10x10mm. Before the test, the samples were submerged in saline solution for 1 hour to ensure a stable open circuit potential.

The idea behind the use of nickel acetate as a surface modification precursor is based on the reduction of Ni^{2+} as a mixt basic Ni(II) acetate on the surface of the sample, formed of Fe, due to the largest reduction potential for Ni^{2+}/Ni^0 (E^0 =-0.25V) compared to Fe^{2+}/Fe^0 (E^0= -0.44 V). A localized increasing in temperature at the sample surface determines a further increase in this reduction potential.

Studies on the thermal behaviour of nickel acetate show the development of non-stoichiometric basic Ni(II) acetate mixtures ($xNi(CH_3COO)_2 \cdot yNi(OH_2)$) or even NiO [DEJ05]. Because of the localized heating, the acetate anion might also be converted to form ions and eventually CO and/or CO_2. The CO produced during acetate decomposing may help in the reduction of Ni^{2+} to the metallic state. The chemical processes [Eq. 5.1] that take place throughout this surface modification process are shown below.

$$\begin{aligned} Ni^{2+} + Fe^0 &\longrightarrow Ni^0 + Fe^{2+} \\ NiO + CO &\longrightarrow Ni^0 + CO_2 \end{aligned} \tag{5.1}$$

The decomposition of nickel acetate during laser processing in liquid can affect the convection heating or the plasma generation and in the same time function as nucleation sites for boiling bubbles phenomenon. The low intensity plasma plume that is produced by ablating the surface (Fe and/or deposited Ni) can also produce boiling bubbles. A certain amount of the laser energy may also be converted to mechanical energy [ZBE15]. These combined phenomena may alter the material's surface shape

The surface topography profiles of the steel samples processed in liquid reveal Rz roughness values of 0.7 μm (Figure 5.3), slightly higher than the mechanically polished substrates (0.4 μm). This suggests that (i) a "steady-state" deposition of nickel has taken place and (ii) melting, if it occurs at all, is likely limited to localized areas.

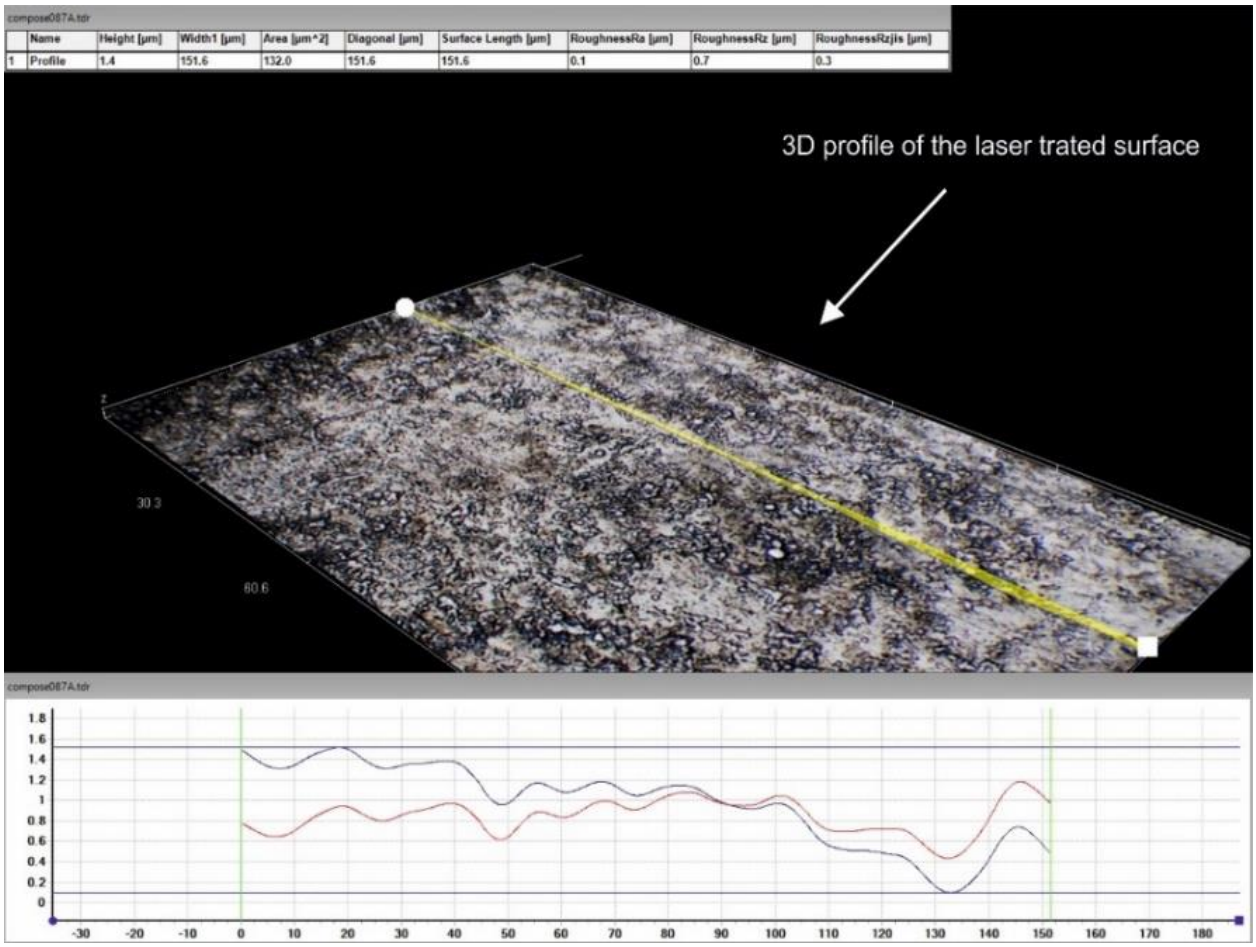

Figure 5.3. 3D scanning and surface profile measure (Hirox KH-8700 digital microscope) [STA23].

The surface of the laser-treated and the cross-section of the samples indicate the presence of a 0.2-3 μm Ni-rich layer (Figures 5.4a and 5.4b). The EDS elemental examination of the layer reveal that the oxygen concentration is practically stoichiometrically equivalent to NiO,

"anchored" to the substrate by its presence of Fe. This layer was removed by gentle polishing since it appeared to be poorly attached to the substrate.

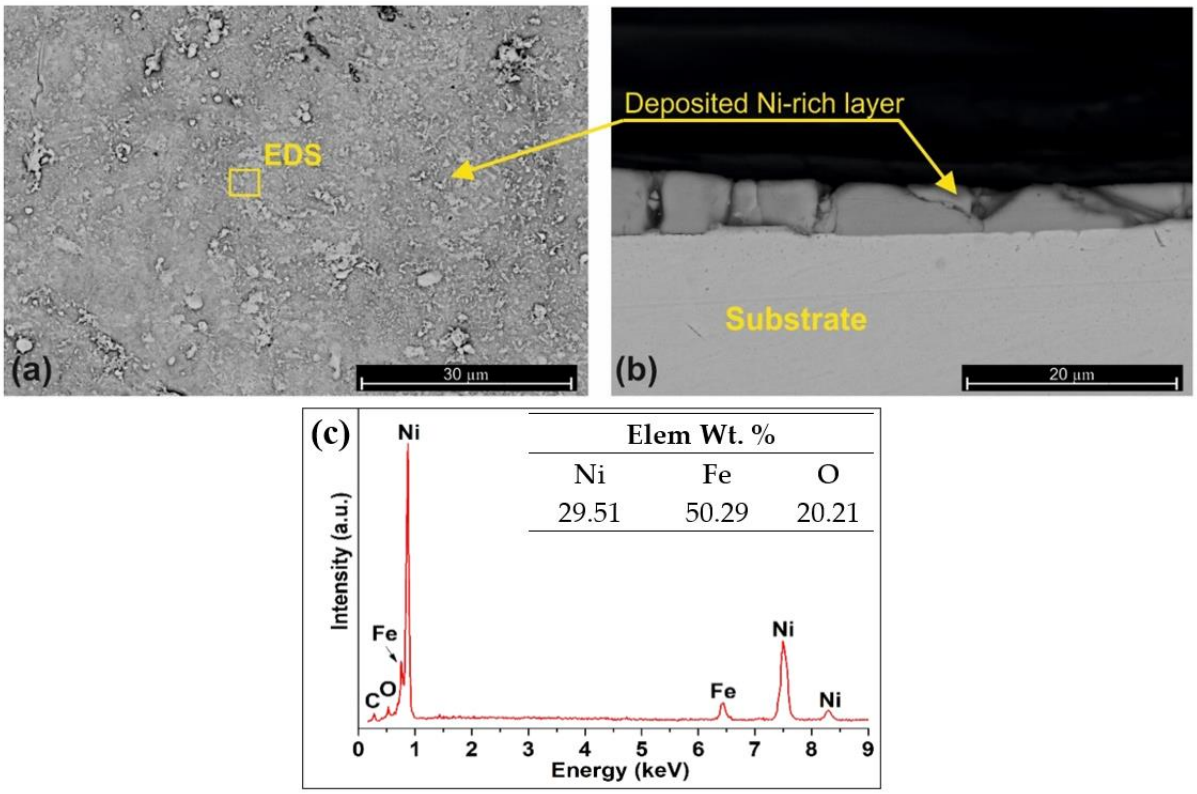

Figure 5.4. SEM images of the sample surface (a) and cross-section (b) after laser processing; (c) EDS analysis of the surface top sample [STA23].

X-ray diffraction was used to evaluate potential structural modifications. The diffraction patterns for the liquid media laser treated sample and the reference sample are shown in Figure 5.5.

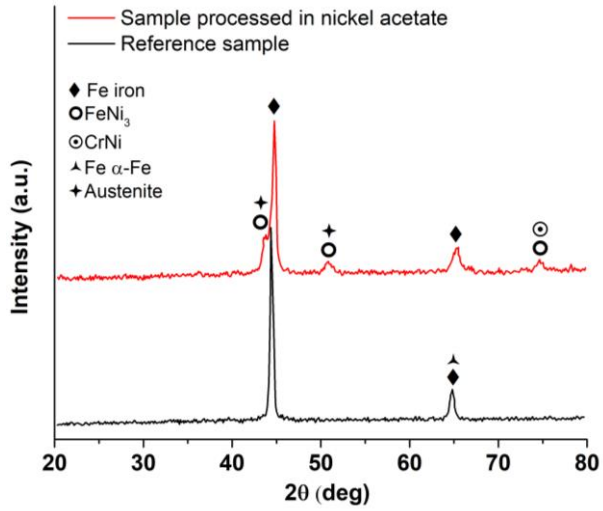

Figure 5.5. XRD pattern, where the black line represents the reference sample (without processing), and the red line represents the sample processed in nickel acetate. [STA23].

C45E steel contains two diffraction patterns that can be attributed to Fe (44.6°) and -ferrite (65°). The peaks attributed to these phases appear at higher diffraction angles (44.8° and 65.4°) for the laser-processed sample, which might suggest a reduction in the α-ferrite unit cell size due to internal tensions. In addition, other peaks in the diffraction pattern have been identified as $FeNi_3$ and residual Cr, Ni-"alloyed" austenite (γ -Fe). Because the quenching rate is quite high during processing in liquid environments, nickel can stabilizes the austenite.

The broadening of the diffraction peaks attributed to ferrite (which has a body centred cubic lattice) may be due to the Bain strain occurrence during quenching, which causes the crystalline lattice to be distorted to a body centered tetragonal one.

The millisecond pulsed laser has a high energy density per pulse, and the heat must be quickly dispersed into the bulk of the material. The liquid medium provides direct quenching with rapid cooling rates while keeping the work piece below 50 °C. The XRD examination, on the other hand, verifies the predicted microalloying processes resulting from nickel diffusion from the nickel acetate solution, mostly through the formation of CrNi-type intermetallic compounds. Furthermore, given the chemical composition of C45E steel, the Ni concentration would be unable to produce the $FeNi_3$ compound without some Ni addition from the liquid solution. These results offer confidence in the innovative method of using nickel acetate as a precursor for the release of Ni atoms during plasma formation.

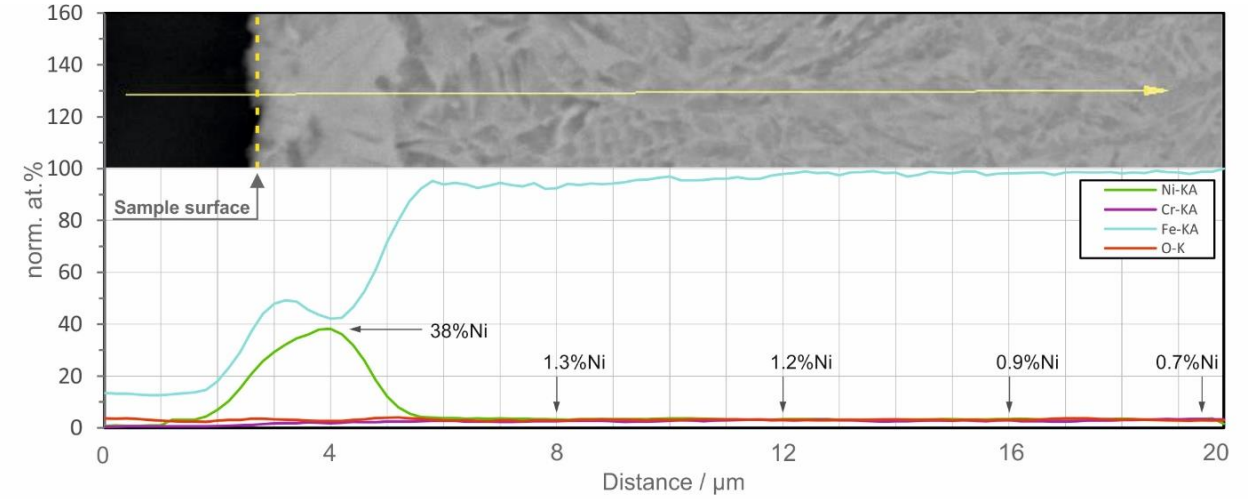

Figure 5.6. EDS line scan illustrating the elemental composition across the processed area [STA23].

In case of the Fe-Ni system, it is essential to note that the pre-exponential diffusion coefficient (D_o) is determined to be 6.92 cm^2/s, and the diffusion activation energy (Q) is calculated as 77.6 kcal/mole. However, these constants are originally derived for pure solids in direct contact.

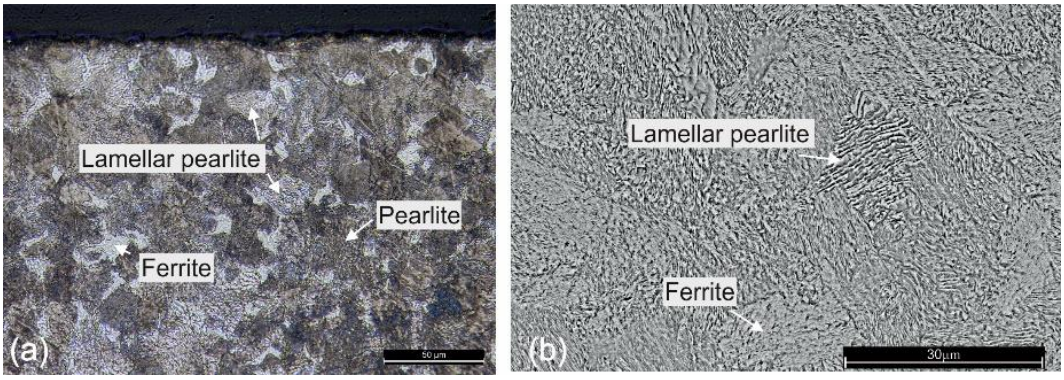

Figure 5.7. Optical and SEM analyses of the C45 base material [STA23].

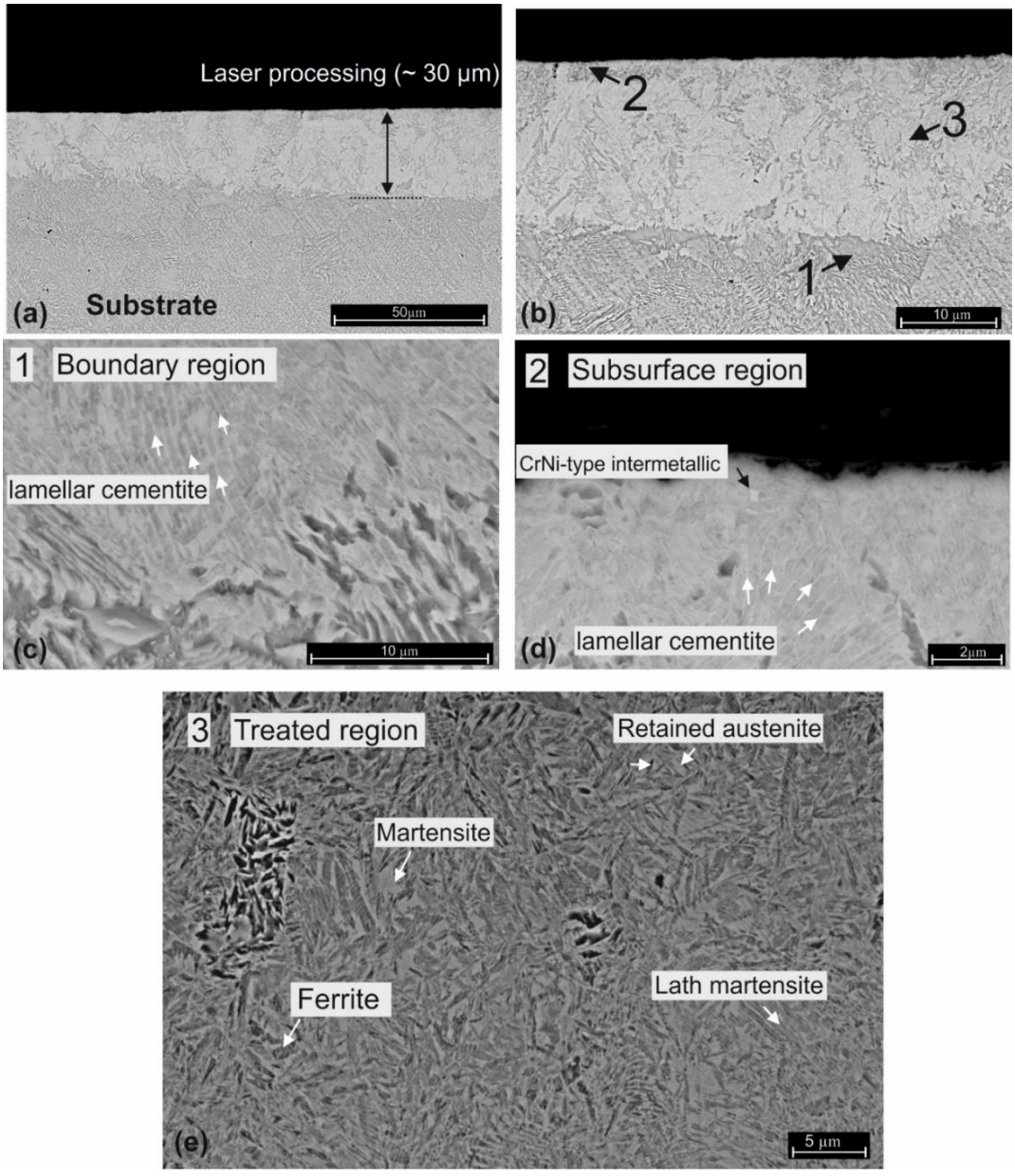

Figure 5.8. SEM micrographs of the specimen's cross-section: (a) and (b) show the laser-treated area at various magnifications; (c) illustrates the boundary between the treated and untreated regions; (d) focus on the subsurface region, and (e) detail on the treated region after aqua regia etching [STA23].

The maximum Ni concentration observed is approximately 38 atomic percent, identified at a distance of 2 µm from the top surface of the workpiece. Comparable data were obtained through a conventional diffusion experiment conducted at 450 °C over 1200 hours [ARI15]. Nevertheless, in this specific experimental setup, diffusion is anticipated to occur at a considerably higher rate due to the involvement of Ni diffusion primarily from the liquid phase. Considering a diffusional length of 2 µm, a diffusion area of 1.130 cm^2 (accounting for the sample's diameter), and an average processing duration of 20 seconds, a calculated diffusion coefficient (D) amounts to 1.17×10^{-8} cm^2/s. It is noteworthy that such diffusion coefficients are typically encountered in solid-state diffusion experiments conducted at temperatures surpassing 1390°C. However, an exact comparison is intricate because diffusion in this case arises from Ni° originating from Ni^{2+} present in the solution. A comprehensive structural analysis, outlined in subsequent sections, provides detailed insights into this phenomenon. The base material, in its annealed state, exhibits a ferrite-pearlite structure, wherein coarse lamellar perlite formations are distinctly visible (as illustrated in Figure 5.7, a and b).

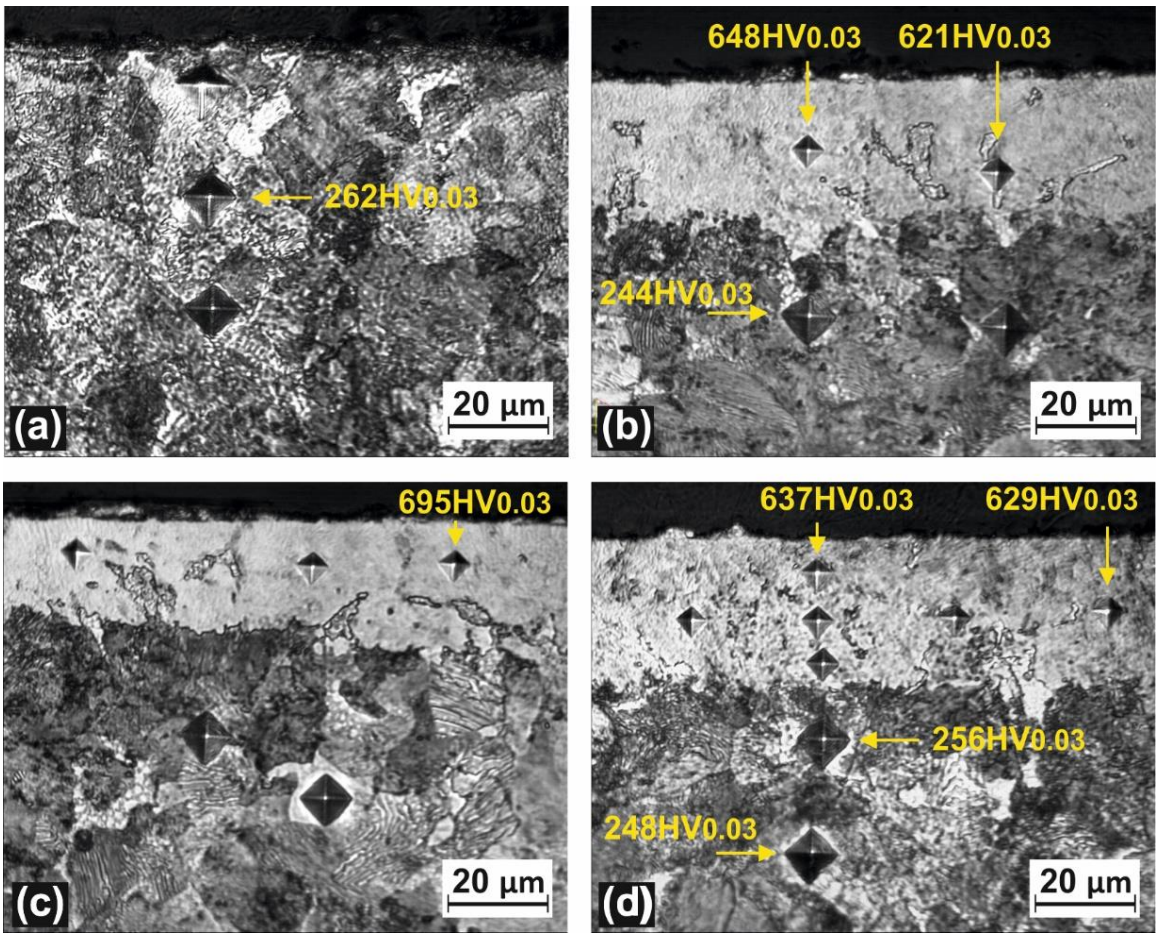

Figure 5.9. Indentation marks (HV0.03) on the cross-section of the untreated sample (a) and on laser treated sample (b, c and d) [STA23].

Figure 5.8 (a) illustrates a clear phase transformation occurring within a depth of 15 - 30 μm from the surface. This region, depicted in both Figure 5.8 (a) and (b), highlight the boundary where the ferrite-to-austenite and pearlite-to-austenite transformations take place, representing the layer with the highest nickel diffusion. Despite the oxidizing nature of the nickel acetate aqueous solution, rapid heating and cooling prevented decarburization. However, due to the high cooling rate, complete homogenization of austenite was not achieved. At the heat-treated zone boundary, clearly demarcated near the thermal processing limit (30 μm depth), the microstructure comprises Widmanstätten ferrite structures, retained austenite, and lath martensite phases (Figure 5.8e). Additionally, the presence of lamellar cementite phase near the surface (Figure 5.8c) indicates the incomplete transformation of austenite. The primary objective of any surface engineering process is to enhance specific proprieties relevant to the intended application, such as hardness, wear and corrosion resistance. The mechanical behaviour of the treated surfaces was evaluated through microhardness analyses and instrumented indentation. Figure 5.9 depicts microhardness indentations on both untreated (a) and laser-treated samples (b, c, and d), while Table 5.3 provides the microhardness profile depending on the distance from the surface.

Microhardness values at various depths from the treated surface Table 5.3.

Region	Depth from the surface [μm]	Microhardness $HV0_{0.03}$
Treated region	10	663 ± 9.2
	20	627 ± 3.6
	30	621 ± 4.6
Boundary region	40 - 50	459 ±11.0
Untreated region	60	259 ± 3.6
	70	248 ± 1.4
	80	246 ± 1.1

As resulted from Figure 5.9 and Table 5.3, laser processing in a liquid medium induces a significant hardening effect, a favorable outcome arising from the synergistic effects of microalloying and rapid pseudothermal processing facilitated by the pulsed laser beam. The application of laser processing in a nickel acetate solution resulted in a higher maximal cross-section microhardness of 695 Vickers. The presence of the liquid solution plays a key role: it

prevents surface melting by efficiently transferring a substantial amount of laser energy to the surface. Simultaneously, the liquid solution rapidly cools the treated surface, leading to a substantial increase in hardness.

The microhardness results, corroborated with SEM and EDS analyses, show that the material experienced microalloying and thermal processing up to a depth of 30 μm, followed by a boundary zone extending 10 – 15 μm from the surface. EDS analyses further reveal a heightened Ni concentration at subsurface levels, specifically at depths ranging from 1-2 μm. To investigate the influence of this microalloying phenomenon on subsurface mechanical properties, instrumented indentation tests were conducted on the laser-processed sample, penetrating to a depth of 2500 nm. Figure 5.10 illustrates the variation of instrumented indentation hardness and elastic modulus concerning depth, providing insights into the subsurface mechanical behavior induced by the laser processing in the liquid medium.

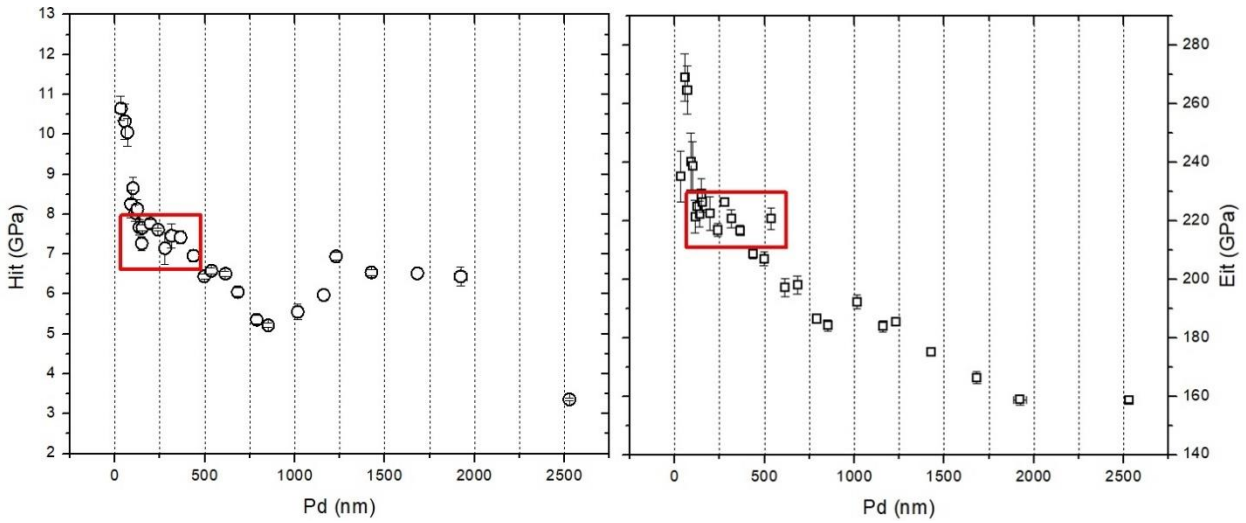

Figure 5.10. The variation of the hardness and elastic modulus as function of the penetration depth [STA23].

The enhancement in hardness can be attributed to the formation of Ni-Fe substitutional solutions and Ni-Cr intermetallic compounds within the material structure, distinct alterations that contribute to the increase in hardness when compared to the untreated substrate. The diffusion of Ni into the metallic matrix induces distortions within the crystalline network, exerting a clear influence on the material's hardness.

Upon evaluating the near-surface region (up to a penetration depth of 2000 nm), the obtained hardness and elastic modulus values can be correlated with the Ni-rich subsurface layer. Figure 5.10 illustrates that the peak indentation hardness, reaching up to 11 GPa

(approximately 1100 HV), occurs near the surface at 100 nm. Subsequently, a stabilization phase, denoted by red rectangles, signifies values characteristic of the region with the highest Ni content, approximately 38% (as indicated by the EDS line scan in Figure 5.6). Within this stabilized region, hardness values range between 6 and 8 GPa (around 800 HV), and elastic modulus values are between 210 and 230 GPa. Upon increasing the indenter load and subsequently reaching greater penetration depths, a noticeable decline in elastic modulus occurs, particularly evident after 500 nm. A similar drop is observed in the evolution of hardness concerning penetration depth after 1500 nm, potentially associated with a work-hardening phenomenon induced by the diamond indenter.

Figure 5.11 presents the potentiodynamic polarization curves of the tested samples in a 9% NaCl electrolyte. Upon analysis of the presented plots, it is evident that the laser-processed surface exhibits superior corrosion resistance in comparison to the reference surface, highlighting the effectiveness of the laser processing method in enhancing the material's resistance to corrosion.

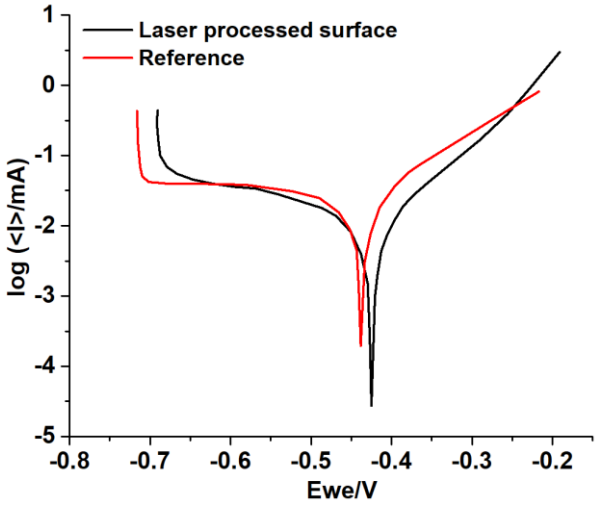

Figure 5.11. Polarization curves of the reference surface and of the laser processed surface [STA23].

Corrosion test parameters and results Table 5.4

Operational parameters	No processing	Laser processing
E_{corr}	-437.4 mV	-435.5 mV
I_{corr}	25.0 µA	11.3 µA
b_c	669.9 mV	285.1 mV
b_a	141.9 mV	117.1 mV
Corrosion rate	0.094 mm/year ±0.006	0.042 mm/year ±0.003

Table 5.4 provides a summary of the corrosion test parameters derived from the polarization curves depicted in Figure 5.11, including Tafel slope constants related to anodic (ba) and cathodic (bc) processes, potential (E) and corrosion potential (Ecorr), as well as corrosion current density (icorr). Upon comparing the polarization curves and electrochemical data, it becomes evident that the laser-treated surface exhibits enhanced corrosion resistance. Specifically, a notable decreasing in corrosion current is observed for the laser-processed sample, as indicated in Table 4, resulting in an improvement of corrosion rate by more than 50%.

This improvement in corrosion resistance can be attributed to several factors. The presence of nickel within the material may act as a passivating agent when the steel sample is exposed to a saline environment, enhancing the surface's resistance to corrosion. Furthermore, the existence of intermetallic compounds and the martensite phase could exert a favorable effect, mitigating the corrosion rate of the material. These factors collectively contribute to the observed enhancement in corrosion resistance on the laser-treated surface, underscoring the beneficial impact of the laser processing method on the material's durability in corrosive environments.

Laser processing in liquid media is a potential technique for improving the surface mechanical properties of materials by combining thermal impact and micro-alloying at the subsurface level. When nickel acetate is used in the laser processing of C45E steel samples, it led to subsurface micro-alloying and phase transformation reaching a depth of up to 30 μm from the surface. This transformative process resulted in significant enhancements of the micro and nanoscale hardness and elastic modulus, coupled with a masive reduction in the corrosion rate [STA23].

The laser-processed region exhibits a distinctive non-equilibrium martensite structure with residual austenite phase, alongside the formation of CrNi and Cr_2Ni_3 intermetallic compounds due to nickel diffusion from the liquid solution. The simultaneous occurrence of phase transformation and microalloying phenomena is instrumental in achieving a robust mechanical response. Microhardness values surged from 250 to 660 Vickers units (HV0.03) due to this process. The heightened subsurface nickel content further amplified hardness to 8 GPa and elastic modulus to 230 GPa, concurrently enhancing corrosion resistance [STA23].

This innovative laser processing technique not only holds potential for designing novel active liquid media but also offers opportunities for optimizing process parameters across diverse materials. Particularly in the biomedical domain, this technique finds application in modifying

implant materials' surfaces, enhancing their hardness and corrosion resistance. Such enhancements are crucial for prolonging the lifespan and performance of implants. Moreover, owing to the formation of a plasma plume in liquid media, this technique can be effectively utilized in micro- and nano-fabrication processes, as well as in the field of microfluidics and microelectromechanical systems (MEMS) manufacturing.

CONCLUSIONS AND CONTRIBUTIONS

This Habilitation thesis presents the numerous applications of laser technology in the industrial engineering field primarily based on studies conducted at the Research Institute of the Transilvania University of Brasov.

The results presented within the thesis represent only a part of my personal intensive research carried out in this field, emphasizing the evolution of laser technology and its utilization in welding, cladding, heat treatment, and various surface engineering processes. Several contributions in the field of laser material processing can be outlined as follows:

1. A comprehensive overview of the contemporary utilization of the laser technology in industrial applications was presented. Laser welding, cladding, and diverse surface techniques were described, providing an in-depth literature review of this advanced processing techniques.
2. Optimization of laser cladding parameters and determination of the influence of cladding speed on the properties of the cladded layer. The use of WC-Co/NiCrBSi/NiAl powder as filler material demonstrated that preheating the base material, coupled with the addition of aluminum, can further enhance the quality of cladded layers by preserving the integrity of the hard phases within the cladded layer.
3. Development of an active flux (SiO_2 + Poly (vinyl alcohol)) to enhance the absorption of the laser beam in welding applications. This active flux also facilitated the formation of ferrite during solidification.
4. Optimization of laser welding parameters for AISI 316L stainless steel using a pulsed laser. The parameter window for laser power, pulse duration, and repetition rate was determined, and their influence on weld bead geometry was defined as a function of input parameters.
5. Heterogeneous laser welding of carbon steel and stainless steel was carried out using AISI 1010 steel and AISI 321, resulting in obtaining of high-quality dissimilar butt joints.

It was shown that the total energy introduced into the process can impact the overall composition of the weld bead, and there is a direct correlation between energy level and the extent of the non-homogeneous region within the weld bead.

6. Development of a novel method for laser surface processing using a liquid medium that acts as both as confinement media and as precursor for microalloying. Enhanced corrosion resistance and surface hardness were achieved by laser processing of C45 steel in a nickel acetate solution.
7. Determination of the influence of the technological cladding setup on layer geometry using cladding units at 20, 25, and 32-degree angles. The variation in powder stem angle can significantly influence dilution and the mechanical properties of the cladded layer.
8. Designing and further laser processing of novel FeCrAl alloys were presented, illustrating that laser surface processing is a practical solution for improving surface properties by refining the grains. Enhanced corrosion resistance and hardness were achieved by melting and remelting the surface of the novel FeCrAl alloys, with direct applications in 4th generation nuclear power plants.

It can be stated that laser technology is the technology of the future in terms of materials processing. As presented in this thesis, laser processing has become, nowadays, a common tool for macro or micro processing of materials. Laser technology is now available at lower prices compared to 20 years ago, and due to the continuous development of new types of lasers with improved properties in terms of beam quality and wall plug efficiency, lasers will be increasingly utilized for industrial applications such as welding, cladding, and surface processing.

The aim of the Habilitation thesis was to contribute to this field by providing information about the actual state of the technology and by presenting the current direction of research activities within the laser processing.

B3. EVOLUTION AND DEVELOPMENT PLANS FOR CAREER DEVELOPMENT

The plans for evolution of my future career are based on two main pylons:

1. Development of the didactic career
2. Development of the research career

Both directions will be developed within the Transilvania University of Brasov at Faculty of Materials Science and Engineering. After obtaining the title of PhD supervisor, my intention is to further develop my academic career, contributing substantively to the didactic and research activities within the university.

Didactic plans

I am the adept of long-life learning and I intend to continually enhance my teaching skills through participation in training programs and by participating in Erasmus mobility programs for teachings, my goal being to acquire modern teaching -learning methods. I intend to participate in at least one Erasmus teaching program each year at a university where I already have strong collaborations and extensive teaching experience, such as Universidad Politécnica de Madrid and Universidad Las Palmas de Gran Canaria.

I intent to further develop the practical application labs that nowadays, are so important for the engineering students and for that I plan to:

- Implement new interactive methods for teaching in order to attract students and to increase the presence to the practical labs. As example, for the laboratory of Non-destructive testing (NDT) I intend to create a virtual training method in which the student can access the equipment (Olympus/Evident OmniScan X3) trough ZOOM platform and to be able to solve by there one real's tasks from the industry.
- I intent to further develop the course of Materials Technology and to update the content of the course and laboratory to the contemporary technologies and demands form the industry
- Regarding the course of Tolerance and Dimension Control, my plan is to update the course content and to create new practical applications that uses the latest dimensional control devices commonly used in industry as standard.

In addition to those disciplines, my overall plan is to continuously update and modernize various aspects of the educational curriculum in all the courses I teach.

Currently, I am the coordinator of the Bachelor's study program in Welding Engineering, and within this field, I intend to keep pace with industry trends and evolving technologies in this comprehensive profession. To achieve this, I will collaborate with industry experts, and together with the students, I will attend relevant workshops and participate in practical visits to economic partners.

From the teaching perspective, the most important aspect is the feedback from the students. I will try to consistently be a good professional/teacher while also adapting to the current needs of the students. It is important to continually adapt the teaching methods to meet the requirements of the present and future generations of students.

The next step in my career involves supervising PhD students, and for that, I intent to encourage innovative thinking and promote high-quality research practice among the doctoral students under my supervision. Ethics in research will be a fundamental base for all my future students. All of the future research plans presented ahead can be developed into main research subjects for upcoming PhD students.

Research plans

The current and future research activity will be based on fundamental and applicative study that involve the laser technology.

As presented in this Habilitation thesis, the field of laser technology is comprehensive and allows for indefinite growth within this domain. Currently, the L8 / L3 laboratory at the Research Institute of Transilvania University in Brasov is equipped with two lasers. Within the 2024-year, equipment for teaching and research, totalling one million euros, will be added, completing the requirements for conducting high standards of research in the field of industrial engineering. Based on that, I intent to continue the research in the field of laser technology and examples of future research can be outlined as:

1. **Developing of a new method for real time monitoring of laser processing**. Laser processing is a highly dependent process with various parameters and for that it can be difficult to predict the influence of certain factors on the laser welding, cladding or cutting processes. It can be crucial to create a system that can identify, in real time, the possible issues / defects that are produced during the laser welding or cladding. I aim to research this matter

and to define a solution based of laser spectroscopy which can give valuable information, in real time about the evolution of the laser welding / cladding process. The project will involve developing of a new technology and algorithms for monitoring the welding / cladding process.

2. **Heterogenous laser welding of titanium with stainless steel.** It is well known that titanium posses lots of advantages for use in medical and industrial application, but welding of pure Ti and Ti alloy can be challenging. Laser welding of titanium presents even more difficulties due to the fast heating-cooling cycle and due to the increased welding speed, that makes challenging the protection of the welding bead until the temperature is below 350 °C. Moreover, heterogenous laser welding of titanium can lead to formation of hard phases and because of that there is a high cracking susceptibility. I aim to investigate the possibility of laser welding of titanium in similar and dissimilar configuration by using enhanced gas flow protection trough a special designed welding head or by welding in controlled atmosphere environment.
3. **Designing and processing of advanced HEA alloys.** Advances in metallurgy and laser processing opens new directions in creating of new materials, with special mechanical and chemical proprieties suitable for exploitation even in the worst environments, like nuclear power plants. Based on the good collaboration with LAMET and ERAMET laboratories from Politehnica University of Brasov I intend to develop new recipes of advanced alloys, FeCrAl and HEA, that can be further subjected to various methods of laser processing. This research direction is a continuation of current studies that are already in progress.

Several others research studies are considered but cannot be mentioned due to the incipient phase of the research.

To quantify the results of the research, I intent to publish each year at least one Q1 /Q2 article as principal author and to participate in at least one international conference per year.
Attracting founds trough research projects is mandatory nowadays, and I aim to participate in all the project competitions in which I am qualified.

B4. REFERENCES

1.	[AKB09]	Akbari Mousavi, S.A.A., Sufizadeh, A.R. Metallurgical investigations of pulsed Nd:YAG laser welding of AISI 321 and AISI 630 stainless steels. Materials and Design, 30, 8, pp. 3150–3157, DOI: 10.1016/j.matdes.2008.11.026, 2009.
2.	[ANA08]	Anawa, E.M., Olabi, A.G. Optimization of tensile strength of ferritic/austenitic laser-welded components. Optics and Lasers in Engineering, 46, 8, pp. 571– 577, DOI: 10.1016/j.optlaseng.2008.04.014, 2008.
3.	[ANA20]	Anas A. S., Avanish K. D., Engineering Steels and High Entropy-Alloys, ISBN 978-1-78985-948-5, DOI: 10.5772/intechopen.91800, 2020.
4.	[AND08]	Andreescu. B., Andreescu F. G., Gas laser for thermal processing, (Laseri cu gaz pentru prelucrări termice), Brasov, Lux Libris, 2008, ISBN 978-973-9458-99-3, 2008.
5.	[ARI11]	Arivazhagan, N., Surendra, S., Satya P., Reddy, G.M. Investigation on AISI 304 austenitic stainless steel to AISI 4140 low alloy steel dissimilar joints by gas tungsten arc, electron beam and friction welding, Materials and Design, 32, 5, pp. 3036–3050, DOI:10.1016/j.matdes.2011.01.037, 2011.
6.	[ARI15]	Arioka, K., Iijima, Y., Miyamoto, T. Rapid nickel diffusion in cold-worked carbon steel at 320–450 °C, Philosophical Magazine, 95(32), 1-13, 2015.
7.	[BAG14]	Baghjari, S.H., Akbari Mousavi, S.A.A. Experimental investigation on dissimilar pulsed Nd:YAG laser welding of AISI 420 stainless steel to kovar alloy. Materials and Design, 57, pp. 128–134 DOI: 10.1016/j.matdes.2013.12.050, 2014.
8.	[CAO23]	Cao B.S., Wu C.L., Wang L., Zhang S., Zhang C.H., Sun X.Y., Effect of residual stress and phase constituents on corrosion-cavitation erosion behavior of 304 stainless steel by iso-material manufacturing of laser surface melting, Journal of Materials Research and Technology, Volume 26, pp. 6532-6551, ISSN 2238-7854, https://doi.org/10.1016/j.jmrt.2023.09.027, 2023.
9.	[CEY22]	Ceyhun K., Effect of heat input and post weld heat treatment on the texture, microstructure and mechanical properties of laser beam welded AISI 317L austenitic stainless steel, Materials Science & Engineering A 855, 143966, 2022.
10.	[CHL21]	Chludzinskia M, Santosa R E, Churiaquea C, Fernandez-Vidalb S R, Ortega M, and Sanchez-Amayaa J M 2021 Optics and Laser Technology, 134, 106583, 2021.

11.	[DEJ05]	De Jesus, J. C., González, I., Quevedo, A., Puerta, T. Thermal decomposition of nickel acetate tetrahydrate: an integrated study by TGA, QMS and XPS techniques, Journal of Molecular Catalysis A: Chemical, 228, 283-291, 2005.
12.	[FCZ19]	Feng, X., Cui, X., Zheng, W., Wen, X., Zhao, Y., Jin, G., Lu, B., Dong, M. Performance of underwater laser cladded nickel aluminum bronze by applying zinc protective layer and titanium additives, Journal of Materials Processing Technology, 266, 544-550, 2019.
13.	[FEN18]	Feng, X.R., Cui, X.F., Jin, G., Zheng, W., Cai, Z.B., Wen, X., Cai, Z.B., Wen, X., Lu, B.W., Liu, J.M. Underwater laser cladding in full wet surroundings for fabrication of nickel aluminum bronze coatings. Surf. Coat. Technol. 333, 104–114, 2018.
14.	[FEN19]	Feng, X., Cui, X., Zheng, W., Lu, B., Dong, M., Wen, X., Zhao, Y., Jin, G. Effect of the protective materials and water on the repairing quality of nickel aluminum bronze during underwater wet laser repairing, Optics & Laser Technology, 114, 140-145, 2019.
15.	[GEA19]	Geanta V., Voiculescu I., Stefanoiu R., Jianu A., Milosan I., Stanciu E.M., Pascu A., Vasile I.M., Titanium Influence on the Microstructure of FeCrAl Alloys Used for 4R Generation Nuclear Power Plants, Revista de chimie, 70 (2), pp. 549-554, 2019.
16.	[GEA20]	Geanta V., Voiculescu I., Tenciu D., Baschir L., Stanciu E.M., Pascu A., Effect of laser processing on the microstructure of the FeCrAl alloys, Journal of Optoelectronics and Advanced Materials, 22(7-8), pp 411-418, 2020.
17.	[GUO17]	Guo, N., Xing, X., Zhao, H.Y., Tan, C.W., Feng, J.C., Deng, Z.Q. Effect of water depth on weld quality and welding process in underwater fiber laser welding, Mater. Des., 115, 112–120, 2017.
18.	[GUO23]	Guo-Dong Chen, Xiu-Bo Liu, Fei-Zhi Zhang, Qing-Shuai Liu, Hou-Zheng Ou, Shi-Hong Zhang, Fabrication and tribological properties of laser cladding WC-Cu/Co-based composite coatings, Surface and Coatings Technology, Volume 472, 129930, ISSN 0257-8972, https://doi.org/10.1016/j.surfcoat.2023.129930, 2023.
19.	[HAM16]	Hamad, A. H. Effects of Different Laser Pulse Regimes (Nanosecond, Picosecond and Femtosecond) on the Ablation of Materials for Production of Nanoparticles in Liquid Solution. In High Energy and Short Pulse Lasers, IntechOpen, 2016.
20.	[HAN98]	Hanna D. C. Principles of lasers, fourth edition, Southampton University, England, Printed in the United State of America 9876543, 1998.
21.	[HEC17]	Hecht, E., Optics. Pearson Education, ISBN 0133977226, 2017.
22.	[HOF17]	Hoffman, J., Chrzanowska, J., Moscicki, T., Radziejewska,J., Stobinski, L., Szymanski, Z. Plasma generated during underwater pulsed laser processing, Applied Surface Science, 417, 130–135, 2017.

23.	[HOP18]	Hoppius, J. S., Kukreja, L.M., Knyazeva, M., Pöhl, F., Walther, F., Ostendorf, A., Gurevich, E. L. On femtosecond laser shock peening of stainless steel AISI 316, Applied Surface Science, 435, 1120-1124, 2018
24.	[HUL21]	Hulka, I., Utu, I.D., Avram, D., Dan, M.L., Pascu, A., Stanciu, E.M., Roata, I.C. Influence of the Laser Cladding Parameters on the Morphology, Wear and Corrosion Resistance of WC-Co/NiCrBSi Composite Coatings. Materials, 14, 5583, 2021.
25.	[IOD11]	Iordachescu, D., Scutelnicu, E., Iordachescu, M., Valiente, A., Hervias, J. R., Ocaña, J. L. Specific properties of ferritic/austenitic DISSIMILAR METALS WELDED JOINTS. Welding in the World, 55, 3-4, pp 2-11, DOI: 10.1007/BF03321280, 2011.
26.	[ION05]	Ion J. C., Laser Processing of Engineering Materials principles, procedure and industrial application, Elsevier Butterworth-Heinemann, ISBN 0 7506 6079 1, 2005.
27.	[IOR10]	Iordachescu D., Scutelnicu E., Iordachescu M., Ruiz-Jervias J.,Temperature Field Features in Case of Dissimilars Metals Arc Welding, Metalurgia International, vol. XV(4), 26-31, 2010.
28.	[IOR11]	Iordachescu, D., Blasco, M., Lopez, R., Cuesta, A., Iordachescu, M., Ocaña, J. L. Recent achievements and trends in laser welding of thin plates. // Journal of Optoelectronics and Advanced Materials, 13, 8, pp. 981-985, 2011.
29.	[JIA22]	Jiahao Z, Ke H, Jiayi Z, Shuyao D, and Xiaohong Z, Materials Today Communications 30, 103054, 2022.
30.	[JOH05]	John, C. I. Laser processing of engineering materials, Elsevier Butterworth-Heinemann, Oxford, UK, 2005.
31.	[KAN19]	Kanitz, A., Kalus, M.-R., Gurevich, E. L., Ostendorf, A., Barcikowski, S., Amans, D. Review on experimental and theoretical investigations of the early stage, femtoseconds to microseconds processes during laser ablation in liquid-phase for the synthesis of colloidal nanoparticles, Plasma Sources Science and Technology, 28, 10, 2019.
32.	[KEN04]	Kennedy, E., Byrne, G., Collins, D.N. A review of the use of high power diode lasers in surface hardening, Journal of Materials Processing Technology, 155, 1855-1860, 2004
33.	[KEV17]	Kevin G. Field, Mary A. Snead, Yukinori Yamamoto, Kurt A. Terrani , Handbook on the Material Properties of FeCrAl Alloys for Nuclear Power Production Application, U.S. Department of Energy Nuclear Technology R&D Advanced Fuels Campaign, 2017.
34.	[KHA12]	Khan, M.M.A., Romoli, L., Fiaschi, M., Dini, G., Sarri, F. Laser beam welding of dissimilar stainless steels in a fillet joint configuration. // Journal of Materials

		Processing Technology, 212, 4, pp. 856– 867 DOI:10.1016/j.jmatprotec.2011.11.011, 2012
35.	[KIH12]	Ki, H., So, S. Process map for laser heat treatment of carbon steels, Elsevier Optics & Laser Technology, 44, 2106-2114, 2012.
36.	[KLI07]	Klimpel, A., Lisiecki, A. Laser welding of butt joints of austenitic stainless steel AISI 321. // Journal of Achievements in Materials and Manufacturing Engineering, 25, 1, pp. 63-66, 2007.
37.	[KOR11]	Korneev, N., Rodriguez Montero, P., Ramos-García, R., Ramirez-San-Juan, J. C., Padilla-Martinez, J. P. Ultrasound induced by CW laser cavitation bubbles, J. Phys.: Conf. Ser., 278, 012029, 2011.
38.	[KOS22]	Kose C., Heat treatment and heat input effects on the dissimilar laser beam welded AISI 904L super austenitic stainless steel to AISI 317L austenitic stainless steel: Surface, texture, microstructure and mechanical properties, Vacuum 205 111440, 2022.
39.	[KUM17]	Kumar, N., Mukherjee, M., Bandyopadhyay, A., Comparative study of pulsed Nd:YAG laser welding of AISI 304 and AISI 316 stainless steels. Optics & Laser Technology. 88. 10.1016/j.optlastec.2016.08.018, 2017.
40.	[LAP19]	Lapouge, P., Dirrenberger, J., Coste, F., Schneider, M. Laser heat treatment of martensitic steel and dual-phase steel with high martensite content, Materials Science and Engineering: A Volume, 752, 128-135, 2019.
41.	[LEE11]	Lee, H., Gojani, A. B., Han, T., Yoh, J. J. Dynamics of laser-induced bubble collapse visualized by time-resolved optical shadowgraph. J. Visual., 14, 331–337, 2011.
42.	[LEI11]	Leitz, K.-H., Redlingshöfer, B., Reg, Y., Otto, A., Schmidt, M. Metal ablation with short and ultrashort laser pulses, Physics Procedia, 12, 230–238, 2011.
43.	[LID23]	Lidong Yu, Yang Bai, TianXuan Bian, YunTeng Qu, ZhiWei Xu, Yi Li, Heng Zhang, Influence of laser parameters on corrosion resistance of laser melting layer on C45E4 steel surface, Journal of Manufacturing Processes, Volume 91, pp. 1-9, ISSN 1526-6125, https://doi.org/10.1016/j.jmapro.2023.02.029, 2023.
44.	[LIM05]	Lima, A.S., Nascimento, A.M., Abreu, H.F.G., P. de Lima-Neto. Sensitization evaluation of the austenitic stainless steel AISI 304L, 316L, 321 and 347. // Journal of Materials Science, 40, 1, pp. 139-144, 2005.
45.	[LIP05]	Lippold J.C., Kotechki, D.J. Welding Metallurgy and Weldability of Stainless Steels. John Wiley and Sons, New Jersey, USA, 2005.
46.	[LOK09]	Lo, K.H., Shek, C.H., Lai, J.K.L. Recent developments in stainless steels. // Materials Science and Engineering R 65, 4-6, pp. 39–104. DOI:10.1016/j.mser.2009.03.001, 2009

47.	[LON23]	Longlong Guo, Lu Cui, Fei Xiao, Binrong Xu, Zebing Wu, Yinping Cao, Zebing Wei, Influence of process parameters on surface properties and corrosion resistasnce of Inconel 625 coating prepared by laser cladding, International Journal of Electrochemical Science, Volume 18, Issue 8, 100213, ISSN 1452-3981, https://doi.org/10.1016/j.ijoes.2023.100213, 2023.
48.	[MAH10]	Mahmoudi, B., Torkamany, M.J., Sabour Rouh Aghdam, A. R., Sabbaghzade, J. Laser surface hardening of AISI 420 stainless steel treated by pulsed Nd:YAG laser, Materials & Design, 31, 2553-2560, 2010.
49.	[MAH19]	Maharjan, N., Zhou, W., Zhou, Y., Guan, Y., Wu, N. Comparative study of laser surface hardening of 50CrMo4 steel using continuous-wave laser and pulsed lasers with ms, ns, ps and fs pulse duration, Surface and Coatings Technology, 366, 311-320, 2019.
50.	[MAR08]	Marczak J, Koss A, Targowski P, Góra M, Strzelec M, Sarzyński A, Skrzeczanowski W, Ostrowski R, Rycyk A., Characterization of Laser Cleaning of Artworks. Sensors. 8. 10.3390/s8106507, 2008.
51.	[MAR17]	Martínez-Conde, A., Krenke, T., Frybort, S. et al. Review: Comparative analysis of CO2 laser and conventional sawing for cutting of lumber and wood-based materials. Wood Sci Technol 51, 943–966, https://doi.org/10.1007/s00226-017-0914-9, 2017.
52.	[MIS14]	Mishra, D., Vignesh, M.K., Ganesh Raj, B., Srungavarapu, P., Ramkumar, K. D., Arivazhagan, N., Narayanan, S. Mechanical Characterization of Monel 400 and 316 Stainless Steel Weldments, Procedia Engineering, 75, pp. 24-28, DOI:10.1016/j.proeng.2013.11.005, 2014.
53.	[MOL17]	Moldovan E., Tierean M.H., Stanciu E.M., Overview of joining dissimilar materials: metals and polymers, Bulletin of the Transilvania University of Braşov , Vol. 10 (59) No. 1, Series I: Engineering Sciences, 2017.
54.	[MOL22]	Moldovan E.R., Doria C.C., Ocana J.L., Baltes L.S., Stanciu E.M., Croitoru C., Pascu A., Roata I.C., Tiereanu M.H., Wettability and Surface Roughness Analysis of Laser Surface Texturing of AISI 430 Stainless Steel, Materials, 5(8), 2955, e-ISSN 1996-1944, 2022.
55.	[NAF09]	Naffakh, H., Shamanian, M., & Ashrafizadeh, F. Dissimilar welding of AISI 310 austenitic stainless steel to nickel-based alloy Inconel 657. Journal of materials processing technology, 209(7), 3628-3639, https://doi.org/10.1016/j.jmatprotec.2008.08.019, 2009.
56.	[NIK16]	Nikolic´, V., Petkovic´, D., Lazov, L., Milovanc˘evic´, M. Selection of the most influential factors on the water-jet assisted underwater laser process by adaptive neuro-fuzzy technique, Infrared Physics & Technology, 77, 45–50, 2016.

57.	[OHS19]	Oh, S., Ki, H. Deep learning model for predicting hardness distribution in laser heat treatment of AISI H13 tool steel, Applied Thermal Engineering, 153, 583-595, 2019.
58.	[PAD11]	Padilla-Martinez, J. P., Aguilar, G., Ramirez-San-Juan, J. C., Ramos-García, R. Temporal evolution of thermocavitation bubbles using high speed video camera, Optical trapping and optical micromanipulation, VIII, 809727, 2011.
59.	[PAD14]	Padilla-Martinez, J. P., Berrospe-Rodriguez, C., Aguilar, G., Ramirez-San-Juan, J. C., Ramos-Garcia, R. Optic cavitation with CW lasers: A review, Physics of fluids, 26, 122007, 2014.
60.	[PAR14]	Parisa F., Shuang L., Zhe Z., Radovan K., Laser cladding assisted by induction heating of Ni–WC composite enhanced by nano-WC and La2O3, Ceramics International, Volume 40, Issue 10, Part A, pp. 15421-15438, ISSN 0272-8842, https://doi.org/10.1016/j.ceramint.2014.06.097, 2014.
61.	[PAS13]	Pascu, A. Parameters of the laser cladding process, LUXLibris Publishing House, Brasov, Romania, 2013.
62.	[PAS16]	Pascu A., Stanciu E.M., Roata I.C., Croitoru C., Baltes L.S., Tierean M.H., Parameters and Behaviour of NiCrFeSiB Laser Cladding in Overlapped Geometry, Bulletin of the Transilvania University of Braşov, Vol. 9 (58) No. 2, Series I: Engineering Sciences, 2016.
63.	[PAS17]	Pascu A., Stanciu E. M., Croitoru C., Roata I. C., Tierean M. H., Pulsed Laser Cladding of Ni Based Powder, IOP Conference Series: Materials Science and Engineering , 209, 012058 doi:10.1088/1757-899X/209/1/012058, 2017.
64.	[PAS22]	Pascu A., Stanciu E. M., Cuculea D., Ardelean G., Iatan C., Moldovan E. R., Machedon T., Influences of the Nozzle Shape on Bead Appearance and Morphology in Coaxial Laser Cladding, International Conference on Innovative Research, May 26th to 27th, 2022, Iasi – Romania, ISSN Print 2601-4580, 2022.
65.	[PAV23]	Pavan A.R., Arivazhagan B., Vasudevan M., Prasanthi T.N., Sudha C.,Study on the microstructure and mechanical properties of hybrid laser + MIG welded joints of 316LN stainless steel, Optics & Laser Technology 163, 109410, 2023.
66.	[PEI21]	Peilei Z, Zhiyuan J, Zhishui Y, Haichuan S, Shaowei L, Di W, Hua Y, Xin Y, Jieshi C, Fuxin W, and Yingtao T, Optics & Laser Technology 140 107094, 2021.
67.	[PHO20]	Phuong N., T. T., Tanabe-Yamagishi, R., Ito, Y. Effects of liquid depth on the expansion and collapse of a hemispherical cavitation bubble induced in nanosecond pulsed laser ablation of a solid in liquid, Optics and Lasers in Engineering, 126, 2020.
68.	[SEN20]	Senegačnik, M., Jezeršek, M., Gregorčič, P. Propulsion effects after laser ablation in water, confined by different geometries. Appl. Phys. A, 126, 136, 2020.

69.	[SHE22]	Shenghong Y, Zheng M, Bo C, Caiwang T, Xiaoguo S, and Guodong W, Optics & Laser Technology 145 107493, 2022.
70.	[SHI17]	Shin, J.S., Oh, S.Y., Park, H., Chung, C.-M., Seon, S., Kim, T.-S., Lee, L., Choi, B.-S., Moon, J.-K. High-speed fiber laser cutting of thick stainless steel for dismantling tasks, Opt. Laser. Technol., 94, 244-247, 2017.
71.	[SHI18]	Shin, J.S., Oh, S.Y., Park, H., Chung, C.-M., Seon, S., Kim, T.-S., Lee, L., Lee, J. Laser cutting of steel plates up to 100 mm in thickness with a 6-kW fiber laser for application to dismantling of nuclear facilities, Opt. Laser Eng., 100, 98-104, 2018.
72.	[SIN03]	Sindo Kou, Welding Metallurgy Second Edition, John Wiley & Sons, Inc., Hoboken, New Jersey, 2003.
73.	[SOP19]	Shin, J. S., Oh, S. Y., Park, H., Kim, T.-S., Lee, L., Chung, C.-M., Lee, J. Underwater cutting of 50 and 60 mm thick stainless-steel plates using a 6-kW fiber laser for dismantling nuclear facilities, Optics & Laser Technology, 115, 1-8, 2019.
74.	[STA14]	Stanciu E. M., Pascu A., Roată I. C., Edge fillet laser welding of AISI 304 stainless steel, Solid State Phenomena, Vol 216, 304-309, 2014.
75.	[STA17]	Stanciu E.M., Pascu A., Gheorghiu I., CMT Welding of Low Carbon Steel Thin Sheets, IOP Conference Series: Materials Science and Engineering , 209, 012051, 2017.
76.	[STA18]	Stanciu E.M., Pascu A., Tierean M.H., Roata I.C., Voiculescu I., Hulka I., Croitoru C., Dissimilar Laser Welding of AISI 321 and AISI 1010, Technical Gazette, ISSN 1330-3651, Vol. 25/No. 2, 2018.
77.	[STA19]	Stanciu E.M., Pascu A., Roata I.C., Croitoru C., Tierean M.H., Laser welding of dissimilar materials, Materials Today-Proceedings, 19, pp 1066-1072, ISSN 2214-7853, 2019.
78.	[STA22]	Stanciu E.M., Pascu A., Roată I.C., Iatan C., Moldovan E.R. and Tierean M.H., Millisecond pulsed laser welding of AISI 316 stainless steel, IOP Conf. Series: Materials Science and Engineering, IOP Publishing, 1251, 012012, 2022.
79.	[STA23]	Stanciu E.M., Pascu A., Croitoru C., Roata I. C., Cristea D., Tierean M.H., Hulka I., Petre I.M., Mirza Rosca J. C., Functional Surfaces via Laser Processing in Nickel Acetate Solution, Materials, 16, 3087, 2023.
80.	[STE18]	Stanciu E.M., Pascu A., Roată I.C., Croitoru C., Tierean M., Mirza Rosca J., Hulka I., Solar radiation synthesis of functional carbonaceous materials using Al_2O_3/TiO_2-Cu-HA doped catalyst, Applied Surface Science 438, pp 33–40, ISSN 0169-4332, 2018.
81.	[SUM19]	Suman C, Siba S M, Vijay B, Brahma N U, Khushvinder S B, and Joji T, Optics and Laser Technology 117 186–199, 2019.

82.	[TBM18]	Telrandhe, S. V., Bhagyaraj, J., Mishra, S., Karagadde, S. A new approach to control and optimize the laser surface heat treatment of materials, Journal of Materials Processing Technology, 262, 492-502, 2018.
83.	[TOR12]	Torkamany, M.J., Sabbaghzadeh, J., Hamedi, M.J. Effect of laser welding mode on the microstructure and mechanical performance of dissimilar laser spot welds between low carbon and austenitic stainless steels. // Materials and Design, 34, pp. 666–672 DOI: 10.1016/j.matdes.2011.05.024, 2012.
84.	[TOY05]	TOYSERKANI Ehsan, KHAJEPOUR Amir, CORBIN Stephen, Laser cladding, CRC Press, ISBN 0-8493-2172-7
85.	[VOG01]	Vogel, A., Noack, J. Numerical simulation of optical breakdown for cellular surgery at nanosecond to femtosecond time scales, Proc. SPIE 4260, Optical Diagnostics of Living Cells IV, 2001.
86.	[VOI18]	Voiculescu I., Geanta V., Stanciu E.M., Jianu D.A., Postolache C., Fugaru V., Effect of Irradiation and Temperature on Microstructural Characteristic of FeCrAl Alloys, Acta Physica Polonica A, 134(1), pp116-118, ISSN: 0587-4246, 2018.
87.	[WAN17]	Wang X., Zhou Shengfeng, Dai Xiaoqin, Lei Jianbo, Guo Jinbo, Gu Zhenjie, Wang Tao, Evaluation and mechanisms on heat damage of WC particles in Ni60/WC composite coatings by laser induction hybrid cladding, International Journal of Refractory Metals and Hard Materials, Volume 64, pp. 234-241, ISSN 0263-4368, https://doi.org/10.1016/j.ijrmhm.2016.11.001, 2017.
88.	[WAN18]	Wang, H., Huang, Y., Zhang, W. The study of laser shock peening with side-water spraying and coaxial-water feeding technology, International Journal of Lightweight Materials and Manufacture, 1, 102-107, 2018.
89.	[WAN18]	Wanga, J., Suna, Q., Jiang, Y., Zhang, T., Ma, J., Fenga, J. Analysis and improvement of underwater wet welding process stability with static mechanical constraint support, Journal of Manufacturing Processes, 34, 238-250, 2018.
90.	[WAN19]	Wang, H., Pöhl, F., Yan, K., Decker, P., Gurevich, E. L., Ostendorf, A. Effects of femtosecond laser shock peening in distilled water on the surface characterizations of NiTi shape memory alloy, Applied Surface Science, 471, 869-877, 2019.
91.	[WEI23]	Wei C., Guangchun X., Hui Z., Hui C., Mingdong Y., Jingjie Z., Zhaoqiang Chen, Chonghai Xu, Effects of pulse wave laser frequency on microstructure and properties of TiN/Co-based cladding layer, Optics & Laser Technology, Volume 163, 109439, ISSN 0030-3992, https://doi.org/10.1016/j.optlastec.2023.109439, 2023.
92.	[WEI23]	Wei Zhang, Xianhe Shang, Minglei Hu, Xing He, Bing Yang, Kunjie Dai, Xiaoqing Ni, Lin Lu, Liangdong Zhou, Liang Zhang, Decheng Kong, Chaofang Dong, Microstructure and corrosion-wear behaviors for laser cladding repaired

		martensitic stainless steels using Co-based and Ni-based powders, Materials Today Communications, Volume 35, 106287, ISSN 2352-4928, https://doi.org/10.1016/j.mtcomm.2023.106287, 2023.
93.	[WEN19]	Wen, X., Jin, G., Cui, X., Feng, X., Lu, B., Caia, Z., Zhao, Y., Fang, Y. Underwater wet laser cladding on 316L stainless steel: A protective material assisted method, Optics & Laser Technology, 111, 814-824, 2019.
94.	[WIE08]	WIELLIGH Louis George, Characterizing the influence of process variables in laser cladding Al-20wt%Si onto an aluminium substrate, PhD thesis, Technology at the Nelson Mandela Metropolitan University, http://hdl.handle.net/10948/721,
95.	[XIA17]	Xiao, J., Liu, P., Wang, C. X., Yang, G. W. External field-assisted laser ablation in liquid: An efficient strategy for nanocrystal synthesis and nanostructure assembly, Progress in Materials Science, 87, 140-220, 2017.
96.	[XIN24]	Xinlin Wang, Zengxia Zhang, Yanqin Zhao, Zhiqiang Hu, Xiang Li, Macroscopic morphology and properties of cobalt-based laser cladding layers on rail steel based on pulse shaping, Optics & Laser Technology, Volume 168, 109940, ISSN 0030-3992, https://doi.org/10.1016/j.optlastec.2023.109940, 2024.
97.	[YAN10]	Yan, J., Gao, M., Zeng, X. Study on microstructure and mechanical properties of 304 stainless steel joints by TIG, laser and laser-TIG hybrid welding, Optics and Lasers in Engineering, 48, pp. 512–517, DOI: 10.1016/j.optlaseng.2009.08.009, 2010.
98.	[YAN10]	Yan, J., Gao, M., Zeng, X. Study on microstructure and mechanical properties of 304 stainless steel joints by TIG, laser and laser-TIG hybrid welding, Optics and Lasers in Engineering, 48, pp. 512–517, DOI: 10.1016/j.optlaseng.2009.08.009, 2010.
99.	[YAN23]	Yanlong Luan, Jia Liu, Yan Shi, Effect of surface texture on quality of stainless steel-PET transmission welding, Optics & Laser Technology, Volume 161, 109144, 2023.
100.	[YAX23]	Yaxin Ma, Hong Zhang, Long He, Lixia Yang, Zhengxing Men, Influence of laser power on the high-temperature creep rupture life of 304L stainless steel manufactured by selective laser melting, Vacuum, Volume 211, 111957, ISSN 0042-207X, 2023.
101.	[YON23]	Yongfeng Li, Jian Zhang, Xuehong Huang, Jing Liu, Lijun Deng, Peiyuan Han, Influence of laser power on microstructure evolution and properties of laser cladded FeNiCoCrMo HEA coatings, Materials Today Communications, Volume 35, 105615, ISSN 2352-4928, 2023.
102.	[ZHA06]	Zhang, X., Ashida, E., Shono, S., Matsuda F. Effect of shielding conditions of local dry cavity on weld quality in underwater Nd:YAG laser welding. J. Mater. Process. Technol., 174 (1), 34–41, 2006.

103. [ZHA15]	Zhang, N., Brugger, J., Etschmann, B., Ngothai, Y., Zeng, D. Thermodynamic modelling of poorly complexing metals in concentrated electrolyte solutions: an X-Ray absorption and UV-Vis spectroscopic study of Ni(II) in the NiCl2-MgCl2-H2O system, PLoS ONE, 10(4), 1-23, 2015.
104. [ZHA23]	Zhang Bo, Wang Huaming, Zhang Shuquan, He Bei, Optimization of the dilution parameters to improve wear resistance of laser cladding 15-5PH steel coating on U75V pearlitic steel, Surface and Coatings Technology, Volume 465, 129571, ISSN 0257-8972, https://doi.org/10.1016/j.surfcoat.2023.129571, 2023.
105. [ZHE21]	Zhenlin Zhang, Yue Zhao, Yang Chen, Zhen Su, Jiguo Shan, Aiping Wu, Yutaka S. Sato, Huaipeng Gu, Xin Tang, The role of the pulsed-wave laser characteristics on restraining hot cracking in laser cladding non-weldable nickel-based superalloy, Materials & Design, Volume 198, 109346, ISSN 0264-1275, https://doi.org/10.1016/j.matdes.2020.109346, 2021.
106. [ZHO20]	Zhong, X., Eshraghi, J., Vlachos, P., Dabiri, S., Ardekani, A. M. A model for a laser-induced cavitation bubble, International Journal of Multiphase Flow, 2020.
107. [ZHU12]	Zhu, J., Jiao, X., Zhou, C., Gao, H. Applications of underwater laser peening in nuclear power plant maintenance, Energy Procedia, 16, 153-158, 2012.
108. [***LAS]	https://www.laserfocusworld.com/lasers-sources/article/16548135/annual-laser-market-review-forecast-where-have-all-the-lasers-gone